

Southern binaries with the Zorro Speckle Camera @ Gemini-South

RENE A. MENDEZ,¹ ANDREI TOKOVININ,² EDGARDO COSTA,¹ AND MAXIMILIANO DIRK³

¹*Departamento de Astronomia
Universidad de Chile*

Casilla 36-D, Santiago, Chile

²*Cerro Tololo Inter-American Observatory
NOIRLab*

Casilla 603, La Serena, Chile

³*Centre for Astrophysics Research
University of Hertfordshire*

Hatfield, Hertfordshire AL10 9AB, UK

ABSTRACT

We present measurements in the context of a survey of southern hemisphere binary and multiple stellar systems observed with the Zorro Speckle dual diffraction-limited optical imaging camera on the 8.1 m Gemini-South telescope carried out between 2019 and 2023. The overall motivation of our survey, as well as some initial results of these observations, are outlined to demonstrate the capabilities - and limitations - of Zorro. We report on the astrometric characterization of the instrument in terms of the precision and accuracy of our measurements and provide details of our custom-made data reduction pipeline. For targets with separations smaller than $0''.4$, an overall precision of 1 mas in the radial and tangential directions is obtained, while the uncertainty in position angle is $0''.2$. Relative astrometry and contrast brightness in the two Zorro filters at 562 and 832 nm are reported for 70 pairs on 64 distinct systems (six are triples). Eleven new binaries are found, mostly of small separations (down to 15 mas), and large brightness contrast (up to $\Delta m = 6$ in the red channel). Our results indicate that the Zorro instrument, when properly calibrated, delivers excellent quality data for visual binary studies of tight and/or faint companions.

Keywords: Classical Novae (251) — Ultraviolet astronomy(1736) — History of astronomy(1868) — Interdisciplinary astronomy(804)

1. INTRODUCTION

Vogt-Russell’s theorem (Kahler 1972) predicts that the most fundamental parameter determining the internal structure and evolution of stars of a given chemical composition is their initial mass (see e.g. Massey & Meyer (2001); Iben (2013)). One of the main relationships reflecting the dependency of the star’s properties on mass is the mass-luminosity relation (MLR), first discovered empirically in the early 20th century, and later explained on theoretical grounds by Eddington (1924). Improving the observational MLR is not a simple task, because it involves not only determining precise distances¹, but also another elusive parameter: mass. To further complicate things, the observational MLR has a statistical dispersion which cannot be explained exclusively by observational errors in the luminosity or mass; there seems to be an intrinsic dispersion caused by differences in age and/or chemical composition (see e.g. Gafeira et al. (2012)).

Currently, the best MLRs for main sequence stars are those of Torres et al. (2010) and Benedict et al. (2016), but (except for one object with $[\text{Fe}/\text{H}] < 0.25$ in Torres et al. (2010)) neither of them include low-metallicity stars. Although there are other studies, using long-base optical interferometry of binary systems, that have begun to address

¹ A classical problem in binary-star research, now largely solved by Gaia.

metallicity effects (e.g. [Boyajian et al. \(2012a,b\)](#), [Feiden & Chaboyer \(2012\)](#)), these have reached only as low as about $[\text{Fe}/\text{H}] = -0.5$.

Another pioneering effort to this end, which in fact provided the motivation for the present survey, has been that of [Horch et al. \(2015, 2019\)](#) who have been using the high-resolution Speckle camera Alopeke mounted on the Gemini-North 8.1 m telescope (GN hereafter) to determine an empirical low-metallicity MLR for the Solar Neighborhood. So far, that work has resolved over twenty systems that span a range of Iron abundance from $[\text{Fe}/\text{H}]$ of +0.1 down to -2.0, with spectral types that range from mid-F to mid-K².

The dependence of total mass on metallicity (for a given luminosity) for the eleven systems with the best data that they had available is shown in Figure 7 of [Horch et al. \(2019\)](#). Alopeke observations on GN for these eleven binaries with a reliable mass determination confirm that the data appears to follow the theoretically expected trend in stellar mass as a function of metallicity. This was a significant step forward, albeit further data are clearly needed to fully constrain the models.

This latter reality prompted us to start in 2019 an observational campaign in the southern hemisphere using the Zorro Speckle camera (a twin of Alopeke) on the Gemini-South 8.1 m telescope (GS hereafter), to increase the sample of low-metallicity objects with well determined orbits and mass sums. Zorro@GS provides a unique opportunity to add an important number of southern systems that will fill in the current metallicity range, and to provide further data on objects that have been scarcely observed at GN. With the full data set, it will be possible to make a relevant contribution to the main-sequence MLR for metal-poor stars.

Determining high-quality individual masses is time-consuming, and requires precise astrometric (mass sum) and high-resolution spectroscopic (mass ratios) observations that must span a significant part of the orbital period. Direct determination of individual masses of spectroscopic binaries is possible if the components can be resolved and their angular separation in the sky (denoted by ρ hereafter) can be accurately determined over time. For double-lined systems, the combined spectroscopic/astrometric orbit solution yields individual masses as well as a distance to the system without the need for parallax measurements (the so-called self-consistent “orbital parallaxes”, [Anguita-Aguero et al. \(2022\)](#)). An independent distance measure (e.g., from Gaia) is needed for single-lined systems to complete the path to individual masses. With a spectroscopic orbit and parallax in hand, several resolved observations adequately spread out along the orbit can be used to determine the semi-major axis and inclination reliably, and therefore provide the basis for individual masses ([Anguita-Aguero et al. \(2023\)](#)).

Given the small space density of local Halo stars, metal-poor binary systems are typically farther away from the sun than solar metallicity stars and, therefore fainter and/or more compact spatially, making them difficult objects for optical interferometry with small (4m or less) telescopes. Thanks to their dual-detector design, Zorro@GS and Alopeke@GN have the ability to resolve binary systems even slightly below its natural diffraction limit of 20 milliarcseconds (mas). These speckle cameras provide an excellent opportunity to make relatively quick progress on a number of low-metallicity binary systems (given the tight and hence short periods involved), by combining conclusive observations obtained at Gemini with spectroscopic data and lower-precision astrometry from other facilities, already available from the literature.

It is extremely important to precisely calibrate masses and luminosities of metal-poor stars. Typically, the Population II main sequence has been defined by nearby metal-poor stars (e.g. [Reid \(1997\)](#), [Gratton et al. \(1997\)](#)), a number of which could be binary systems. If binaries currently included in the Population II main sequence definition are resolved, and individual luminosities can be obtained, these new data will reduce the current scatter, allowing for more stringent constraints on stellar models, as well as better ages and distances to Galactic globular clusters.

In cases where one component has evolved away from the main sequence, age determinations are also possible using, e.g., the method of [Davidson et al. \(2009\)](#) to place the components on the H-R diagram. A hint of this is shown in Figures 1 and 8, on Sections 1 and 4, respectively, of [Mendez et al. \(2017\)](#), and on Figs. 5 and 6, on Sections 4 and 5 of [Anguita-Aguero et al. \(2022\)](#). Also, the secondary components of metal-poor binaries are especially important in that they will have undergone considerably less change in color and luminosity, and their current observables should thus be close to their zero-age locations in the color-magnitude diagram, and in this way, speckle observations could be directly compared with stellar models ([Spada et al. 2013](#)). Thus, our Zorro@GS survey, together with the Alopeke@GN program, will not only add a significant number of new points to the MLR, but also provide sensitive

² A more recent study by [Mann et al. \(2019\)](#) discusses the effects of metallicity on the MLR for later spectral types and masses $M < 0.7 M_{\odot}$.

tests of stellar evolution theory. We expect to be able to investigate the effect of metallicity and age on the MLR for the first time. Also, in general, an increase in the number of well-studied binary stars will also contribute to other astrophysical areas, such as star formation and comprehensive studies of the Solar Neighborhood, which require a knowledge of the multiplicity fraction.

Several low-metallicity binary stars targeted by the Alopeke@GN survey turned out to be multiple systems (some pending confirmation of common motion). These objects are quite interesting because the architecture of stellar hierarchical systems results from their formation and early evolution; thus their study helps to understand the formation of stars and planets (Moe & Di Stefano 2017; Moe & Kratter 2018). We have included these compact hierarchical systems in our program, in order to provide further observational constraints on the orbital architecture. In principle, both inner and outer orbits could be determined, and our goal in this respect is to increase the still modest number of multiples where both orbits are known precisely (see, e.g., Tokovinin & Latham (2020)), enabling the study of relative orbit orientation, mutual resonances, and eccentricities in multiple systems.

In this paper, we report on the preliminary results from our Zorro@GS survey and its medium-term prospects. In a forthcoming paper, we will analyze in detail a few of the objects for which enough data permits a precise determination of their orbits, including radial velocities (RV hereafter) from an ongoing effort with Echelle spectrographs to determine RVs for the system’s components.

The outline of the paper is as follows: In Section 2 we describe the selection of our sample and provide a log of our observing runs. In Section 3, we describe the data reduction steps, including the astrometric calibration and an assessment of the data quality and overall performance of Zorro@GS. In Section 3.5 we highlight our main results and provide comments on selected individual objects. Finally, Section 5 presents our main conclusions.

2. SAMPLE SELECTION

Our initial sample consisted of assorted southern hemisphere targets kindly provided by E. Horch and collaborators, from their study of low-metallicity binaries that lacked orbital coverage or were pending confirmation of their architecture (actually, at least three of the systems targeted by Horch and collaborators were discovered to be trines; sustained observations of the new components (if bound) would further shed light to our knowledge of metal-poor stars).

This list quickly evolved in time as observations progressed and some targets were removed from the observing list (e.g., due to non-detection or possibly very long periods), while other promising low-metallicity or multiple-system targets were added from our own survey of southern binaries. Indeed, in 2014, we began a systematic campaign with the HRCam speckle camera at the SOAR 4.1 m telescope to observe nearby southern binary and multiple stellar systems (both visual and spectroscopic). The science goals of that project have been described in Mendez et al. (2017). Many publications have resulted from this effort (for the latest, see e.g., Anguita-Aguero et al. (2023)).

Among the stars observed with HRCam@SOAR, we have identified many tight binary systems that are at the resolution limit of this instrument and, therefore, have large astrometric uncertainties. These are short-period systems (~ 10 yr or less) with very small projected ρ , equal to or smaller than the diffraction limit of the SOAR telescope (~ 35 mas at 5500 \AA), in which cases speckle observations with 4 m facilities are of insufficient precision to determine high-quality orbits. Therefore, in addition to including bona-fide low-metallicity targets in our GS program, we also included some of these tight systems. We have also included some targets from the survey of multiple stellar systems in the southern hemisphere being carried out by A. Tokovinin (see, e.g., Tokovinin (2023)) which proved to be too tight for the resolution of HRCam@SOAR.

We must emphasize that, as a result of our selection process, our final sample is very heterogeneous and it should not be considered complete or representative of these systems in any astrophysical sense. From this point of view, this work’s main contribution is adding new orbits and mass ratios (when possible) for a variety of tight binaries and multiple systems.

2.1. Observing strategy and observing runs

Zorro is a fast, low-noise, dual channel and dual-plate-scale imager, which in speckle mode provides simultaneous two-color (blue and red) diffraction-limited optical imaging (FWHM 20 mas at 650 nm) of objects as faint as $V \sim 17$ mag over a FOV of $6''.7$. The detector consists of two 1024×1024 iXon Ultra 888 back-illuminated Electron Multi-

plying CCDs with $13\ \mu\text{m}$ pixels³. In speckle mode, four narrow band filters are available⁴, two of which can be used simultaneously in the blue and red "arms" of the instrument. For our survey we selected the Edmund Optics filter #562 in the blue side (562 nm central wavelength, 54 nm wide), and filter #832 (832 nm central wavelength, 40 nm wide) on the red side.

In general, we followed the standard recommendations given on the Gemini web page for the instrument, but added two sensitive observing constraints. We requested that airmass be kept as small as possible and that the observations be limited to hour angles within ± 1.5 hours from the meridian to minimize the effects of atmospheric dispersion (AD), which was especially noticeable in the blue filter (see Section 3.3.3). Unfortunately, due to the queue nature of the observations, combined with the declination of some targets, this rule was not always possible to strictly enforce.

In our list of targets we included well-observed, relatively wide, binaries for calibration purposes (further details are given below), which were typically observed at a rate of at least two systems per run. We also assigned a PSF reference star to each target; these are bona-fide single stars closer than about 3° to the target used for modelling the power spectrum of an isolated star. While the Gemini Zorro web pages recommend selecting bright objects ($5 < V < 6$ mag), after our first few runs we found that such bright objects did not provide a good match to the binary fit (see Section 3.3.3), so we opted instead for slightly fainter objects, with $V \geq 6$ mag, selected from the Bright Star Catalog (which is limited to $V \leq 6.5$).

Between 2019 and 2023, we have been awarded more than 74 hours of mostly highest-priority (Band 1) time with Zorro@GS through highly rated proposals by the time allocation committee, but, due to the COVID pandemic, a fraction of this time ($\sim 30\%$) could not be executed, significantly delaying our original observing plan. Very high-quality observations have been secured, however, for several tight binaries, and we do have a few new orbital points for them, but in some cases, it has not been possible to obtain the number of epochs needed to derive reliable visual orbits.

In Table 1, we present the details of our eleven observing runs, including the number of hours allocated, the completion rate, the epochs involved, the total number of usable frames, and the number of individual targets observed.

³ Full description of the instrument can be found in: <https://www.gemini.edu/instrumentation/alopeke-zorro>

⁴ Narrow band filters are preferred to increase the speckle contrast.

Table 1. Observing log from the Gemini Observatory archive: Gemini-Zorro program IDs and dates.

Gemini Program ID	Allocated time (hrs)/ Completion rate (%)	Dates	Number of frames ^a	Number of targets ^b
GS-2019A-Q-110	8.5 / 100	2019-05-19 to 2019-07-19	315	38
GS-2019A-Q-311	2.9 / 66	2019-05-21 to 2019-06-20	34	7
GS-2019B-Q-116	8.9 / 78	2019-09-12 to 2019-01-15	288	41
GS-2019B-Q-223	2.3 / 26	2019-09-13 to 2019-10-10	22	4
GS-2020A-Q-116	8.0 / 58	2020-03-15 to 2020-03-12	256	34
GS-2020B-Q-142	9.2 / 99	2020-10-29 to 2021-07-21	333	42
GS-2021A-Q-141 ^c	7.7 / 87	2021-01-14 to 2021-07-19	160	44
GS-2021B-Q-145	5.7 / 99	2021-09-18 to 2021-12-22	116	38
GS-2022A-Q-150	7.9 / 95	2022-03-15 to 2022-05-18	116	38
GS-2022B-Q-143	6.8 / 93	2022-10-07 to 2023-01-09	191	58
GS-2023A-Q-142	7.3 / 86	2023-03-05 to 2023-07-05	172	47

^aUsable frames (256×256 pix²).

^bBoth filters. Includes astrometric calibration binaries (typically two per observing run), and PSF reconstruction bona-fide single stars (typically one per object, either target or calibration binary).

^cThis run was split into two. In the second one the camera on the blue channel was out of focus, and no data was acquired with it. For calibration purposes we used the same values as those derived from the first run of this semester.

3. DATA REDUCTION, CALIBRATION, AND PRECISION ASSESSMENT

3.1. Introduction and data

In this section, we describe an adaptation of the HRCam@SOAR⁵ speckle pipeline made to process the data secured with the Zorro@GS. This pipeline is described in Tokovinin et al. (2010) and Tokovinin (2018a). We note that the SOAR pipeline has also been recently used to process the data from NESSI, a similar 2-channel speckle instrument at the WIYN telescope (Tokovinin et al. 2019).

The pipeline was adapted by one of the authors (AT) using as test bench the first-epoch data from 2019A, which serve here as example. Initially, the Zorro data (being a visiting instrument) was not ingested regularly to the Gemini Observatory Archive; therefore, these data were instead kindly provided by the Zorro instrument scientist at GS, Dr. R. Salinas, as tar-files, one per night. There are 8 nights from 2019-05-19 to 2019-07-19 (see Table 2.1). Each tar file contains FITS data cubes compressed with `bzip2`. A standard cube has a format of $256 \text{ pix} \times 256 \text{ pix} \times 1000$ frames (comprising one data cube), with a file size of 131 GB. The compressed data cubes have only a slightly smaller size (between 80 to 100 Gb), so the compression does not save much disk space but adds time for a decompression. The files are named like `S20190519Z0318b.fits` and `S20190519Z0318r.fits` for the blue and red channels, respectively, and include the date and a sequential number. The naming is important for the data organization, and the code has been properly adapted to it.

3.2. Pipeline presentation

The pipeline is written in IDL[®] (version 7.1 or higher⁶), and requires the ASTRO IDL library⁷. Our pipeline has been developed for personal use and is not meant to be a commercial software product, which means that a potential user must understand the algorithms and be able to fix problems. In the pipeline, the work is organized by means of arrays of IDL structures, saved on disk (Figure 1). The `log` and `bindat` arrays have one element per data cube and contain all essential meta-information, as well as the results of binary-star processing. In contrast, the `obsres` array

⁵ For information regarding this instrument, see <https://www.ctio.noirlab.edu/~atokovin/speckle/index.html>

⁶ IDL is a product by NV5 Geospatial software, see <https://www.nv5geospatialsoftware.com/>

⁷ Maintained by NASA's Goddard Space Flight center, and which can be downloaded from <https://asd.gsfc.nasa.gov/archive/idlastro/>

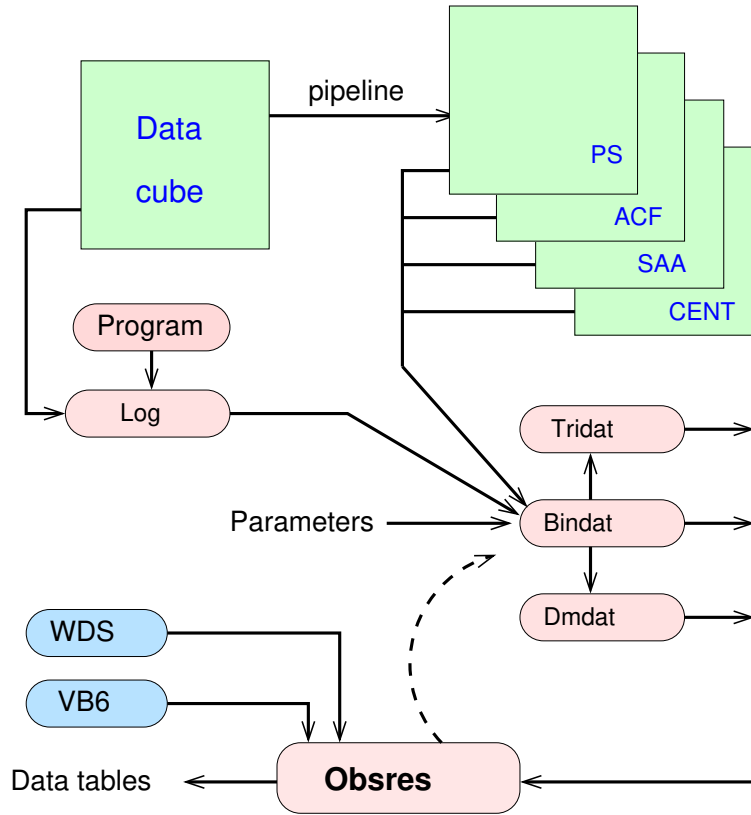


Figure 1. Data flow diagram of the Zorro Speckle data reduction process, which has been adapted from the SOAR/HRCam pipeline (Tokovinin 2018a).

(results) has one element per measurement, normally from averaging several data cubes (see further details below). Another important item is the parameter file that specifies path to the data and results, pixel scale, orientation, etc. Each observing run has its own parameter file, and its results (structures) are saved in a separate directory. A parameter file for one observing run, `z19a.par`, is reproduced below:

```

{param,
tel: 'GemS', ; telescope name
D: 8.1, ; aperture diam., m
pixel: 0.00991, ; nominal pixel scale, arcsec, blue; 0.1093 red, from Zorro/Gemini web page
long: -70.73669D0, ; longitude, degrees, Gemini site
lat: -30.24075D0, ; latitude, degrees, Gemini site
altitude: 2722., ; altitude a.s.l. for refraction, Gemini page
dirdat: '/19a/Raw/', ; image files
dirps: '/19a/Reduced/ps/', ; power spectra directory
diracf: '/19a/Reduced/acf/', ; ACFs directory
dirav: '/19a/Reduced/av/', ; average directory
filters: ['562','716','832'], ; filter names
lambda: [562.3,716.0,832.0], ; central wavelength for each filter, nm
dlambda: [43.6,51.5,40.4], ; FWHM, nm
paoffset: +0.42, ; add to get true PA **Always start with this value at 0.0!
scale: 0.9606, ; multiply by scale to get true separation **Always start with this value at 1.0!
redbluescale: 0.9719, ; pixel(red)/pixel(blue) **Always start with this value at 1.0!
redbluetheta: 0.439, ; theta(red)-theta(blue) **Always start with this value at 0.0!
log: '/19a/Results/log.idl', ; log-file
bindat: '/19a/Results/bindat.idl', ; bindat structure
tridat: '/19a/Results/tridat.idl', ; tridat structure
wdsid: '/19a/Results/wdsid.txt', ; created by avres2, edited
avres: '/19a/Results/avres.idl', ; averaged results

```

```
obsres: '/19a/Results/obsres.idl'} ; final results
```

3.3. Data processing

3.3.1. Calculation of the power spectra

The SOAR routine `getpowerixon.pro`, adapted to NESSI, was used for Zorro without changes. To subtract the bias, we compute the median signal in 10×10 pixel boxes in the lower-left and top-right corners and take the smallest of the two numbers as the (fixed) bias value.

The main calculation proceeds in the same way as done at SOAR. During the first pass through the cube, the bias is subtracted from each frame, centroids and other parameters are computed and saved, and the bias-subtracted cube is created. On the second pass, the power spectrum is accumulated using this cube. Also, the centered and "shift and add" (SAA hereafter) images (useful for quadrant disambiguation) are computed. The individual image parameters were used to reject poor frames (e.g. target too close to the border). Of the full 1024×1024 pix detector we used only a small region of interest (ROI) of 256×256 pix, so the fraction of rejected images is substantial for some cubes.

Also (especially in the earlier runs) a few data cubes were recorded with the full FOV on each night. These huge cubes (16 times normal) are rejected by the power calculation and not processed any further (these are considered unusable frames, and are excluded from Table 1).

Due to its optical layout, the two Zorro detectors have different orientations on the sky. To avoid potential confusion in further data reduction, we flip the red channel images along the horizontal axis, leaving the blue channel unchanged. As a result, all images have the same orientation: North to the right, East down. The resulting 2D images are named using the standard prefixes `ps-`, `av-`, `cent-`, `saa-`, and can be automatically retrieved during data processing from the names stored in the `log` or `bindat` structures. The results of `getpowerixon` are placed in the directories specified by the parameter file (all nights for a given observing run are put together).

3.3.2. The log structure and the parameter file

The log structure, identical to that of SOAR, is created and filled by several procedures in `getlog.pro`. The first procedure, `getlog`, reads all FITS files in the chosen directory, extracts relevant parameters from the headers, and creates the log structure, one element per data cube. The structure is saved in the log file specified by the parameters, or appended to it if the keyword `/append` is given. The log is created by calling the program for each night and appending successive nights of the same run. The filter names in the log (strings) equals the wavelength in nm, e.g. '562'. The procedure `getzen` computes the zenith distance and parallactic angle, using star coordinates and the geographical coordinates of the site in the parameter file. The routine `listlog` in `getlog.pro` creates the text `listlog.txt`, to be consulted during binary processing (e.g. to find a proper PSF reference star for a given binary). For example, for 2019a, the log contains 456 lines, including the full-frame cubes not processed here.

The code `getacf.pro` computes all ACFs from the power spectra. It operates on the log structure and adds to it important parameters such as models of the power spectrum (used in the binary-star processing), detection limits, and parameters of the AD. At this point, the log structure is complete. It is copied under the name `bindat` and used in the binary-star processing, which is the next step.

3.3.3. Binary star processing

The SOAR procedure for binary-star fitting `bin8.pro` and its GUI interface `xb.pro` were slightly adapted. The default reference spectrum calculated by azimuthal average (Tokovinin et al. 2010) includes modeling of the AD. However, the Zorro filters have a rectangular passband, hence their transfer function is modeled by the sinc^2 function rather than by a Gaussian. Figure 2 shows the power spectra of a tight binary (HIP 89000) in the blue and red channels. The power spectrum of the associated nearby PSF reference star is shown on the right side. Unfortunately, we found that the resolution in the blue channel is severely degraded by AD in one direction⁸. If the 21 mas separation binary were oriented parallel to the AD, it would probably remain unresolved in the blue channel. The situation is much better in the red channel with the 832 nm filter. In fact, the red channel resolution *always* supersedes the blue channel resolution, despite the longer wavelength. The formal astrometric and photometric accuracy (from the binary fits) are also worse in the blue channel. Note also that the blue image is under-sampled by the Zorro pixels.

⁸ Unfortunately, GS lacks an AD corrector, which would greatly alleviate this problem, as has been demonstrated in the case of HRCam@SOAR (Tighe et al. 2016).

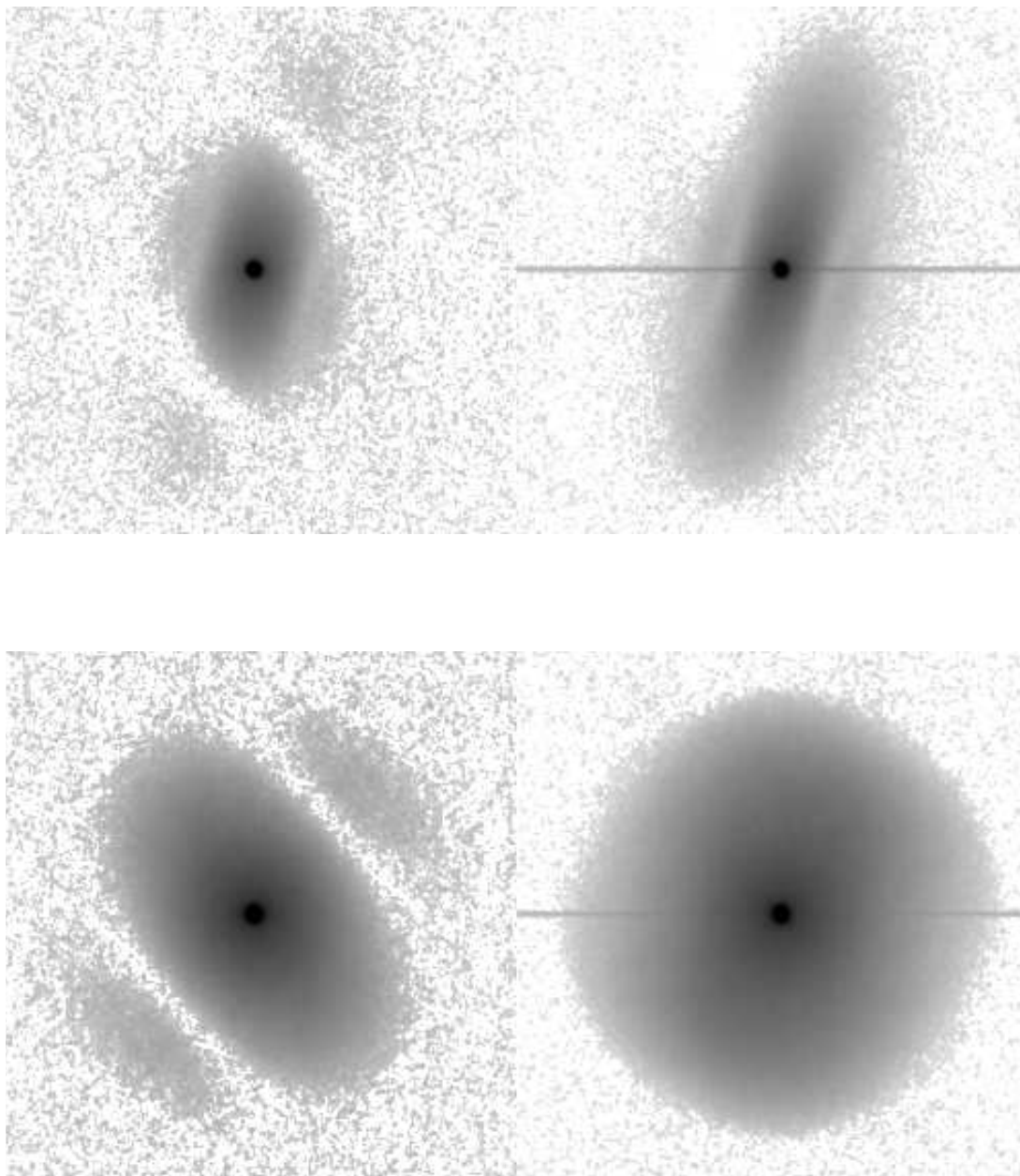


Figure 2. Example of power spectra for the data cube S20190519Z18, displayed with a negative logarithmic stretch. Top: blue channel, bottom: red channel. To the right of each spectrum, the spectrum of the associated PSF reference star is shown. The object is the 21 mas separation binary HIP 89000 observed at a zenith distance of 35° . The horizontal line in the reference spectra is an artifact caused by the image truncation owing to imperfect centering of the star in the ROI.

The use of a PSF reference star takes the AD and other instrumental effects into account, at least to first order. When a PSF reference star is not available, the reference spectrum is constructed from the object itself, by angular averaging, taking into account the AD (we call this the "RAD" model). Figure 3 shows an example of the blue channel power spectrum with a RAD reference. The AD is modeled using the calculated parallactic angle, zenith distance, and filter parameters. In some cases, the binary star fit using a RAD reference gives smaller residuals than the fit using a reference star, and then RAD is preferred.

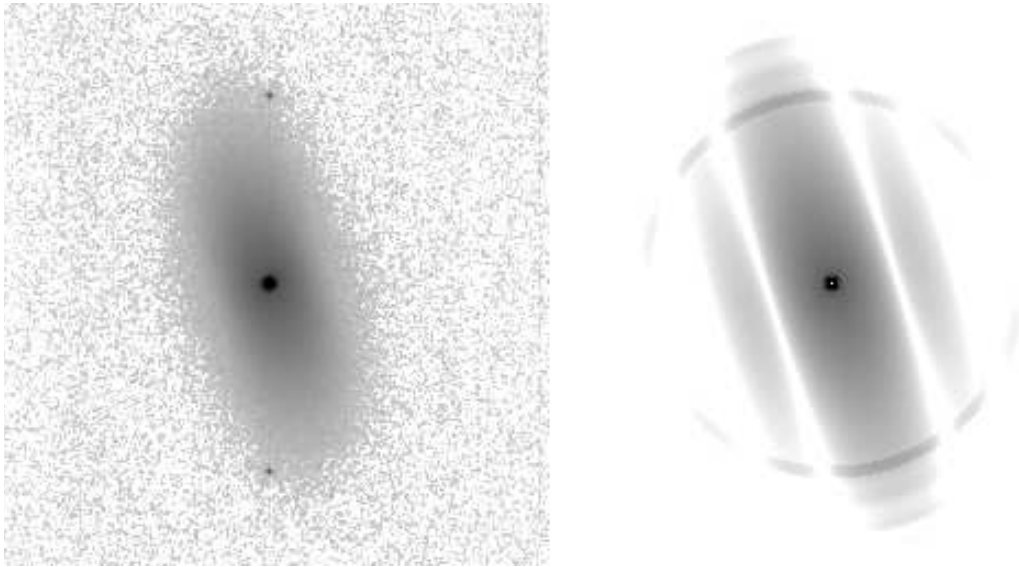


Figure 3. Left panel: Power spectrum in the blue channel of the cube S20190717Z0990b. Black dots are the consequence of a periodic noise. In this case, the reference spectrum on the right is the RAD model. Its similarity to the object spectrum illustrates the correctness of the AD model.

Several data cubes taken in 2019 July, including the one shown in Figure 3, are affected by periodic noise in the form of horizontal stripes. It is manifested in the power spectrum by two strong peaks above and below the center (see the left panel). The peaks create a "ring" in the reference spectrum (right panel) and stripes in the ACF. Such peaks can be easily masked, but this has not been implemented so far in our pipeline. None of the iXon CCDs used so far have had similar defects; and in Zorro, it is also intermittent. The red channel is affected by the stripes at the same time, but to a smaller degree.

The quality of the binary fit is characterized by the reduced χ^2/N . This metric rarely reaches small values, close to one or two. The residuals are typically dominated by the large-scale mismatch between data and model. When the χ^2/N with a real PSF reference star exceeds the χ^2/N with the RAD reference, the latter is preferred. During data processing, the reference star is identified by the cube number only, given by the 4 digits of the file name following 'Z', e.g. '0284'. The function `reference()` in `xb.pro` finds the name of the PSF reference image, given the name of the target file. It automatically selects the correct channel using the 'b' and 'r' letters in the file name.

Several data cubes are usually taken for each binary, producing e.g. a 'b-r-b-r-b-r' sequence in the log file. To automate the processing, we fit the first data cube and use the command `clone` for the following cubes. It copies the results (including the reference name) from the previous `bindat` record to be used as an initial approximation for the fit. Considering that the blue and red channels are different, we typically used `clone, s=-2` to copy from 2 cubes before, i.e. in the same channel. The fitting of triple stars is adapted in a similar way and does not present any additional problems. The final reduced data are stored in the sub-directory `RUN/19a/` in files `bindat.idl` and `tridat.idl`.

The IDL procedure `av` in `avres2.pro` averages the results from similar data cubes (per epoch and filter), producing one record for each subsystem in each filter. Another procedure `wdsid` creates the 'dictionary' file `wdsid.txt` to translate object names to standard WDS discoverer designation codes⁹ (when they are not available, the original names are retained). Then a group of procedures in `obsres.pro` creates the `obsres` structure with final results, which is used in further analysis. The data browser `xd.pro` allows to view and, if necessary, re-process individual data (e.g., for quadrant adjustments).

⁹ See the on-line WDS catalog at <http://www.astro.gsu.edu/wds/>

3.4. Calibration

3.4.1. Matching red and blue channels

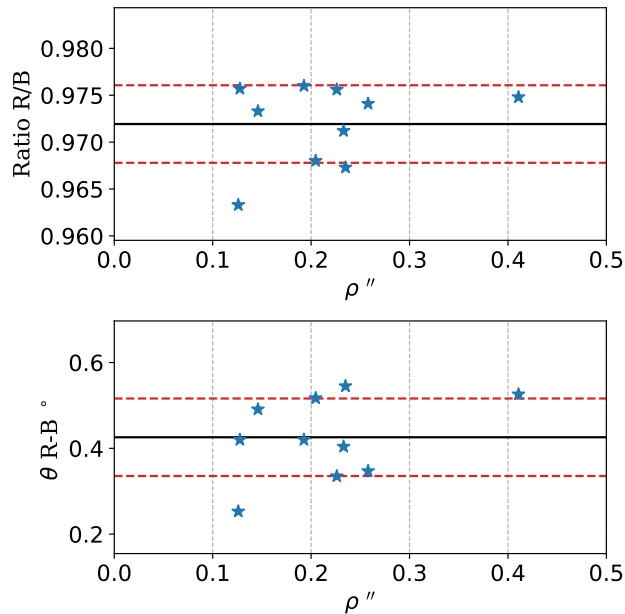


Figure 4. Comparison of measurements between the blue and red channels for 10 binary stars observed in the 2019A run. Top panel: ratio of red/blue separations; lower panel: difference in position angle. This comparison is used to correct the red channel to the same scale and orientation as that of the blue channel. The solid line shows the mean, while the dashed lines indicate the $\pm 1\sigma$ range.

The detectors of the blue and red channels have slightly different orientation and pixel scales. The nominal values of the pixel scales are 9.91 and 10.93 mas for the blue and red cameras, respectively, but for the data processing we used a common pixel scale of 9.91 mas for both channels (see the parameter file in Section 3.2). The code `redblue.pro` selects from `obsres` binaries with ρ between $0''.05$ and $1''.2$ and $\Delta m_b < 5.5$ mag, measured in both channels. In the 2019A run there are ten such pairs. Taking the blue channel as a reference, the ratio of scales is plotted in Figure 4. The mean ρ ratio red/blue is 0.9719 (with an rms over the ten frames of 0.0044), not the 1.1029 ratio inferred from the nominal pixel scales. The mean difference in the position angle (θ hereafter), separation-weighted, is $0^\circ 439$ with an rms scatter of $0^\circ 095$. The procedure `redcorrect` in `redblue.pro` corrects the data in the red channel to match the blue one. After this correction is applied, the pipeline’s measurement errors roughly match the channel’s difference if an “instrumental” error offset of 0.4 mas is added in quadrature. This agreement between the channels is similar to the one found for NESSI, after correcting the inter-channel systematics (Tokovinin et al. 2019). The typical number of red and blue pairs in all our observing runs varied between 7 and 17, and the precision of the scale ratio was between 0.12% for the best correction, up to 0.67% for the worst correction, while the θ uncertainty correction remained below $0''.5$ for all runs.

3.4.2. Absolute Calibration

For the purpose of absolute pixel scale and sky orientation calibration, binaries with ρ between $0''.5$ and $1''.2$ and moderate Δm have been selected as “astrometric calibrators”. Their motion is typically slow and it can be accurately modeled if good modern data are available. The current standard Zorro calibration plan does not contain such binaries, therefore in each observing run we have included them in our target list. These calibrators have been inherited from the SOAR program. We note that the accuracy of the models has nothing to do with the accuracy of their corresponding orbits that may remain poorly constrained for some time. The SOAR calibrator models have been updated in Tokovinin et al. (2022) and references, as a whole, to the relative positions measured by Gaia DR3. If, in the future, more accurate models of the calibrators become available, the observations can be corrected a-posteriori.

In addition to our astrometric calibrators, the 2019A data also includes several binaries with well-known orbits (including two of grade 1), probably added as part of the Zorro standard calibration plan. These latter binaries are mostly tight, $< 0''.2$, and the accuracy of their orbits is always worse than the intrinsic data accuracy (additionally, observations of the two grade-1 binaries at SOAR indicate that both orbits require minor corrections). Moreover, the accuracy (weight) of calibration in scale and orientation is proportional to the binary ρ , so binaries with larger ρ should be preferred. Note also that relying on orbits or data from smaller telescopes is a poor calibration strategy.

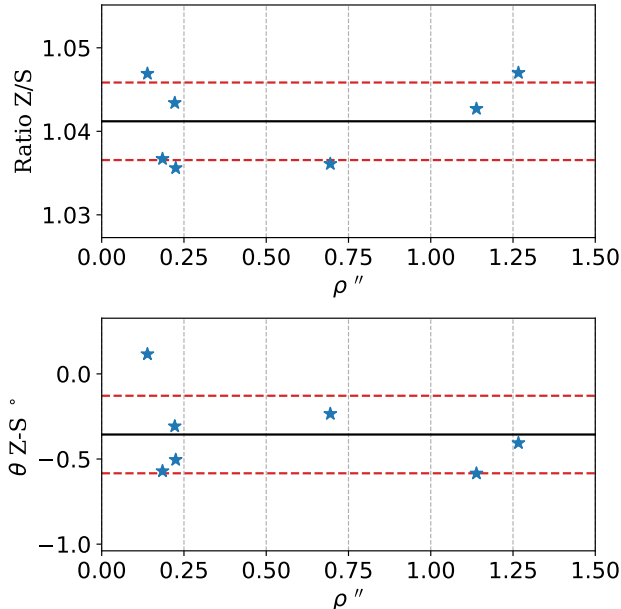


Figure 5. Calibration of Zorro astrometry relative to SOAR. The top panel shows the scale ratio, while the lower panel shows the difference in θ for the calibration binaries included in the 2019A run. The solid line shows the mean, while the dashed lines indicate the $\pm 1\sigma$ range.

Lacking "perfect" absolute calibrators, we can only compare data from Zorro with those from SOAR. Excluding triples, there are seven systems in common observed at SOAR in 2019A and before. These include our own astrometric calibrators and the tighter calibration binaries provided by the observatory mentioned in the previous paragraph. We first interpolated the SOAR positions linearly to the epoch of the Zorro observations and then compared with Zorro (red and blue channels of Zorro are now in good agreement and are averaged, see previous sub-section). The plots in Figure 5 show the comparison between the Zorro and SOAR measurements. The mean ρ ratio Z/S is 1.041 (rms 0.005) and the separation-weighted difference in θ is Z-S = $-0''.42$ (rms $0''.25$). These corrections were introduced into `obsres` manually (see the parameter file in Section 3.2). The pixel scale of the blue and red Zorro channels resulting from this calibration for the 2019A dataset turned out to be 9.520 and 9.252 mas, respectively.

The same procedures outlined above were applied to all successive observing runs for which we had always at least two of these astrometric calibrators. The uncertainty of the calibration varied between 0.02% and 0.50% in scale ratio, while the θ uncertainty correction remained below $0''.25$.

Table 2. Resolved systems.

WDS	DD	HIP	Epoch +2000.0 yr	Filt	Ncub	θ	$\rho \times \sigma_\theta$	ρ	σ_ρ	Δm	Code	$\Delta \theta$	$\Delta \rho$	Ref	Comments
						''	mas	''	mas	mag		''	''		
01011+1622	DSG 9	4754	20.8246	832	5	35.9	10.3	1.3461	10.5	7.5					[Fe/H] = -1.72, large proper-motion.
01059-2529	HD 6516	5146	19.5439	832	3	158.1	5.0	0.1821	4.6	5.3					
01205-1957	TOK 203	6273	21.7198	562	2	127.0	2.0	0.2707	1.7	6.1		17.7	0.057	Tok2019c	
			21.7198	832	2	127.2	0.1	0.2726	0.1	3.7	q	18.0	0.059	Tok2019c	
01262-6751	DON 17	6703	20.8246	562	5	291.0	0.2	1.4060	0.2	1.5	q	0.0	-0.008	Izm2019	Exclude, measurements, corrupted
			20.8246	832	5	291.1	0.1	1.4087	0.3	1.2	q	0.1	-0.005	Izm2019	Outside/edge FOV! Corrupted ACF.
			21.7200	562	2	248.0	0.5	1.1937	0.1	1.8	q	-43.2	-0.231	Izm2019	
			21.7200	832	2	249.5	0.2	1.2637	0.0	1.3	q	-41.7	-0.161	Izm2019	
			22.7632	562	2	246.8	0.1	1.1866	0.1	1.7		-44.7	-0.251	Izm2019	
			22.7632	832	2	248.4	0.3	1.2508	0.1	1.3		-43.0	-0.187	Izm2019	
			22.8506	562	2	247.1	0.6	1.1877	0.6	1.4		-44.4	-0.251	Izm2019	
			22.8506	832	2	249.0	1.0	1.2580	1.0	1.2	q	-42.5	-0.181	Izm2019	
01412-6741	HD 10607Aa,Ab	7869	19.5439	832	5	192.3	0.2	0.0256	0.2	0.7					[Fe/H] = -1.1, large proper-motion.
			20.8982	832	5	188.4	0.3	0.0347	0.2	0.9					
01559+0151	STF 186	8998	20.9065	562	5	255.9	0.0	0.6163	0.1	0.3	q	180.2	-0.002	Jte2018	Large θ diff, but firm q on SAA images.
			20.9065	832	5	255.8	0.0	0.6179	0.1	0.2	q	180.1	-0.001	Jte2018	Large θ diff, but firm q on SAA images.
			20.9121	562	5	255.6	0.1	0.6177	0.2	0.5	q	179.9	-0.001	Jte2018	Large θ diff, but firm q on SAA images.
			20.9121	832	5	255.6	0.1	0.6170	0.3	0.3	q	179.9	-0.002	Jte2018	Large θ diff, but firm q on SAA images.
			23.0200	562	2	258.2	0.0	0.5688	0.1	0.4	q	179.8	-0.004	Jte2018	Large θ diff, but firm q on SAA images.
			23.0200	832	2	258.4	0.0	0.5754	0.0	0.2	q	180.0	0.003	Jte2018	Large θ diff, but firm q on SAA images.
02128-0224	TOK 39Aa,Ab	10305	20.8247	562	1	125.9	0.0	0.0217	0.0	0.3		-38.6	0.005	SOAR2019	Part of a triple system, B component at ~ 17 arcsec.
			20.8247	832	1	124.8	0.0	0.0213	0.0	0.4		-39.7	0.004	SOAR2019	Tok 39Aa,Ab is an SB2 with $P = 95$ days.
03124-4425	JC 8AB	14913	20.8984	562	5	120.8	0.0	0.1897	0.0	0.6	q	-0.3	-0.000	SOAR2021	
			20.8984	832	5	120.9	0.0	0.1896	0.1	0.6	q	-0.3	-0.000	SOAR2021	
			20.9066	562	5	120.9	0.0	0.1888	0.0	0.7	q	-0.1	-0.000	SOAR2021	
			20.9066	832	5	120.9	0.0	0.1892	0.0	0.6	q	-0.1	-0.000	SOAR2021	
			20.9121	562	5	120.6	0.0	0.1884	0.0	0.6	q	-0.3	-0.000	SOAR2021	
			20.9121	832	5	120.7	0.0	0.1883	0.0	0.6	q	-0.2	-0.001	SOAR2021	
			21.7202	562	2	99.2	0.0	0.1137	0.0	0.7	q	-0.2	0.001	SOAR2021	
			21.7202	832	2	99.4	0.0	0.1137	0.0	0.6	q	-0.0	0.001	SOAR2021	
			22.7633	562	2	288.9	0.1	0.0589	0.0	0.7		4.2	-0.002	SOAR2021	
			22.7633	832	2	288.9	0.0	0.0590	0.0	0.6		4.2	-0.002	SOAR2021	
			22.8507	562	2	276.0	0.0	0.0675	0.0	0.6	q	3.1	-0.002	SOAR2021	
			22.8507	832	2	276.0	0.0	0.0676	0.0	0.6	q	3.1	-0.002	SOAR2021	
04059+1530	HD 25788	19120	20.0276	832	5	277.4	1.9	0.2661	1.9	5.6					[Fe/H] = -0.86.
04584-0344	HDS 644	23116	20.0223	562	2	174.9	0.2	0.6790	0.3	3.8	q	0.1	-0.001	Tok2019d	
			20.0223	832	2	174.8	0.1	0.6803	0.1	2.8	q	-0.0	0.000	Tok2019d	

Table 2 continued on next page

Table 2 (continued)

WDS	DD	HIP	Epoch +2000.0_yr	Filt	Ncub	θ o	$\rho \times \sigma_\theta$ mas	ρ "	σ_ρ mas	Δm mag	Code	$\Delta\theta$ o	$\Delta\rho$ "	Ref	Comments
05019-7638	RST 2368	23413	21.0354	562	2	176.7	0.2	0.6874	0.2	3.4	q	0.0	-0.002	Tok2019d	
			21.0354	832	2	176.7	0.2	0.6904	0.0	2.7	q	0.1	0.001	Tok2019d	
			21.9718	562	2	178.4	0.2	0.6968	0.3	3.8	q	0.1	-0.001	Tok2019d	
			21.9718	832	2	178.4	0.1	0.6974	0.1	2.7	q	0.0	-0.000	Tok2019d	
			21.1417	562	2	155.5	0.6	0.8294	0.4	2.7					
			21.1417	832	2	155.8	0.1	0.8257	0.1	2.2	q				
			22.8510	562	2	156.6	0.4	0.8337	0.3	2.5	q				
			22.8510	832	2	156.6	0.2	0.8327	0.1	2.1	q				
			23.1704	562	2	156.9	0.2	0.8362	0.2	2.6	q				
			23.1704	832	2	156.7	0.2	0.8377	0.5	2.3	q				
05514-6402	HD 39963	27660	21.7205	832	1	322.8	0.1	0.1002	0.1	3.4					Was PSF star.
			23.0205	562	1	327.7	0.1	0.0973	0.1	2.6					
			23.0205	832	1	327.1	0.1	0.1009	0.1	2.9	q				
05598-4814	HDS 814	28393	22.2041	562	2	148.6	0.3	0.2286	0.3	3.8		-0.0	0.002	Tok2018e	
			22.2041	832	2	148.4	0.1	0.2278	0.1	2.2	q	-0.2	0.001	Tok2018e	
			22.7635	562	2	147.4	0.3	0.2217	0.4	3.7	q	0.0	0.000	Tok2018e	
			22.7635	832	2	147.3	0.0	0.2211	0.0	2.2	q	-0.1	-0.001	Tok2018e	
06298-5014	R 65AB	30953	20.0171	562	2	239.7	0.0	0.1713	0.1	0.2		27.9	-0.241	Dec2014d	
			20.0171	832	2	239.7	0.0	0.1715	0.0	0.2		27.9	-0.241	Dec2014d	
			20.0198	562	2	239.5	0.0	0.1710	0.0	0.1		27.8	-0.241	Dec2014d	
			20.0198	832	2	239.6	0.0	0.1712	0.0	0.1		27.8	-0.241	Dec2014d	
			21.0355	562	2	218.0	0.0	0.0677	0.0	0.1		1.1	-0.353	Dec2014d	
			21.0355	832	2	218.0	0.0	0.0679	0.0	0.1		1.1	-0.353	Dec2014d	
			21.1417	562	2	209.7	0.0	0.0523	0.0	0.0		-7.6	-0.369	Dec2014d	
			21.1417	832	2	209.8	0.0	0.0525	0.0	0.1		-7.6	-0.369	Dec2014d	
			22.2041	562	2	306.6	0.0	0.1183	0.0	0.1		84.2	-0.313	Dec2014d	Note large θ difference. Up-date orbit? See notes.
			22.2041	832	2	306.6	0.0	0.1178	0.0	0.1		84.2	-0.313	Dec2014d	
			22.7690	562	2	298.7	0.0	0.1674	0.0	0.1		73.6	-0.269	Dec2014d	
			22.7690	832	2	298.6	0.0	0.1681	0.0	0.1		73.6	-0.269	Dec2014d	
			23.0205	562	2	296.8	0.0	0.1867	0.0	0.1		70.6	-0.253	Dec2014d	
			23.0205	832	2	296.7	0.0	0.1879	0.0	0.1		70.5	-0.251	Dec2014d	
			23.1733	562	2	296.1	0.0	0.1997	0.1	0.2		69.2	-0.241	Dec2014d	
			23.1733	832	2	296.0	0.1	0.2007	0.1	0.1		69.2	-0.240	Dec2014d	
07043-5645	DSG 11	34105	20.1946	562	5	283.3	0.1	0.0314	0.1	1.1					
			20.1946	832	5	283.0	0.2	0.0321	0.3	1.0					
			20.8988	562	5	342.6	0.3	0.0242	0.4	1.1					
			20.8988	832	5	341.7	0.4	0.0244	0.9	1.0					
			21.0355	562	2	329.5	0.0	0.0312	0.0	1.0					
			21.0355	832	2	329.7	0.4	0.0317	0.2	0.9	q				
			22.2013	562	2	300.9	0.1	0.0674	0.0	1.1	q				
			22.2013	832	2	301.0	0.0	0.0669	0.0	1.0	q				
			23.0205	562	2	287.6	0.0	0.0529	0.0	1.0	q				
			23.0205	832	2	287.3	0.1	0.0537	0.1	1.0	q				
07284-3749	HD 59466	36304	20.8989	562	2	295.2	0.8	0.0497	1.1	2.5					Was PSF star. [Fe/H] = -1.31.
			20.8989	832	2	293.6	0.3	0.0515	0.6	2.2					
			21.0355	562	1	295.7	0.0	0.0482	0.0	2.6					
			21.0355	832	1	298.4	0.0	0.0549	0.0	2.4					

Table 2 continued on next page

Table 2 (continued)

WDS	DD	HIP	Epoch +2000.0_yr	Filt	Ncub	θ o	$\rho \times \sigma_\theta$ mas	ρ "	σ_ρ mas	Δm mag	Code	$\Delta\theta$ o	$\Delta\rho$ "	Ref	Comments			
07292+1246	TOK 787	36371	21.9720	562	1	330.0	0.0	0.0430	0.0	2.2								
			21.9720	832	1	328.3	0.0	0.0437	0.0	2.2								
			20.9071	562	2	58.0	0.4	0.3666	0.4	3.8								
			20.9071	832	2	58.3	0.2	0.3659	0.1	3.2	q							
			21.0354	562	1	57.9	0.2	0.3675	0.2	3.8	q							
			21.0354	832	1	58.0	0.1	0.3657	0.1	3.2	q							
			22.3737	562	1	56.0	1.4	0.3689	1.5	3.8								
			22.3737	832	1	56.7	0.2	0.3706	0.2	3.3								
			23.0206	562	1	55.4	0.3	0.3685	0.3	3.8	q							
			23.0206	832	1	56.1	0.1	0.3709	0.1	3.3	q							
07293+1227	LSC 45	36387	20.0281	562	5	315.8	0.5	0.0434	1.2	1.4		1.0	0.001	SOAR2021				
			20.0281	832	5	315.9	0.3	0.0451	0.4	1.5			1.0	0.002	SOAR2021			
			20.1973	562	5	319.7	0.4	0.0445	1.1	1.4			1.0	0.002	SOAR2021			
			20.1973	832	5	319.1	0.1	0.0438	0.4	1.4			0.4	0.002	SOAR2021			
			20.9070	832	5	335.6	0.2	0.0424	0.8	1.5			-0.4	0.003	SOAR2021			
			21.0354	562	2	335.2	0.5	0.0382	0.1	1.1			-4.2	-0.000	SOAR2021			
			21.0354	832	2	338.0	0.3	0.0421	2.3	1.6			-1.5	0.004	SOAR2021			
			20.1973	562	5	331.6	0.6	0.7885	0.7	4.8								
			20.1973	832	5	331.4	0.1	0.7862	0.1	3.3	q							
			20.9070	832	5	330.9	0.7	0.7780	0.8	4.9								
07546-0125	YSC 198Aa,Ab	38625	20.9070	832	5	330.7	0.2	0.7765	0.2	3.4								
			21.0355	562	2	331.1	0.4	0.7738	0.4	4.5								
			21.0355	832	2	330.7	0.2	0.7676	0.1	3.4	q							
			21.9720	562	2	331.1	0.9	0.7382	1.1	4.8								
			21.9720	832	2	331.1	0.1	0.7376	0.1	3.5	q							
			22.3737	562	2	332.0	2.1	0.7467	2.1	5.1								
			22.3737	832	2	332.4	0.1	0.7418	0.3	3.4	q							
			23.0096	562	2	332.4	0.4	0.6807	0.4	4.4	q							
			23.0096	832	2	332.1	0.1	0.6594	0.3	3.3	q							
			20.2002	562	2	114.8	0.1	0.8921	0.0	0.9	q		-0.1	0.001	Mut2010b			
09285+0903	STF 1356	46454	20.2002	832	2	114.8	0.1	0.8931	0.1	0.9	q	-0.2	0.003	Mut2010b				
			21.1559	562	3	115.3	0.1	0.9043	0.1	1.2	q	-0.5	0.001	Mut2010b				
			21.1559	832	3	115.5	0.0	0.9027	0.2	1.1	q	-0.4	-0.000	Mut2010b				
			21.1586	562	2	115.4	0.1	0.9041	0.1	1.2	q	-0.4	0.001	Mut2010b				
			21.1586	832	2	115.5	0.1	0.9048	0.0	1.1	q	-0.4	0.002	Mut2010b				
			23.0098	562	2	117.4	0.0	0.9206	0.1	0.9	q	-0.1	-0.006	Mut2010b				
			23.0098	832	2	117.4	0.0	0.9275	0.1	1.0	q	-0.1	0.001	Mut2010b				
			20.0173	562	5	229.3	0.2	0.0245	0.4	0.0								
			20.0173	832	5	233.0	0.2	0.0258	0.3	0.3								
			09511-2829	HD 85432	48333	20.2002	562	5	192.2	1.3	0.0197	0.5	0.5					
20.2002	832	5				192.3	1.3	0.0195	0.5	0.6								
21.0355	562	2				196.7	0.0	0.0299	0.1	0.3								
21.0355	832	2				196.4	0.1	0.0301	0.1	0.3								
21.9722	562	2				254.9	0.1	0.0291	0.1	0.2								
21.9722	832	2				255.9	0.0	0.0291	0.1	0.3								
22.1989	562	2				215.7	0.1	0.0233	0.0	0.3								
22.1989	832	2				216.6	0.0	0.0236	0.2	0.4								
23.0098	562	2				215.7	0.1	0.0295	0.2	0.4								
23.0098	832	2				215.7	0.1	0.0295	0.2	0.4								

Table 2 continued on next page

Table 2 (continued)

WDS	DD	HIP	Epoch +2000.0_yr	Filt	Ncub	θ o	$\rho \times \sigma_\theta$ mas	ρ "	σ_ρ mas	Δm mag	Code	$\Delta\theta$ o	$\Delta\rho$ "	Ref	Comments
10375-0932	RST 3708	-----	23.0098	832	2	214.1	0.0	0.0295	0.2	0.2	q				
			23.1682	562	2	193.5	0.2	0.0303	0.1	0.5	q				
			23.1682	832	2	193.1	0.0	0.0305	0.1	0.4	q				
			20.1948	562	2	2.6	0.0	0.5435	0.1	1.6	q	1.8	-0.000	Tok2015c	This is HD 92015.
			20.1948	832	2	2.6	0.0	0.5419	0.1	1.4	q	1.7	-0.002	Tok2015c	
			21.1560	562	2	3.0	0.1	0.5466	0.1	1.6	q	1.5	-0.002	Tok2015c	
			21.1560	832	2	2.8	0.0	0.5448	0.0	1.3	q	1.3	-0.004	Tok2015c	
			21.1587	562	2	3.0	0.1	0.5468	0.4	1.6	q	1.5	-0.002	Tok2015c	
			21.1587	832	2	2.9	0.2	0.5458	0.5	1.3	q	1.4	-0.003	Tok2015c	
			22.2018	562	2	4.1	0.1	0.5543	0.1	1.6	q	1.9	0.001	Tok2015c	
			22.2018	832	2	4.1	0.0	0.5473	0.1	1.4	q	1.9	-0.006	Tok2015c	
			23.1683	562	2	5.2	0.1	0.5564	0.3	1.7	q	2.3	-0.001	Tok2015c	
			23.1683	832	2	5.5	0.1	0.5487	0.3	1.4	q	2.6	-0.009	Tok2015c	
11221-2447	I 507AB	55505	22.2018	562	2	8.1	0.0	0.3037	0.0	0.6	q	0.2	0.003	Tok2018e	
			22.2018	832	2	8.2	0.3	0.3028	0.2	0.4	q	0.2	0.002	Tok2018e	
			23.0099	562	2	8.7	0.1	0.2663	0.0	0.7	q	0.1	0.003	Tok2018e	
			23.0099	832	2	9.1	0.1	0.2672	0.1	0.4	q	0.5	0.004	Tok2018e	
11328-4026	HD 100378	56319	20.0366	562	2	308.5	0.2	0.4065	0.4	4.8	q				Was PSF star.
			20.0366	832	2	308.5	0.6	0.4047	0.6	6.0	q				
			20.1923	562	2	308.8	0.3	0.4067	0.3	4.7	q				
			20.1923	832	2	308.9	0.7	0.4108	0.5	5.7	q				
11464-2758	DSG 13AC	57421	19.3785	832	1	151.5	0.0	0.4690	0.0	5.7	q				
			21.0359	832	2	149.8	0.0	0.4702	0.1	5.6	q				
			22.2046	832	2	149.0	0.9	0.4681	1.0	5.5	q				
			23.1711	832	2	148.6	0.7	0.4683	0.0	5.9	q				
11464-2758	LSC 49AB	57421	19.3785	562	2	63.6	0.2	0.1959	1.0	2.9	q				
			19.3785	832	1	63.8	0.1	0.1956	0.1	2.6	q				
			19.3785	832	1	63.6	0.0	0.1943	0.0	2.7	q				
			19.3815	832	1	63.8	0.1	0.1960	0.1	2.7	q				
			21.0359	562	2	54.1	0.1	0.1865	0.2	3.2	q				
			21.0359	832	2	54.1	0.1	0.1866	0.2	2.8	q				
			22.2046	562	2	46.6	0.1	0.1795	0.1	2.9	q				
			22.2046	832	2	46.9	0.3	0.1795	0.1	2.7	q				
			23.1711	562	2	40.2	0.0	0.1729	0.2	2.9	q				
			23.1711	832	2	40.5	0.2	0.1736	0.3	2.7	q				
11520-4357	SBE 137	57860	22.2046	832	2	313.8	0.1	1.6284	0.1	0.6	q				Outer pair of a triple system.
			23.0209	832	2	313.4	0.3	1.6271	0.2	0.7	q				Aa,Ab is an SB2 at ~27 mas, and 892 day period.
12018-3439	I 215AB	58669	23.1713	832	2	313.4	0.1	1.6280	0.2	0.8	q				Aa,Ab unresolved on the Zorro data.
			19.3815	562	5	324.7	0.1	0.2283	0.4	1.0	q	1.3	0.003	Tok2015a	AaAb is an SB2 with ~150 day period.
			19.3815	832	5	324.6	0.1	0.2229	0.1	0.9	q	1.2	0.003	Tok2015a	AaAb unresolved on Zorro data.
			20.1921	562	5	317.0	0.1	0.2441	0.1	0.8	q	1.2	0.003	Tok2015a	
			20.1921	832	5	317.0	0.0	0.2445	0.1	0.8	q	1.2	0.004	Tok2015a	
			21.0359	562	2	310.7	0.1	0.2697	0.0	0.9	q	1.5	0.005	Tok2015a	
			21.0359	832	2	310.7	0.1	0.2700	0.1	0.7	q	1.5	0.005	Tok2015a	
			22.2046	562	2	303.5	0.0	0.3073	0.0	0.9	q	1.5	0.006	Tok2015a	

Table 2 continued on next page

Table 2 (continued)

WDS	DD	HIP	Epoch +2000.0_yr	Filt	Ncub	θ o	$\rho \times \sigma_\theta$ mas	ρ "	σ_ρ mas	Δm mag	Code	$\Delta\theta$ o	$\Delta\rho$ "	Ref	Comments
12114-1647	S 634Aa,Ab	59426	22.2046	832	2	303.5	0.0	0.3065	0.0	0.8	q	1.5	0.006	Tok2015a	Uses binary fit.
			20.0367	562	5	272.4	0.6	0.0222	0.6	0.6					Uses trinary fit.
			20.0367	832	5	266.9	0.4	0.0239	0.5	0.8					Uses binary fit.
			23.5043	562	2	267.4	0.1	0.0238	0.0	0.8					Uses trinary fit.
			23.5043	832	2	263.9	0.0	0.0272	0.0	0.9					Uses trinary fit.
12114-1647	S 634Aa,Ac	59426	20.0367	832	5	215.6	1.6	0.3360	1.2	5.9					New sub-system.
			23.5043	832	2	246.5	0.1	0.2813	0.2	6.0					New sub-system.
12314-5659	RST 2802	-----	20.0367	562	5	50.4	0.1	1.2430	0.2	1.8	q				This is HD 108938.
			20.0367	832	5	50.3	0.1	1.2428	0.2	1.9	q				
			20.1924	562	5	50.4	0.2	1.2509	0.3	2.0	q				
			20.1924	832	5	50.4	0.2	1.2486	0.3	2.1	q				
			21.1589	562	2	50.1	0.1	1.2444	0.1	1.9	q				
			21.1589	832	2	49.8	0.2	1.2375	0.1	2.2	q				
			22.3739	562	2	50.6	0.1	1.2514	0.3	2.0	q				
			22.3739	832	2	50.7	0.1	1.2526	0.3	2.1	q				
12319-6330	DSG 15	61158	19.3815	562	3	47.4	0.2	0.1224	0.2	3.5					
			19.3815	832	3	47.3	0.2	0.1227	0.1	3.1	q				
			21.1588	562	2	45.1	0.3	0.1392	0.3	3.6					
			21.1588	832	2	45.0	0.1	0.1408	0.0	3.1	q				
			22.3712	562	2	44.3	0.1	0.1389	0.2	3.5					
			22.3712	832	2	44.1	0.0	0.1400	0.0	3.1	q				
			23.5044	832	2	43.4	0.1	0.1216	0.2	3.1	q				
12428-5557	KOU 15	62026	21.1589	562	1	210.3	0.1	0.1198	0.1	2.6		-0.5	-0.001	SOAR2021	Tertiary is at ~ 14 arcsec, UC 2437AB.
			21.1589	832	1	210.3	0.0	0.1199	0.0	2.1	q	-0.6	-0.001	SOAR2021	
			22.3739	562	1	200.7	0.1	0.1410	0.1	2.7		-0.2	0.002	SOAR2021	
			22.3739	832	1	200.8	0.0	0.1413	0.0	2.1	q	-0.0	0.002	SOAR2021	
			23.4008	562	2	194.2	0.1	0.1571	0.2	2.7	q	0.2	0.007	SOAR2021	
			23.4008	832	2	194.3	0.0	0.1575	0.0	2.1	q	0.3	0.007	SOAR2021	
12565-2635	YSC 216Aa,Ab	63162	19.3816	562	5	39.2	0.1	0.1402	0.1	0.9					
			19.3816	832	5	39.2	0.1	0.1402	0.1	1.0	q				
			21.1588	562	3	50.9	0.0	0.1368	0.0	0.9	q				
			21.1588	832	3	50.8	0.1	0.1365	0.0	1.0	q				
			22.2046	562	2	58.8	0.1	0.1360	0.0	0.9	q				
			22.2046	832	2	58.8	0.1	0.1360	0.1	1.0	q				
12592-6256	TOK 722Aa,Ab	63377	19.5319	832	3	63.1	0.2	0.0293	0.2	0.1	q				
			21.1589	832	2	50.8	0.7	0.0240	0.1	0.2	q				
			22.3739	832	2	63.6	0.1	0.0177	0.1	1.6					Marginal resolution—see notes.
12592-6256	TOK 722Aa,Ac	63377	23.4006	832	2	52.1	0.2	0.0285	0.2	0.1					
			19.5319	832	3	54.9	0.2	0.4588	0.2	2.0					
			21.1589	832	2	53.9	0.2	0.4649	0.8	1.8					
			22.3739	832	2	54.4	0.1	0.4678	0.0	2.1	q				
			23.4006	832	2	54.6	0.2	0.4861	0.2	2.0					
12592-6256	TOK 722A*Ac	63377	19.5319	562	3	54.6	0.4	0.4411	1.4	2.7	q				In the blue filter. Aa,Ab is not resolved. A* means photocenter.
			21.1589	562	2	54.3	0.6	0.4538	0.3	2.5	q				

Table 2 continued on next page

Table 2 (continued)

WDS	DD	HIP	Epoch +2000.0_yr	Filt	Ncub	θ o	$\rho \times \sigma_\theta$ mas	ρ "	σ_ρ mas	Δm mag	Code	$\Delta\theta$ o	$\Delta\rho$ "	Ref	Comments
13495-2621	TOK 405	67458	22.3739 23.4006	562 562	2 6	54.7 54.3	0.9 1.1	0.4632 0.4721	0.5 1.1	2.7 2.8					
			19.3871 20.1926 20.1926 21.1589 21.1589 22.2047 22.2047	832 562 562 562 832 562 832	7 5 5 2 2 2 2	192.0 191.4 191.6 190.3 190.4 189.8 189.9	1.4 1.0 1.3 1.3 0.2 1.2 0.2	0.6917 0.6879 0.6844 0.6766 0.6757 0.6630 0.6616	1.4 1.0 0.2 1.1 0.3 1.3 0.2	5.9 5.8 4.4 5.9 4.5 5.9 4.4	q q q q q q q				
13535-3540	HWE 28AB	67819	20.1925 20.1952 20.1952 20.1979 20.1979 20.2007 21.5468 22.2047 22.2047 22.3713 22.3713 23.1713 23.1713 23.4008 23.4008 23.4990 23.4990	832 562 832 562 832 562 832 562 832 562 832 562 832 562 832 562 832	2 2 2 2 2 2 2 2 2 2 2 2 2 2 2 2 2	316.6 316.6 316.8 316.8 316.7 316.7 316.7 317.2 317.5 317.5 317.5 317.5 317.9 317.7 318.0 317.8 317.9 317.9	0.1 0.0 0.0 0.1 0.2 0.0 0.0 0.0 0.0 0.2 0.1 0.1 0.1 0.1 0.1 0.1 0.0 0.1	1.0093 1.0093 1.0109 1.0109 1.0079 1.0110 1.0111 1.0090 1.0096 1.0072 1.0026 1.0010 1.0059 1.0051 1.0043 0.9934 1.0063 1.0131	0.1 0.3 0.0 0.2 0.1 0.0 0.0 0.3 0.6 0.1 0.0 0.1 0.2 0.4 0.3 0.7 0.4 0.2 0.0	0.5 0.4 0.2 0.2 0.4 0.3 0.2 0.2 0.5 0.5 0.6 0.4 0.3 0.9 1.1 0.8	q q q q q q q q q q q q q q q q q q	Izm2019 Izm2019 Izm2019 Izm2019 Izm2019 Izm2019 Izm2019 Izm2019 Izm2019 Izm2019 Izm2019 Izm2019 Izm2019 Izm2019 Izm2019 Izm2019 Izm2019 Izm2019			
14025-2440	B 263AB	68587	19.3870 19.3870 21.1591 21.1591 22.2047 22.2047	562 832 562 832 562 832	7 7 2 2 2 2	142.1 142.2 152.7 152.8 158.4 158.4	0.1 0.1 0.0 0.0 0.1 0.1	0.2251 0.2238 0.2536 0.2537 0.2718 0.2707	0.1 0.1 0.0 0.0 0.0 0.0	2.1 1.9 2.1 1.9 2.1 1.9	q q q q q q	-1.7 -1.6 -3.5 -3.3 -4.0 -4.0	0.012 0.011 0.019 0.019 0.023 0.022	Tok2015c Tok2015c Tok2015c Tok2015c Tok2015c Tok2015c	
14509-1603	DSG 17Aa,Ab	72622	19.3872 19.3872 20.1927	562 832 832	3 3 5	173.2 174.3 181.6	0.1 0.0 **	0.0272 0.0268 0.0180	0.2 0.2 **	0.3 0.3 0.0					dm=0 enforced.
15092+1431	HIP 74165	74165	21.1592 21.1592 23.1688	562 832 832	2 2 2	107.0 91.9 309.9	0.6 1.3 2.8	0.0162 0.0133 0.0231	0.9 1.7 2.3	0.0 0.2 1.5					proper - motion.
15317+0053	TOK 48	76031	19.3817 19.3817 21.1592 21.1592 22.1995	562 832 562 832 562	6 6 2 2 5	359.9 359.5 339.8 340.9 333.6	3.0 0.5 1.7 0.3 2.7	0.2170 0.2136 0.2443 0.2475 0.2665	2.2 0.5 1.8 0.2 3.7	5.2 4.1 5.7 4.0 5.7					Aa not resolved (into Aa1,a2), Aa* is the photocenter.
15362-0623	TOK 301Aa*,Ab	76400	19.3817 19.3817 21.1592 21.1592 22.1995	562 832 562 832 562	6 6 2 2 5	359.9 359.5 339.8 340.9 333.6	3.0 0.5 1.7 0.3 2.7	0.2170 0.2136 0.2443 0.2475 0.2665	2.2 0.5 1.8 0.2 3.7	5.2 4.1 5.7 4.0 5.7					

Table 2 continued on next page

Table 2 (continued)

WDS	DD	HIP	Epoch +2000.0_yr	Filt	Ncub	θ o	$\rho \times \sigma_\theta$ mas	ρ "	σ_ρ mas	Δm mag	Code	$\Delta\theta$ o	$\Delta\rho$ "	Ref	Comments
15362-0623	TOK 301Aa1,a2	76400	19.3817	832	6	290.02	**	0.0123	**	0.0					dm=0 enforced. Triple fit, uncertain.
15365+1607	DSG 18Aa,Ab	76424	19.3873	832	3	322.0	1.7	1.0119	1.7	6.6					dm=0 enforced. Triple fit, uncertain.
16035-5747	SEE 258AB	78662	19.3817	562	3	18.6	0.0	0.1847	0.0	0.4	q	5.0	-0.017	Tok2015c	dm=0 enforced. Triple fit, uncertain.
16044-1122	STF 1998AB	78727	19.3873	562	1	10.8	0.0	1.1412	0.0	1.0		0.2	0.018	Dec2009g	dm=0 enforced. Triple fit, uncertain.
16142-5047	TOK 409	79576	19.3817	832	4	65.9	1.7	0.4244	2.3	5.8					dm=0 enforced. Triple fit, uncertain.
16329+0315	DSG 7Aab,c	81023	19.4640	832	4	246.9	1.2	0.2528	0.3	4.3	q	216.3	0.244	Hor2019	dm=0 enforced. Triple fit, uncertain.
16391-2759	HD 149960	81521	20.1956	562	5	292.3	3.6	0.4556	2.0	6.1					dm=0 enforced. Triple fit, uncertain.
16478+0515	HD 151525	82216	19.4640	832	1	207.4	0.7	0.7224	0.7	5.9	q				dm=0 enforced. Triple fit, uncertain.
16546-0609	DSG 1AB	82730	19.3846	562	3	268.4	0.3	0.3939	0.3	4.6	q?				dm=0 enforced. Triple fit, uncertain.
17111-2039	TOK 791AB	84056	19.3846	832	3	268.5	1.7	0.3947	2.1	4.9	q?				dm=0 enforced. Triple fit, uncertain.
17127-2136	OCC 1096	84198	19.3818	562	6	171.6	0.5	0.0182	0.2	0.0					dm=0 enforced. Triple fit, uncertain.
17157-0949	A 2592ABa	84430	22.2050	832	2	65.9	0.3	0.2284	0.3	1.9	q	-6.7	0.004	Tok2015c	dm=0 enforced. Triple fit, uncertain.
16391-2759	HD 149960	81521	20.1956	562	5	292.3	3.6	0.4556	2.0	6.1					dm=0 enforced. Triple fit, uncertain.
16329+0315	DSG 7Aab,c	81023	19.4640	832	4	246.9	1.2	0.2528	0.3	4.3	q	216.3	0.244	Hor2019	dm=0 enforced. Triple fit, uncertain.
16391-2759	HD 149960	81521	20.1956	562	5	292.3	3.6	0.4556	2.0	6.1					dm=0 enforced. Triple fit, uncertain.
16478+0515	HD 151525	82216	19.4640	832	1	207.4	0.7	0.7224	0.7	5.9	q				dm=0 enforced. Triple fit, uncertain.
16546-0609	DSG 1AB	82730	19.3846	562	3	268.4	0.3	0.3939	0.3	4.6	q?				dm=0 enforced. Triple fit, uncertain.
17111-2039	TOK 791AB	84056	19.3846	832	3	268.5	1.7	0.3947	2.1	4.9	q?				dm=0 enforced. Triple fit, uncertain.
17127-2136	OCC 1096	84198	19.3818	562	6	171.6	0.5	0.0182	0.2	0.0					dm=0 enforced. Triple fit, uncertain.
17157-0949	A 2592ABa	84430	22.2050	832	2	65.9	0.3	0.2284	0.3	1.9	q	-6.7	0.004	Tok2015c	dm=0 enforced. Triple fit, uncertain.

Table 2 continued on next page

Table 2 (continued)

WDS	DD	HIP	Epoch +2000.0_yr	Filt	Ncub	θ	$\rho \times \sigma_\theta$	ρ	σ_ρ	Δm	Code	$\Delta\theta$	$\Delta\rho$	Ref	Comments
						o	mas	"	mas	mag		o	"		
17157-0949	A 2592ABb	84430	23.5020 22.2050 23.5020	832 832 832	2 2 2	53.5 66.1 61.8	0.0 0.2 0.1	0.2367 0.1915 0.2094	0.0 0.2 0.1	1.6 2.3 2.0	-13.8 -6.5 -5.5	0.001 -0.033 -0.027	Tok2015c Tok2015c Tok2015c		
17157-0949	A 2592AB*	84430	22.2050 23.5020	562 562	2 2	65.8 54.0	0.0 0.2	0.2157 0.2345	0.5 0.1	0.8 1.2	q q	-6.8 -13.3	-0.008 -0.002	Tok2015c Tok2015c	In the blue filter BaBb not resolved, B* is the photocenter.
18099+0307	YSC 132Aa,Ab	89000	19.3765 19.3765 19.3820 21.5500 22.2025 22.2025 19.3765 19.3765 19.3820 19.3820 22.2024 22.2024	562 832 562 832 562 832 562 832 562 832 562 832	3 3 3 2 3 3 3 2 3 3 2 2	135.9 135.4 132.3 134.3 95.2 94.4	0.4 0.4 0.6 0.1 0.3 0.0	0.0213 0.0215 0.0213 0.0215 0.0206 0.0207	0.2 0.1 0.1 0.1 0.0 0.0	0.0 0.0 0.0 0.0 0.1 0.0	0.0 0.0 0.0 0.0 0.0 0.0	-3.0 -3.5 -4.2 -2.2 -1.1 -1.9	0.001 0.001 0.001 0.001 0.001 0.001	Mdz2017 Mdz2017 Mdz2017 Mdz2017 Mdz2017 Mdz2017	[Fe/H] = -0.20.
18191-3509	OL 18	89766	21.7139 21.7139 22.2023 22.2023 22.3719 22.3719 23.2645 23.2645 23.4011 23.4011 23.5051 23.5051	562 832 562 832 562 832 562 832 562 832 562 832	2 2 3 3 2 2 2 2 2 2 2 2	296.1 296.1 296.1 296.0 296.0 296.0 296.7 296.6 296.4 296.2 296.4 296.3	0.0 0.0 0.1 0.0 0.0 0.0 0.0 0.0 0.0 0.1 0.2 0.4	1.0706 1.0709 1.0852 1.0834 1.0846 1.0846 1.1008 1.1010 1.1036 1.1031 1.1047 1.1090	0.1 0.2 0.2 0.2 0.1 0.5 0.2 0.3 0.1 0.1 0.1 0.1	0.8 0.6 q q q q q q q q q q	0.2 0.2 0.1 0.1 0.0 0.6 0.5 0.2 0.0 0.2 0.1	-0.003 -0.003 0.002 0.001 -0.001 -0.001 -0.001 -0.001 -0.001 -0.002 -0.002 0.003	SOAR2021 SOAR2021 SOAR2021 SOAR2021 SOAR2021 SOAR2021 SOAR2021 SOAR2021 SOAR2021 SOAR2021 SOAR2021 SOAR2021		
18340-3301	OU 7	91014	19.3820 19.3820 19.3820 21.7139 21.7139 22.3721 22.3721	562 832 832 562 832 562 832	3 1 3 1 2 2 2	178.1 177.9 177.9 177.9 177.2 176.9 176.9	0.8 0.8 0.4 0.6 1.1 0.8 0.2	0.2475 0.2461 0.2478 0.2480 0.2455 0.2434 0.2430	0.6 0.8 1.1 0.4 1.0 0.4 0.2	5.4 5.6 5.0 4.9 5.5 5.4 5.0	q q q q q q q	5.4 5.6 5.0 4.9 5.5 5.4 5.0	0.7 0.8 1.1 0.4 1.0 1.0 0.2	SOAR2021 SOAR2021 SOAR2021 SOAR2021 SOAR2021 SOAR2021 SOAR2021	[Fe/H] = -1.06, large proper-motion.
19133-0036	YSC 159Aa,Ab	94449	21.7194 21.7194 22.3721 22.3721	562 832 562 832	2 2 2 2	281.1 281.1 281.0 280.9	0.7 0.1 0.4 0.1	0.5608 0.5600 0.5674 0.5682	0.7 0.3 0.4 0.1	3.7 3.1 3.8 3.1	q q q q	3.7 3.1 3.8 3.1	0.7 0.3 0.4 0.1	SOAR2021 SOAR2021 SOAR2021 SOAR2021	
20339-2710	HD 195719	101472	21.5476	832	2	162.3	0.2	0.0179	0.5	0.9	q	0.5	0.9		New tight companion, triple hierarchical system with CBL 178 at 53 arcsec (see WDS).
			21.7141 21.7141 22.3721	562 832 562	2 2 2	166.4 165.6 130.0	0.3 0.1 **	0.0193 0.0199 0.0059	0.2 0.1 **	0.7 0.5 0.0	q q q	0.2 0.1 **	0.7 0.5 0.0		dm=0.0 enforced.

Table 2 continued on next page

Table 2 (continued)

WDS	DD	HIP	Epoch +2000.0_yr	Filt	Ncub	θ	$\rho \times \sigma_\theta$	ρ	σ_ρ	Δm	Code	$\Delta\theta$	$\Delta\rho$	Ref	Comments
						o	mas	"	mas	mag		o	"		
20389+1115	CVN 17Aa,Ab	101966	22.3721	832	2	135.5	*,*	0.0069	*,*	0.0					dm=0.0 enforced.
			21.7141	562	2	35.9	2.8	0.5294	2.0	5.9	q	-3.4	-0.026	Cvn2011	
			21.7141	832	2	36.4	0.2	0.5151	0.2	4.6	q	-2.8	-0.040	Cvn2011	
			22.3748	562	2	34.1	3.1	0.5151	2.1	6.0	q	-3.4	-0.027	Cvn2011	
			22.3748	832	2	34.5	0.2	0.5182	0.2	4.6	q	-3.0	-0.024	Cvn2011	
			22.7682	832	2	32.6	0.3	0.5096	0.3	4.6	q	-3.7	-0.025	Cvn2011	
			23.4995	832	2	30.5	0.7	0.4980	0.3	4.8	q	-3.7	-0.023	Cvn2011	
21041+0300	WSI 6AB	103987	19.4642	562	3	333.5	0.2	0.1207	0.3	2.0		1.3	-0.002	MSN2022	Aa,Ab (DSG 6) with $a = 28$ mas, and $P=1$ yr unresolved at Zorro. $[\text{Fe}/\text{H}] = -1.07$.
22152-0535	A 2599	109874	19.6940	562	2	280.0	0.1	0.6949	0.1	2.3					
			19.6940	832	2	280.1	0.1	0.6968	0.1	3.1					
			19.7401	562	2	280.2	0.1	0.6962	0.1	2.2	q				
			19.7401	832	2	280.3	0.1	0.6954	0.1	3.1	q				
			19.7703	562	2	280.3	0.3	0.6919	0.1	2.4	q				
			19.7703	832	2	280.3	0.1	0.6941	0.1	3.2	q				
22451-0240	A 2696BC	112325	19.6940	562	2	71.5	0.1	0.6112	0.1	1.1		-3.3	-0.015	Hrt2014b	
			19.6940	832	2	71.5	0.0	0.6107	0.0	0.9		-3.2	-0.015	Hrt2014b	
			23.5028	562	2	69.0	0.2	0.6078	0.3	1.3	q	-3.6	-0.027	Hrt2014b	
			23.5028	832	2	69.6	0.0	0.6064	0.1	1.1	q	-3.1	-0.028	Hrt2014b	
23171-1349	BU 182AB	114962	19.7703	562	2	227.7	0.1	0.7386	0.0	0.4	q	0.0	-0.010	Mdz2017	$[\text{Fe}/\text{H}] = -1.46$, large proper-motion.
			19.7703	832	2	227.8	0.1	0.7375	0.0	0.3	q	0.1	-0.011	Mdz2017	
			20.9008	562	5	227.7	0.1	0.7338	0.1	0.4	q	-0.1	-0.009	Mdz2017	
			20.9008	832	5	227.6	0.0	0.7340	0.1	0.3	q	-0.1	-0.009	Mdz2017	
			20.9064	562	6	227.5	0.1	0.7337	0.2	0.4	q	-0.2	-0.009	Mdz2017	
			21.5507	832	2	227.0	0.0	0.7215	0.2	0.3	q	-0.8	-0.018	Mdz2017	
			21.7144	562	2	227.8	0.0	0.7297	0.0	0.4	q	0.0	-0.010	Mdz2017	
			21.7144	832	2	228.1	0.1	0.7299	0.2	0.4	q	0.3	-0.009	Mdz2017	

Since some of our astrometric calibrators were observed over several epochs, we can compare the results of our calibrations over time, which are done independently for each observing run based on the epoch-specific ephemeris. This is shown, as an example, in Figure 6 for HIP 8998 (three distinct epochs) and HIP 46454 (four epochs), with two measurements per epoch (blue and red, usually indistinguishable at the scale of the plots). The actual data is given in Table 2. As seen from Table 3, the calibration renders our measurements consistent with those from the SOAR program. No systematic offsets are evident, and a similar scatter is seen in the zoom inlets of Figure 6, which shows that our calibrations have been applied consistently throughout the different epochs. However, given the small number of comparison points, it is difficult to assess the internal precision of the Zorro data from this comparison; this is done in more detail in the following section.

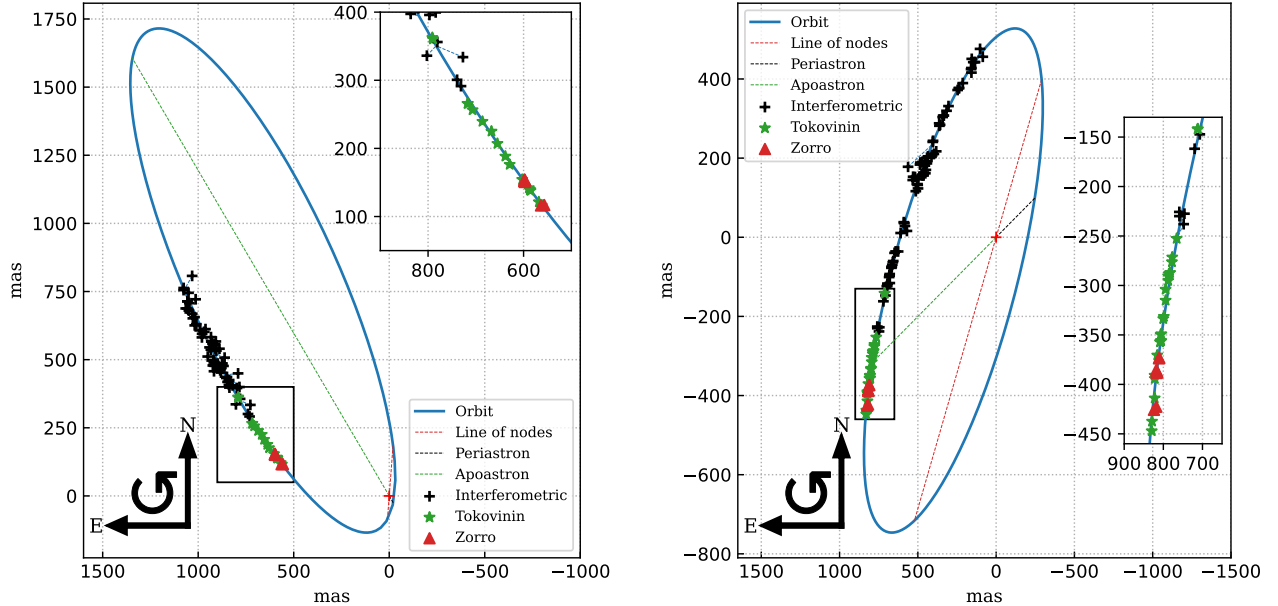


Figure 6. Example results for two astrometric calibrators: HIP 8998 (left panel, three epochs) and HIP 46454 (right panel, four epochs). In both cases blue and red measurements could be secured on each epoch (usually indistinguishable at the scale of the plots). The orbits shown are preliminary and are bound to be modified as more data are acquired. Indeed, these two orbits are currently listed as grade 2 in ORB6, with estimated periods of 167 yr and 118 yr respectively.

Table 3. Residuals for SOAR (first line) and ZORRO (second line) for the two astrometric calibrators (HIP 8998 and HIP 46454) whose tentative orbits are shown in Figure 6.

Binary	$[O - C]_\rho$	σ_ρ	$[O - C]_\theta$	σ_θ	Epoch range	Npoints
	mas	mas	$^\circ$	$^\circ$	yrs	
8998	3.1	2.8	+0.02	0.21	2008.77 - 2023.00	17
	-2.2	2.0	+0.03	0.12	2020.91 - 2023.02	6
46454	3.2	2.0	-0.02	0.17	2009.27 - 2024.15	25
	-2.3	2.8	-0.02	0.15	2020.20 - 2023.01	8

3.5. Results

The final results for a particular run are stored in the `obsres` structure. They can be exported in different formats. The standard export creates the files `double.txt` and `single.txt` for resolved and unresolved sources, respectively. For example, in 2019A there is one resolved triple HIP 63377 with ρ of 29 mas and $0'.46$ between Aa,Ab and Aa,Ac,

respectively (see Table 2). Its outer pair is known as TOK 722. A new faint companion to the PSF reference star HIP 82216 (HD 151526) is detected at $0''.72$. The bright pair STF 1998 (WDS J16044–1122) was observed only once and only in the blue channel; its orbit probably needs a correction. We note that in the earlier epochs (including 2019A) an excessive number of data cubes (6 or even 7) were acquired for some targets. We found that these overabundant data did not improve the quality of the final result but did cost observing time. After the initial runs, we started acquiring typically only two data cubes per target on a regular basis.

3.6. Data Quality: Internal Precision Assessment

In this subsection we provide a look at the quality of the data, based mostly on repeated measurements, which gives us an idea of the internal precision of our relative photometry and astrometry. Because all our targets are observed simultaneously in two filters in every epoch, this allows us to estimate the repeatability of our measurements of ρ and θ (which, in principle, should be independent of the filter used). Because we have observations at different epochs for several systems, we can also assess the precision of the magnitude difference between the components — which should be independent of the epoch of observation — unless, of course, one of the binary components is variable.

In Figure 7 we show, in three columns, the difference between the measured positions in the red and blue filters in the radial and tangent direction, $\Delta\rho$ (in the sense $\rho_{562} - \rho_{832}$), $\bar{\rho} \cdot \Delta\theta$, both in mas, as well as in position angle $\Delta\theta$ (in degrees, in the sense $\theta_{562} - \theta_{832}$), as a function of the mean ρ at a given epoch, for all the objects in our sample that have simultaneous observations in both filters. The first two rows of panels show the residuals considering the whole sample of binaries: In the first (second) row the color-code (on the right to each figure) indicates the brightness difference in the blue (red) filter (Δm hereafter). The third and fourth rows show the effect of applying a 3σ -clipping to the data in order to compute the rms. In these later plots, the dashed lines indicate the 3σ rms. The color coding in all plots shows the magnitude difference between the components, which adds a third dimension to the plots. Smaller, high-contrast, dots depict smaller Δm , while larger low-contrast dots the opposite. Blue dots were used for the blue contrast plots, and red dots for the red contrast plots.

For the whole sample shown, comprising 154 simultaneous observations in the blue and red channels for 50 unique binaries, the overall rms using an iterative 3σ clipping estimate (lower two rows of Figure 7) indicate uncertainties of (1.5 mas, 1.6 mas, $0^\circ 23$ in $(\Delta\rho, \bar{\rho} \cdot \Delta\theta, \Delta\theta)$ respectively, which can be considered as a representative uncertainty of the bulk of our observations. When computing the rms without a σ -clipping, the uncertainties are however substantially larger, indicating that there are some relevant outliers that should be explained.

Regarding the outliers seen in Figure 7, it seems clear that there are no systematic effects as a function of ρ , except that the largest residuals occur mostly on those objects that exhibit the largest Δm between the components. On the other hand, there is an obviously larger scatter in θ at small ρ (see also Figure 8).

The worst offender in ρ is one observation of the large-separation binary ($\sim 0''.8$) HIP 38635 (YSC 198 AaAb) at epoch 2023.01, with a huge blue-red difference of 21.3 mas. This target was observed on other five epochs (see Table 2), with no difficulties. We have examined in detail the binary solution for this target on all epochs, and there are no problems with it, albeit the χ^2 for its solution at the offending epoch is not particularly good: near 7 in the blue channel, and near 20 in the red channel; this having used a nearby PSF star. We note that the blue image is heavily distorted by AD, despite the fact that the zenith distance of this frame was only 30° . In fact, there is an observation at a larger zenith distance (47°) which has smaller residuals (4.9 mas). The observation with the smallest residual (0.6 mas) of this set has a zenith distance of 29° . The seeing on the night when this observation was acquired was good, with quartiles of $0''.38$, $0''.42$ and $0''.45$. At the moment we do not have an explanation for the large difference between the blue and red measurements of this particular target. We note however the rather large magnitude difference of about 5.0 mag in the blue, and 3.5 mag in the red.

For the other targets that exhibit large residuals, we could find a variety of reasonable explanations: For example, for HIP 88937 (HDS 2560 AaAb, 14.6 mas residual at epoch 2022.21), the companion is near the edge of the FOV ($\rho = 1''.24$); in one case even outside the FOV in the blue channel. Then, HIP 101966 (CVN 17AaAb, 14.3 mas residual at epoch 2021.7141) exhibits a very noisy blue channel detection, with a large $\Delta m_{562} \sim 6.0$, in fact the fit to the binary was "guided" by the red channel ACF. Uncomfortably, the next two high-residual objects are both astrometric calibration binaries: the observation at epoch 2023.41 for HIP 67819 (HWE 28AB), with a ρ of $1''.0$ and small Δm , exhibits a residual of 10.9 mas (another eight epochs exhibit a small residual), and HD 92015 (RST 3708) with a ρ of $0''.55$, a moderate Δm , with the next two high residuals at epoch 2023.17 with 7.7 mas, and at epoch 2022.20 with a residual of 7.0 mas (another three observations, at 2020.20, 2021.16, and 2023.17 do not show large residuals).

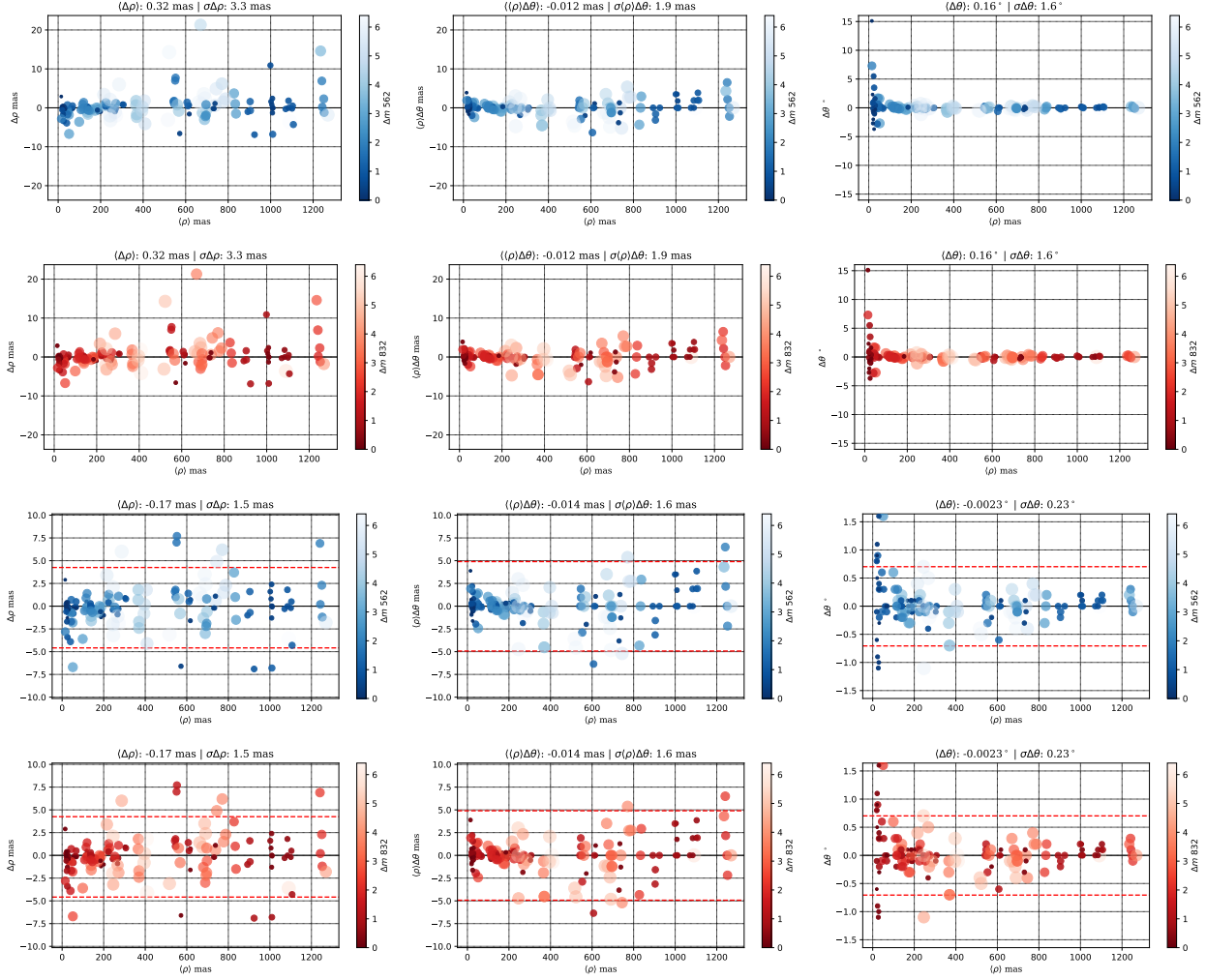


Figure 7. Positional precision: residuals (ordinate) *vs.* ρ (abscissa). Differences between the measured ρ in the radial and tangent direction, $\Delta\rho$, $\bar{\rho} \cdot \Delta\theta$, both in mas, as well as in position angle $\Delta\theta$ (in $^\circ$), as a function of the mean ρ at a given epoch, for all the objects in our sample that have simultaneous observations in both filters. The first two rows of panels show the residuals considering the whole sample of binaries: first row for the blue filter and second row for the red filter. The third and fourth rows show the effect of applying a 3σ -clipping to the data in order to compute the rms, for the blue and red filters, respectively. In these later plots, the dashed lines indicate the 3σ rms. In these figures we have added a color coding to show the magnitude difference between the components, which adds a third dimension to the plots. Smaller, high-contrast, dots depict smaller Δm , while larger low-contrast dots the opposite. Blue dots were used for the blue filter plots, and red dots for the red filter plots. At the top of each figure, we include the mean residual value and its rms in the units of the corresponding ordinate.

Considering that HWE 28AB and RST 3708 are calibrators, and that both show large residuals in the 2023A run, one may be tempted to culprit the blue/red scale correction on that particular run. However, in this run two other astrometric standards were involved, OL 18 with $\Delta\rho = 0.5$ mas (at $\rho = 1''.1$), and RST 2368 with $\Delta\rho = 1.5$ mas and $\rho = 0''.84$. So, the scale correction cannot be the culprit, because it is applied equally to all images. Note that, as further discussed below, at ρ larger than $\sim 0''.4$ the internal precision seems to be worse by a factor of two than at smaller ρ (see Figure 8), and 3σ excursions (implying residuals of 6.0 mas) are not statistically impossible.

Regarding the outliers in θ , it is obvious from the panels in the third column of Figures 7 and 8, that these are systems with very small ρ , close to the diffraction limit, where the binary is only detected typically by one pair of widely separated fringes (see, e.g., Figure 2). The worst offender in this case is HIP 74165, resolved only on epoch 2021.16, with a ρ of 15 mas, and a θ difference of $+15^\circ$. Given its northern declination of $+14^\circ$, it was acquired at a large zenith distance of 45° , so the blue image is very elongated which makes the binary fit uncertain. The next case is HIP 101472, with a similar ρ , and a θ difference of $+7^\circ$ for the measurements on 2022.37. In this case, while

the observations were all done at small zenith distance (5°) the larger magnitude difference (see Table 2) and small ρ means that the fringe contrast is very weak, leading to a somewhat uncertain fit. Then follows HIP 59426, in the inner binary (S 634 Aa,Ab) of this triple system which at epoch 2020.04 and a ρ of 23 mas shows a θ difference of $+5^\circ.5$ (it has also another outlier at epoch 2023.50 and θ difference of $-3^\circ.7$, the second resolution of this system, see Table 2)). The external Aa,Ac sub-system was detected only in the R channel. Accordingly, we performed a binary fit to the Aa,Ab sub-system in the blue frames, and a triple fit to the Aa,Ab plus Aa,Ac sub-systems in the red frames (see Table 2). Therefore, this large θ difference could be caused by the different processing. To check on this suspicion, we have re-processed the system with the binary code alone for both filters. The mean difference in the θ between the binary- and triple-fit for Aa,Ab is $0^\circ.5$ (average over five independent data cubes) so this can not be responsible for the large residual. The observations were done at relatively small zenith distance (16°) with rather moderate elongation of the ACF of the blue channel data, so the reason for the large residual is not obvious, apart from the fact that the fringes had a small contrast and the χ^2 of the fits were not optimal (about 20). The last significant outlier in θ is HIP 48333, at also small ρ (25 mas), with a θ difference of $-3^\circ.7$ at epoch 2020.02. There is a small but noticeable elongation on the blue channel images despite a small zenith distance (11°), but all fits have a reasonable $\chi^2 \sim 2.5$, albeit only one pair of fringes are available for fitting due to the small ρ .

One important outcome that can be appreciated from Figure 7 is that the mean value of the differences in both ρ and θ are well centered on zero (within the rms), which means that our Red-to-Blue scale correction, discussed in Section 3.4.1, has been properly applied in all epochs and that there are no evident systematic offsets neither in ρ nor in θ . Overall, this means that the red and blue measurements can be safely considered as independent measurements of the same quantity and used as such in our orbit fitting later on. Furthermore, by comparing the panels in the first and second columns, we see that the rms of the radial and tangential directions are equivalent.

It is also apparent from Figure 7 that the overall scatter is somewhat dependent on ρ . For example, it appears that the scatter in the radial and tangent directions suffers a change near a ρ of $0''.4$. Several of the large-separation binaries are actually astrometric calibration binaries (see Table 2 and Section 3.4.2), while objects at closer ρ are program stars. This is indeed confirmed by examining Figure 8. At small ρ , we find that the ρ measurement errors would usually surpass 1 mas (e.g., in ρ a 0.87 mas rms of the ρ difference should imply an uncertainty of $0.87/\sqrt{2}$ per measurement), while at large ρ the per-measurement uncertainty would be more like 2 mas (see also Table 3). In terms of PA, we see the opposite trend; at small ρ , the scatter is larger than at large ρ . This is evident in Figure 8, which is due to the much larger scatter in θ at ρ close to the diffraction limit (already mentioned when commenting on in Figure 7). Interestingly, this large rms in θ does not translate into a larger rms in the tangential direction, which exhibits an rms of 0.84 mas similar to that in the radial direction, due to the very small ρ of these binaries (compare the middle and right plots on rows one and two of Figure 8). We note that our pipeline does not correct for differential distortion between channels, nor for possible scale differences in the X and Y axes, as was done by Horch et al. (2009) for the Differential Speckle Survey Instrument (see their Equation (3) on Section 3). It is likely that the intrinsic Zorro optical design could be the main reason for the apparent increase in uncertainty at larger ρ . Another factor that increases the error for larger separation is the atmospheric differential tilt discussed in Tokovinin et al. (2022) (see Equation (19) on Section 2.4).

In terms of the repeatability of the relative photometry, Figure 9 shows the scatter of the repeated measurements over all available epochs, as a function of mean magnitude difference and mean ρ , for both filters (rows one and three). A straight 3σ clipping estimate for the whole sample shown indicates uncertainties of 0.091 mag for both filters (rows two and four). This figure also includes a third dimension: mean ρ in rows one and two, and mean magnitude difference in rows three and four. The color coding in this figure is analogous to that of Figure 7 and Figure 8. In Figure 9 the ordinate $\Delta m - \langle \Delta m \rangle$ is the residual of a particular Δm measurement with respect to the mean of all measurements (over all epochs) in a given filter for that target, this is termed $\Delta\Delta m$ below.

As was the case for the positional uncertainties, some outliers are worth noticing. The tighter component (Tok 722AaAb, ρ of 20 mas) of the triple system HIP 63377 shows in one of its measurements (epoch 2022.37) a very large $\Delta m \sim 1.6$ which is not compatible with previous or posterior observations, which indicate a very small Δm . This sub-system could only be detected in the red channel. We re-processed this sub-system with the binary code instead of the triple-fitting code, and we obtained a $\Delta m = 0.0$, compatible with the other observations. We also note (see Table 2) that its ρ at this epoch is rather discrepant with the values before and after. All the epochs were acquired with a similar zenith distance of $\sim 34^\circ$, and the seeing was commensurable, so there is no obvious reason for the discrepancy. Variability of one of the components could be perhaps advocated, but this does not explain the

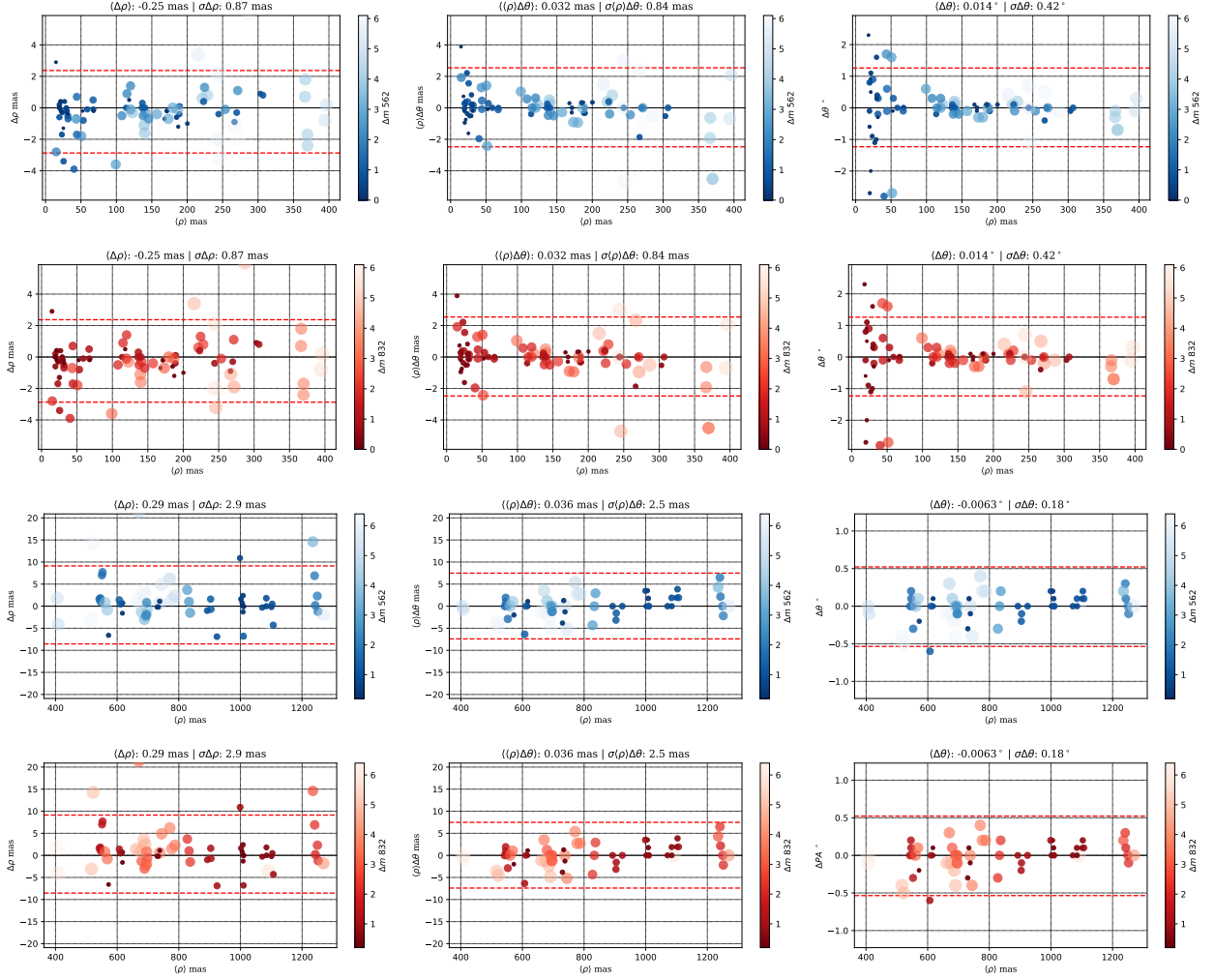


Figure 8. The same general description for rows three and four of Figure 7 are valid for this figure. Here, however, rows one and two are for the range with $\rho < 0.4$ (program stars), while rows three and four are for the larger ρ binaries (mostly astrometric standards).

difference in ρ , and, besides, it is rather large (1.6 mag). Another outlier is HIP 88937; an astrometric binary used earlier on in the program, and later deprecated. It has a large ρ of nearly $1.3''$, which puts the companion very near the edge of the FOV, hence some of its flux is lost making the photometry unreliable. The last outlier worth noting is HIP 101472 at epoch 2022.37, with a difference of $\Delta\Delta m = 0.73$). This is the same outlier mentioned earlier, with a large difference in θ , and likely for the same reasons.

Apart from the outliers mentioned above, there are no obvious trends as a function of either magnitude contrast or ρ . Given the difference in positional precision for small and large ρ noted before, we examined the photometric precision in the same ρ ranges, namely $[0.0, 0.4]''$ and above $0.4''$, which is shown in Figure 10. At large ρ (bottom row) the photometric repeatability seems a bit worse, as already noticed in Section 3.3.3. At small ρ (top row), the red filter seems to be a bit better than the blue one, even considering that the more difficult-to-measure tighter systems are only resolved in that filter (hence the larger number of points at very small ρ).

4. RESULTS AND SOME PRELIMINARY ORBITS

In Table 2 we present our measurements for the systems that could be resolved. In the first column we list the WDS Identification, in the second column the Discoverer Designation (DD) from WDS¹⁰ and in the third column is the

¹⁰ Objects with HD or HIP number in the DD means that they are new binaries, and a DD name is pending from the WDS curators

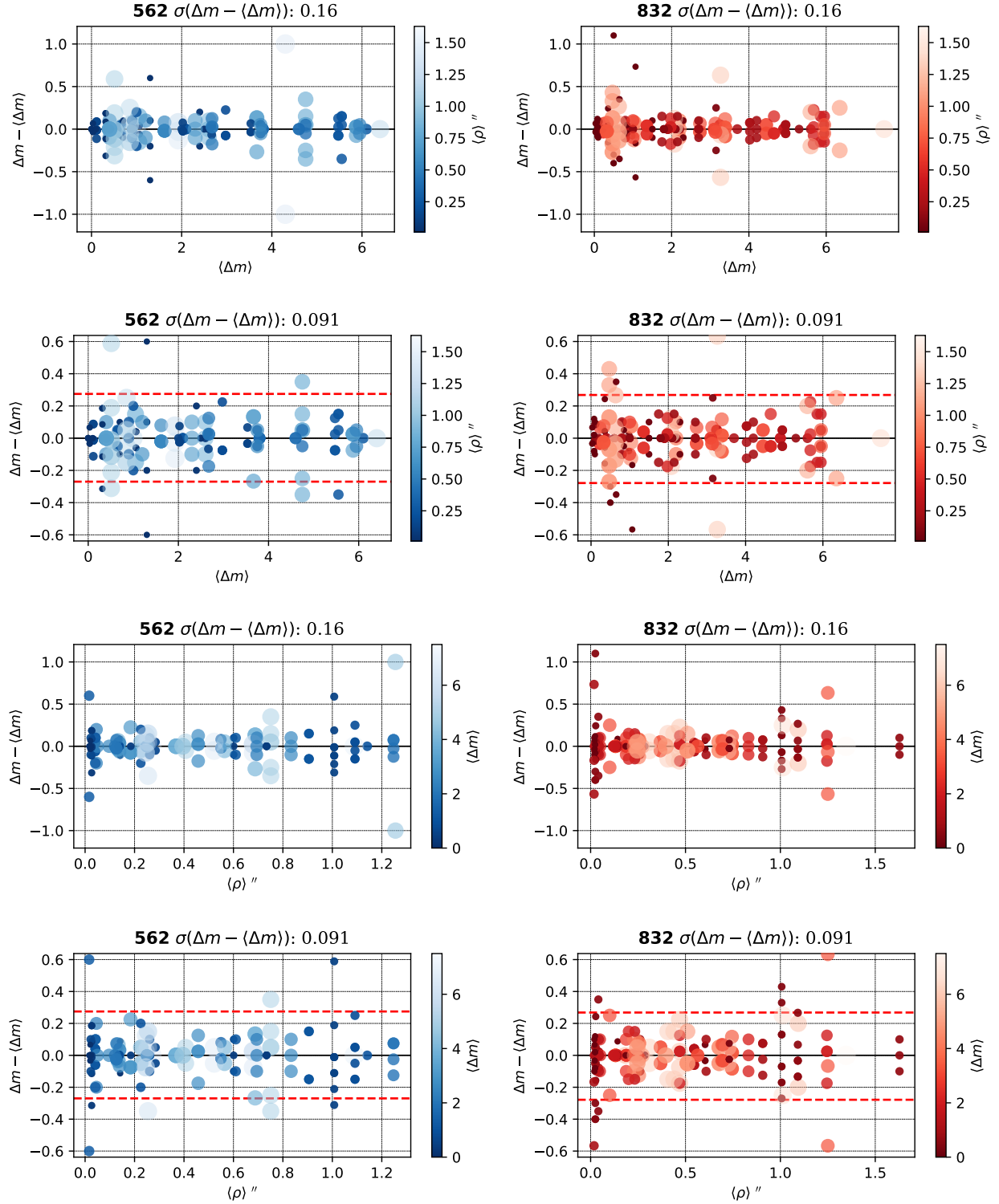


Figure 9. Photometric precision: residuals (ordinate) *vs.* contrast (abscissa) and ρ for the 562nm (left column) and 832nm (right column) filters for all our binaries with observations in the two filters. The first row is for the whole sample, while in the second row applies a 3σ -clipping to compute the rms; in this case, the dotted lines indicate the 3σ rms. The third and fourth rows are similar, but as a function of mean ρ and magnitude difference. The color coding in this figure is analogous to that of Figure 7 and Figure 8. At the top of each figure, we include the mean residual value and its rms in the units of the corresponding ordinate.

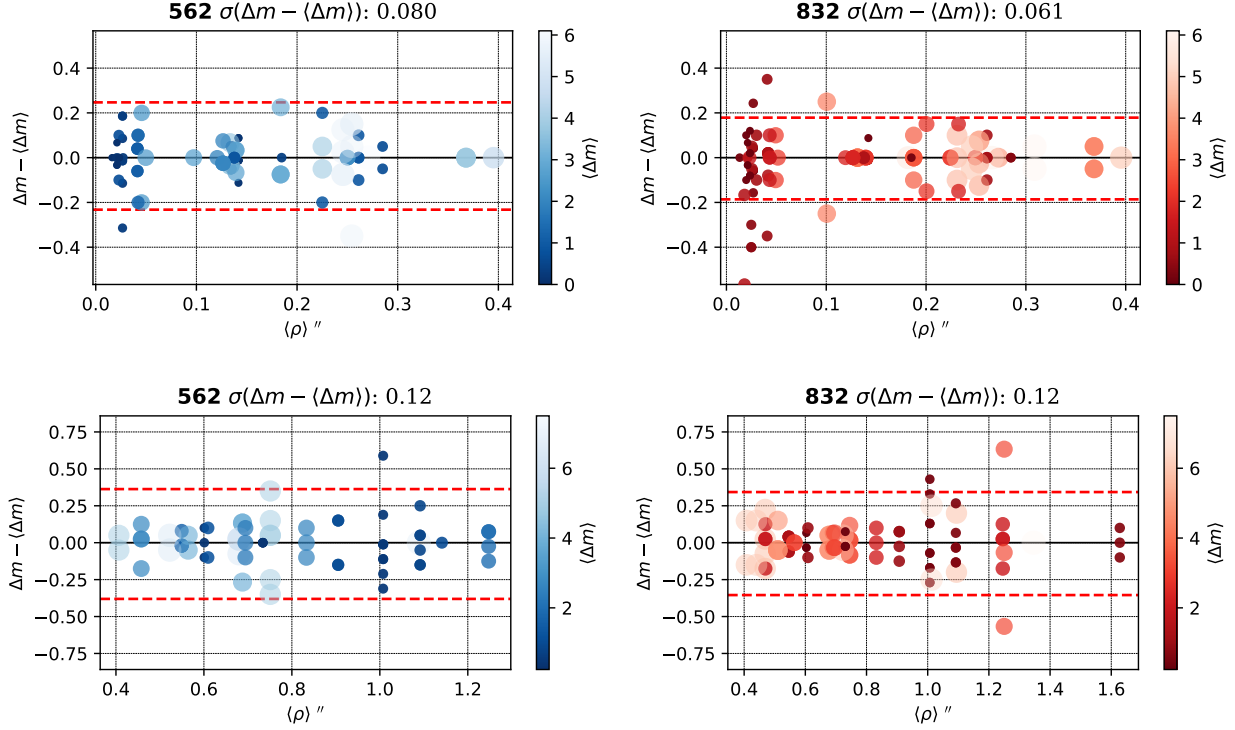


Figure 10. Same as row four on Figure 9, except that the top row is for the range with $\rho < 0''.4$ (program stars), while the bottom row is for the larger ρ binaries (mostly astrometric standards).

HIPPARCOS number (when available). The fourth column gives the epoch in fraction of Julian yr minus 2000.0, the fifth column indicates the filter name and the sixth column gives the number of cubes (of 1000 images each) averaged to produce our measurement. We then give (columns 8, 9 and 10): θ in degrees, the tangential formal error in mas (from the binary or trinary fit code), the ρ in arcsec, and the formal uncertainty in mas (from the binary or trinary fit code). The eleventh column gives the magnitude contrast in the respective filter and in column twelve a code (q means firm quadrant detection on the SAA images, : means uncertain measurement, data are noisy and Δm is likely over-estimated, or tentative resolution). If there is an orbit published for the target, $\Delta\theta$ (in degrees) and $\Delta\rho$ (in mas) indicate the residual of our measurement with respect to the predicted θ and ρ computed for the epoch of observation, in this case we give the orbit reference from Orb6¹¹. The last column gives some relevant comments, when applicable. An overview of the data contents of this table is presented in Figures 11, 12 and 13. We note that there are six (nine) objects with $\Delta m \geq 5.5$ in the blue (red) filter. Of these, only one has $\Delta m \geq 5.5$ in both filters (Tok 791AB), and of the nine objects with large Δm in the red filter, only two of them have measured Δm in both filters (Tok 791AB and HD 100378). In terms of ρ , eleven objects have ρ smaller than 25 mas.

Table 4. Unresolved targets.

WDS	DD	HIP	Epoch	Filt	Ncub	MinSep	Det@0.15	Det@1.00	Comments
			+2000.0 yr			"	mag	mag	
00466-5406	HD 4520	3640	19.5438	562	3	0.014	7.86	7.01	
			19.5438	832	3	0.021	8.43	7.66	
00507-5059	HD 4919	3949	19.5438	562	3	0.014	7.54	7.09	
			19.5438	832	3	0.021	8.07	7.46	

Table 4 continued on next page

¹¹ See <http://www.astro.gsu.edu/wds/orb6.html>.

Table 4 (continued)

WDS	DD	HIP	Epoch	Filt	Ncub	MinSep	Det@0.15	Det@1.00	Comments
			+2000.0 yr			"	mag	mag	
00527-2400	HD 5445	4104	19.5438	562	3	0.014	8.47	6.64	
			19.5438	832	3	0.021	6.05	6.83	
01004+1714	HD 5873	4696	20.8246	562	3	0.014	0.00	4.65	
			20.8246	832	3	0.021	6.10	5.53	
01011+1622	DSG 9	4754	20.8246	562	4	0.014	0.00	4.35	Resolved on 832, same epoch.
01051+1457	YSC 124Aa,Ab	5081	20.9119	562	5	0.014	0.00	5.05	
			20.9119	832	5	0.021	4.84	5.53	
01059-2529	HD 6516	5146	19.5439	562	5	0.014	8.12	6.81	
			19.5439	832	2	0.021	6.81	7.01	Resolved on 832, same epoch.
			20.9065	562	10	0.014	2.86	5.79	
			20.9065	832	10	0.021	1.41	5.28	
01066+1353	HD 6566	5207	20.9120	562	2	0.014	0.00	4.91	
			20.9120	832	2	0.021	4.15	5.34	
			21.7200	562	1	0.014	5.51	6.53	
			21.7200	832	1	0.021	5.15	6.65	
01072-2360	HD 6668	5259	20.9065	562	2	0.014	3.26	5.99	
			20.9065	832	2	0.021	1.66	5.68	
01101-2612	HD 7006	5472	21.7198	562	2	0.014	0.00	5.76	
			21.7198	832	2	0.021	5.77	6.71	
01145-0503	RGS 1Aa,Ab	5806	20.8246	562	3	0.014	0.00	5.65	
			20.8246	832	3	0.021	5.76	6.58	
			21.7200	562	1	0.014	0.00	5.59	
			21.7200	832	1	0.021	5.38	6.48	
			22.7632	562	1	0.014	0.00	5.54	
			22.7632	832	1	0.021	6.03	6.21	
			22.8506	562	1	0.014	0.00	5.54	
			22.8506	832	1	0.021	6.03	6.21	
01206-0315	HD 8120	6283	21.7198	562	1	0.014	0.00	5.96	
			21.7198	832	1	0.021	5.59	6.82	
01349+0817	HD 9657	7366	20.9121	562	2	0.014	0.00	5.07	
			20.9121	832	2	0.021	4.29	6.16	
01380+0946	TOK 688	7604	20.9121	562	5	0.014	0.00	5.14	
			20.9121	832	5	0.021	4.38	6.02	
			23.0200	562	2	0.014	0.00	4.44	
			23.0200	832	2	0.021	0.00	5.42	
01412-6741	HD 10607	7869	19.5439	562	5	0.014	0.00	4.24	Resolved on 832, same epoch.
			20.8982	562	5	0.014	0.00	5.11	Resolved on 832, same epoch.
			21.7200	562	2	0.014	0.00	5.38	
			21.7200	832	2	0.021	6.00	6.51	
			22.7632	562	2	0.014	0.00	5.39	
			22.7632	832	2	0.021	6.32	6.07	
01490+0120	HD 11088	8454	20.9065	562	2	0.014	0.00	5.53	
			20.9065	832	2	0.021	4.01	6.29	
			20.9121	562	2	0.014	0.00	5.53	
			20.9121	832	2	0.021	4.01	6.29	
			23.0200	562	1	0.014	0.00	4.37	
			23.0200	832	1	0.021	5.11	5.59	
01514-4528	HD 11437	8642	20.8983	562	2	0.014	4.57	6.46	
			20.8983	832	2	0.021	3.55	6.54	
01526-6757	HD 11733	8751	20.8983	562	2	0.014	0.00	5.58	
			20.8983	832	2	0.021	4.47	6.24	
			21.7200	562	1	0.014	0.00	5.75	
			21.7200	832	1	0.021	5.64	6.55	
			22.7632	562	1	0.014	0.00	5.49	
01536-4618	HD 11695	8837	22.7632	832	1	0.021	4.75	6.19	
			20.8982	562	5	0.014	5.93	6.46	
01594+1218	HD 12140	9295	20.8982	832	5	0.021	4.88	6.67	
			23.0200	562	1	0.014	0.00	3.97	
02092-0220	HD 13228	10033	23.0200	832	1	0.021	0.00	5.06	
			20.8247	562	3	0.014	0.00	4.80	
02128-0224	TOK 39Aa,Ab	10305	20.8247	832	3	0.021	5.61	5.43	
			21.7198	562	2	0.014	0.00	5.37	Resolved on 562 and 832 on 20.8247.
			21.7198	832	2	0.021	6.20	6.39	
			22.7633	562	2	0.014	0.00	5.23	

Table 4 continued on next page

Table 4 (continued)

WDS	DD	HIP	Epoch	Filt	Ncub	MinSep	Det@0.15	Det@1.00	Comments
			+2000.0 yr			"	mag	mag	
			22.7633	832	2	0.021	4.51	5.73	
02142-6750	HD 5098	10418	19.5439	562	3	0.014	0.00	5.32	
			19.5439	832	3	0.021	8.85	7.35	
02197-0421	HD 14417	10854	21.7198	562	1	0.014	0.00	5.38	
			21.7198	832	1	0.021	5.62	6.52	
			22.7633	832	1	0.021	4.08	5.74	
02418-0313	HD 16824	12584	22.7633	562	1	0.014	0.00	5.49	
			22.7633	832	1	0.021	5.55	5.76	
02440-0601	TOK 75Ba,Bb	12764	22.7633	562	2	0.057	0.00	0.00	:
			22.7633	832	2	0.030	0.00	3.50	:
03024+0421	HD 18883	14143	20.0221	562	2	0.014	0.00	4.88	
			20.0221	832	2	0.021	4.92	6.15	
03064+0316	HD 19304	14443	20.0221	562	3	0.014	0.00	4.66	
			20.0221	832	3	0.021	4.79	6.02	
03151-4540	HD 20407	15131	20.8984	562	2	0.014	5.49	6.63	
			20.8984	832	2	0.021	4.72	6.96	
			20.9067	562	2	0.014	5.49	6.63	
			20.9067	832	2	0.021	4.72	6.96	
			20.9122	562	2	0.014	5.49	6.63	
			20.9122	832	2	0.021	4.72	6.96	
03151-4540	HD 20407	15131	21.7202	562	1	0.014	5.52	6.23	
			21.7202	832	1	0.021	4.21	6.48	
			22.7633	562	1	0.014	5.55	6.33	
			22.7633	832	1	0.021	4.88	6.36	
			22.8508	562	1	0.014	5.55	6.33	
			22.8508	832	1	0.021	4.88	6.36	
03196-3251	HIP 15841	15481	20.8246	562	5	0.016	7.88	5.92	
			20.8246	832	5	0.021	5.78	5.77	
			22.7634	562	2	0.015	4.14	4.26	:
			22.7634	832	2	0.024	2.84	5.24	
03237-3242	HD 21149	15816	20.8247	562	1	0.014	4.52	5.90	
			20.8247	832	1	0.021	4.24	5.47	
			22.7634	562	1	0.014	3.69	5.93	
			22.7634	832	1	0.021	2.47	5.73	
04059+1530	HD 25788	19120	20.0276	562	5	0.014	0.00	5.12	Resolved on 832, same epoch.
04090+1324	HD 26171	19376	20.0277	562	2	0.014	0.00	5.43	
			20.0277	832	2	0.021	6.50	6.22	
04384-7739	HD 30479	21611	21.1417	562	1	0.014	0.00	4.51	
			21.1417	832	1	0.021	2.77	4.88	
			22.8510	562	1	0.014	0.00	4.77	
			22.8510	832	1	0.021	0.00	6.11	
			23.1704	562	1	0.014	0.00	4.42	
			23.1704	832	1	0.021	0.00	4.99	
04444-5944	HD 30478	22040	20.0223	562	2	0.014	0.00	5.90	
			20.0223	832	2	0.021	5.65	6.79	
04549-5833	HD 31746	22844	22.7689	562	1	0.014	0.00	6.13	
			22.7689	832	1	0.021	6.00	6.77	
04571-5804	HD 32065	23029	20.0222	562	5	0.014	0.00	5.99	
			20.0222	832	5	0.021	5.23	6.69	
			22.7688	562	2	0.014	0.00	6.09	
			22.7688	832	2	0.021	5.20	6.80	
05008-0546	HD 32147	--	21.0354	562	1	0.014	0.00	4.51	
			21.0354	832	1	0.021	0.00	5.71	
			21.9718	562	1	0.014	0.00	5.87	
			21.9718	832	1	0.021	6.05	6.40	
05016-4450	HD 32517	23381	20.0222	562	5	0.014	0.00	6.22	
			20.0222	832	5	0.021	5.38	6.83	
05028-0413	HD 32393	23475	20.0223	562	2	0.014	0.00	5.48	
			20.0223	832	2	0.021	5.74	6.53	
05050-4935	HD 33042	23649	20.0225	562	2	0.014	0.00	5.71	
			20.0225	832	2	0.021	4.29	6.49	
05183-4852	HD 273975	24742	20.9069	562	5	0.014	5.71	5.21	
			20.9069	832	5	0.021	4.75	6.20	
05200-4703	HD 35116	24876	20.9069	562	2	0.014	5.08	6.41	
			20.9069	832	2	0.021	4.29	6.57	

Table 4 continued on next page

Table 4 (continued)

WDS	DD	HIP	Epoch	Filt	Ncub	MinSep	Det@0.15	Det@1.00	Comments
			+2000.0 yr			"	mag	mag	
05287-6527	CLO 10Ba,Bb	25647	21.7205	562	2	0.014	0.00	5.42	Quadruple, with Aa,Ab (CLO 10Aa,Ab). Ba,Bb undetected by Zorro. CLO 10Aa,Ab being done at SOAR.
			21.7205	832	2	0.021	6.21	6.41	
			23.0204	562	2	0.014	0.00	4.66	
			23.0204	832	2	0.021	6.08	6.22	
05503-7922	HD 40953	27566	20.0198	562	2	0.014	0.00	5.24	
			20.0198	832	2	0.021	0.00	6.33	
05514-6402	HD 39963	27660	21.7205	562	1	0.014	0.00	5.72	Resolved on 832, same epoch.
05547-4938	HD 40200	27937	22.2041	562	1	0.014	0.00	5.57	
			22.2041	832	1	0.021	5.73	6.13	
			22.7635	562	1	0.014	5.61	6.53	
			22.7635	832	1	0.021	4.73	6.86	
06058-7857	HD 43641	28880	20.0198	562	5	0.014	0.00	4.81	
			20.0198	832	5	0.021	0.00	6.15	
06313-5150	HD 46569	31079	20.0171	562	2	0.014	6.72	6.22	
			20.0171	832	2	0.021	8.69	6.84	
			20.0198	562	2	0.014	6.72	6.22	
			20.0198	832	2	0.021	8.69	6.84	
06318+0647	HD 46122	31118	20.0280	466	5	0.014	0.00	5.38	
			20.0280	716	5	0.018	0.00	5.67	
06323+0451	HD 46241	31159	20.0280	466	2	0.014	0.00	5.29	
			20.0280	716	2	0.018	0.00	5.74	
06334-5220	HD 47001	31265	21.0355	562	1	0.014	0.00	6.21	
			21.0355	832	1	0.021	6.83	6.51	
			21.1418	562	1	0.014	0.00	6.21	
			21.1418	832	1	0.021	6.83	6.51	
			22.2041	562	1	0.014	0.00	5.77	
			22.2041	832	1	0.021	5.14	6.39	
			22.7690	562	1	0.014	0.00	6.12	
			22.7690	832	1	0.021	7.08	6.60	
			23.0205	562	1	0.014	0.00	4.93	
			23.0205	832	1	0.021	5.38	5.86	
06371-3214	HD 47391	31623	20.0172	562	5	0.014	8.33	6.01	
			20.0172	832	5	0.021	7.22	6.42	
			20.0171	562	2	0.014	8.45	6.46	
			20.0171	832	2	0.021	7.14	6.92	
			20.1946	562	2	0.014	0.00	5.05	
			20.1946	832	2	0.021	5.86	6.09	
			23.0095	562	2	0.014	0.00	5.37	
			23.0095	832	2	0.021	6.15	6.18	
			23.0095	562	1	0.014	0.00	5.51	
			23.0095	832	1	0.021	5.94	6.34	
07078+0728	HD 54079	34387	20.0280	562	2	0.014	0.00	5.17	
			20.0280	832	2	0.021	6.06	6.21	
			20.1973	562	2	0.014	0.00	5.79	
			20.1973	832	2	0.021	5.45	6.55	
07081-5720	HD 55105	34417	20.8989	562	2	0.014	0.00	5.86	
			20.8989	832	2	0.021	3.37	6.39	
			21.0355	562	1	0.014	0.00	5.24	
			21.0355	832	1	0.021	2.23	6.00	
			22.2013	562	1	0.014	0.00	5.50	
			22.2013	832	1	0.021	6.16	6.50	
07103+0518	HD 54759	34625	23.0205	562	1	0.014	0.00	3.91	
			23.0205	832	1	0.021	2.47	5.21	
			20.0280	562	5	0.014	0.00	5.23	
			20.0280	832	5	0.021	5.61	6.37	
			20.1973	562	5	0.014	0.00	5.30	
20.1973	832	5	0.021	5.34	6.44				
07250+1140	HD 58187	35987	20.0281	562	2	0.014	0.00	4.70	
			20.0281	832	2	0.021	4.79	5.78	
			20.1973	562	2	0.014	0.00	5.70	
			20.1973	832	2	0.021	6.00	6.59	
07281-3801	HD 59392	36269	20.8988	832	5	0.021	4.31	6.45	
			20.8989	562	4	0.014	4.98	6.06	

Table 4 continued on next page

Table 4 (continued)

WDS	DD	HIP	Epoch	Filt	Ncub	MinSep	Det@0.15	Det@1.00	Comments
			+2000.0 yr			"	mag	mag	
			21.0355	562	2	0.014	3.91	6.16	
			21.0355	832	2	0.021	4.73	6.07	
			21.9720	562	2	0.014	6.84	6.34	
			21.9720	832	2	0.021	4.99	6.23	
			22.2014	562	1	0.014	6.11	6.42	
			22.2014	832	2	0.021	5.23	6.42	
			23.0205	562	2	0.014	0.00	5.51	
			23.0205	832	2	0.021	0.00	5.28	
07284-3749	HD 59466	36304	22.2014	562	1	0.014	6.73	6.26	Resolved on 562 and 832 on.
			22.2014	832	1	0.021	5.83	6.01	20.8989, 21.0355 and 21.9720.
			23.0205	562	1	0.014	0.00	5.06	
			23.0205	832	1	0.021	0.00	4.78	
07293+1227	LSC 45	36387	20.9070	562	5	0.014	0.00	5.13	Resolved on 832, same epoch.
			22.3737	562	2	0.014	0.00	4.26	Resolved on 562 and 832 on.
			22.3737	832	2	0.021	0.00	5.32	20.0281, 20.1973, 21.0354.
			23.0205	562	2	0.014	0.00	3.34	
			23.0205	832	2	0.021	0.00	4.71	
07517+0146	HD 63975	38373	20.1973	562	2	0.014	0.00	5.89	
			20.1973	832	2	0.021	5.03	6.54	
07574-0038	HD 65158	38885	20.9071	562	2	0.014	0.00	5.90	
			20.9071	832	2	0.021	3.91	6.55	
			21.0355	562	1	0.014	0.00	4.63	
			21.0355	832	1	0.021	2.54	5.61	
			21.9720	562	1	0.014	0.00	5.66	
			21.9720	832	1	0.021	5.86	6.18	
			22.3737	562	1	0.014	0.00	5.53	
			22.3737	832	1	0.021	7.63	6.50	
			23.0096	562	1	0.014	0.00	3.93	
			23.0096	832	1	0.021	4.01	5.20	
08143-0554	HD 68879	40348	23.0206	562	2	0.014	0.00	4.09	
			23.0206	832	2	0.021	2.72	5.25	
08203-0520	HD 70148	40859	23.0206	562	1	0.014	0.00	3.89	
			23.0206	832	1	0.021	4.83	5.06	
09370-2518	HD 83332	47187	20.0173	562	2	0.014	8.98	6.48	
			20.0173	832	2	0.021	7.36	6.64	
			20.2002	562	2	0.014	4.04	6.05	
			20.2002	832	2	0.021	3.73	5.73	
09454-3012	HD 84567	47868	21.0355	562	1	0.014	3.88	6.06	
			21.0355	832	1	0.021	4.03	6.03	
			21.9722	562	1	0.014	4.54	6.44	
			21.9722	832	1	0.021	3.77	6.44	
			22.1990	562	1	0.014	6.88	6.63	
			22.1990	832	1	0.021	5.99	6.58	
			23.0098	562	1	0.014	6.81	5.93	
			23.0098	832	1	0.021	7.13	5.80	
			23.1682	562	1	0.014	2.62	5.02	
			23.1682	832	1	0.021	4.38	5.04	
09462+0643	HD 84542	47943	21.1559	562	1	0.014	0.00	5.87	
			21.1559	832	1	0.021	7.51	6.75	
			21.1586	562	1	0.014	0.00	5.87	
			21.1586	832	1	0.021	7.51	6.75	
			23.0098	562	1	0.014	0.00	4.13	
			23.0098	832	1	0.021	3.45	5.05	
10372-1145	HD 91992	51974	21.1560	562	1	0.014	8.22	6.32	
			21.1560	832	1	0.021	6.89	6.51	
			21.1587	562	2	0.014	8.22	6.32	
			21.1587	832	2	0.021	6.89	6.51	
			22.2018	562	1	0.014	0.00	4.42	
			22.2018	832	1	0.021	0.00	5.27	
			23.1683	562	1	0.014	0.00	5.60	
			23.1683	832	1	0.021	5.66	6.10	
10376-1323	HD 92055	52009	20.1948	562	2	0.014	5.41	5.66	
			20.1948	832	2	0.021	3.81	5.93	
11126-2145	HD 97428	54749	22.2019	562	1	0.014	0.00	4.95	
			22.2019	832	1	0.021	2.89	5.13	

Table 4 continued on next page

Table 4 (continued)

WDS	DD	HIP	Epoch	Filt	Ncub	MinSep	Det@0.15	Det@1.00	Comments
			+2000.0 yr			"	mag	mag	
			23.0099	562	1	0.014	5.65	5.78	
			23.0099	832	1	0.021	5.72	5.79	
11394-3923	DSG 12	56851	20.1921	562	5	0.014	5.15	6.30	
			20.1921	832	5	0.021	4.97	6.19	
11439-2945	HD 101959	57217	21.0359	562	1	0.014	2.70	5.44	
			21.0359	832	1	0.021	1.99	5.03	
			22.2046	562	1	0.014	4.40	6.54	
			22.2046	832	1	0.021	3.59	6.49	
			23.1711	562	1	0.014	2.96	5.79	
			23.1711	832	1	0.021	2.91	5.51	
11464-2758	DSG 13AC	57421	19.3785	562	1	0.014	8.31	5.95	
11488-2645	HD 102620	57613	19.3815	562	1	0.014	2.75	5.06	
			19.3815	832	1	0.021	7.95	7.31	
11520-4357	SEE 137	57860	22.2046	562	2	0.014	5.38	5.91	Resolved on 832, same epoch.
			23.0209	562	2	0.014	1.52	4.79	Resolved on 832, same epoch.
			23.1713	562	2	0.014	0.00	5.25	Resolved on 832, same epoch.
11534-3504	HD 103266	57971	21.0359	562	1	0.014	6.78	6.00	
			21.0359	832	1	0.021	5.62	5.83	
			22.2046	562	1	0.014	6.61	6.22	
			22.2046	832	1	0.021	6.39	6.09	
11567-4704	HD 103746	58242	22.2046	562	1	0.014	5.44	5.77	
			22.2046	832	1	0.021	5.21	5.88	
			23.0209	562	1	0.014	0.00	5.63	
			23.0209	832	1	0.021	4.98	5.93	
			23.1713	562	1	0.014	0.00	5.62	
			23.1713	832	1	0.021	4.97	6.04	
12152-1019	HD 106516	59750	19.3815	562	3	0.014	7.87	6.73	
			19.3815	832	3	0.021	8.18	7.27	
12171-1642	HD 106819	59895	23.5044	562	1	0.014	6.68	6.57	
			23.5044	832	1	0.021	5.12	6.80	
12209-1334	HD 107418	60221	19.3815	562	1	0.014	7.63	7.05	
			19.3815	832	1	0.021	6.99	7.47	
12228-5741	HD 107696	60379	20.0366	562	2	0.014	0.00	5.07	
			20.0366	832	2	0.021	5.02	6.22	
			20.1924	562	2	0.014	0.00	5.43	
			20.1924	832	2	0.021	5.99	6.23	
12236-3525	HD 107832	60449	19.3815	562	1	0.014	8.25	7.02	
			19.3815	832	1	0.021	7.83	7.21	
			20.1924	562	2	0.014	3.36	6.28	
			20.1924	832	2	0.021	3.07	6.09	
12284-6148	HD 108530	60861	21.1588	562	2	0.014	0.00	5.76	
			21.1588	832	2	0.021	4.41	6.44	
			22.3712	562	1	0.014	0.00	5.93	
			22.3712	832	1	0.021	5.57	6.76	
			23.5044	562	1	0.014	0.00	5.54	
			23.5044	832	1	0.021	5.15	6.94	
12319-6330	DSG 15	61158	23.5044	562	2	0.014	0.00	5.97	Resolved on 832, same epoch.
12428-6304	HD 110432	62027	19.3815	562	1	0.014	8.08	6.45	
			19.3815	832	1	0.021	7.63	7.16	
			19.5319	562	3	0.014	0.00	6.61	
			19.5319	832	3	0.021	8.84	7.71	
12436-0135	HD 110646	62103	22.3741	562	1	0.014	0.00	3.74	
			22.3741	832	1	0.021	3.55	5.08	
12440-2819	HD 110666	62131	19.3816	562	1	0.014	4.57	5.76	
			19.3816	832	1	0.021	8.05	7.36	
12520-2644	HD 111786	62788	21.1589	562	1	0.014	3.46	6.15	
			21.1589	832	1	0.021	2.66	5.92	
			22.2046	562	1	0.014	6.09	6.06	
			22.2046	832	1	0.021	5.72	5.84	
12532-0333	CHR 38	62875	22.3741	562	3	0.014	0.00	5.67	
			22.3741	832	3	0.021	6.18	6.54	
12544-5826	HD 112044	62986	23.4008	562	1	0.014	0.00	5.65	
			23.4008	832	1	0.021	5.12	6.52	
13014-2723	HD 113083	63559	19.5291	562	5	0.014	0.00	6.63	
			19.5291	832	5	0.021	6.65	7.69	

Table 4 continued on next page

Table 4 (continued)

WDS	DD	HIP	Epoch	Filt	Ncub	MinSep	Det@0.15	Det@1.00	Comments
			+2000.0 yr			"	mag	mag	
13027-2701	HD 113247	63650	19.5291	562	5	0.014	0.00	6.42	
			19.5291	832	5	0.021	6.74	7.53	
13119-6318	HD 114461	64395	21.1589	562	1	0.014	0.00	4.85	
			21.1589	832	1	0.021	4.30	5.80	
			22.3739	562	1	0.014	0.00	5.82	
			22.3739	832	1	0.021	6.34	6.66	
			23.4006	562	1	0.014	0.00	5.96	
13418-3336	HD 119090	66825	23.4006	832	1	0.021	5.30	6.82	
			20.1925	562	2	0.014	4.23	6.29	
			20.1925	832	2	0.021	3.45	6.12	
			20.1952	562	2	0.014	4.23	6.29	
			20.1952	832	2	0.021	3.45	6.12	
			20.1979	562	2	0.014	4.23	6.29	
			20.1979	832	2	0.021	3.45	6.12	
			20.2007	562	2	0.014	4.23	6.29	
			20.2007	832	2	0.021	3.45	6.12	
			21.5468	832	1	0.021	5.20	6.61	
			22.2047	562	1	0.014	2.86	5.94	
			22.2047	832	1	0.021	2.77	5.74	
			22.3713	562	1	0.014	5.03	6.48	
			22.3713	832	1	0.021	4.91	6.24	
			23.1713	562	1	0.014	6.38	6.64	
			23.1713	832	1	0.021	6.05	6.66	
			23.4008	562	1	0.014	6.38	6.64	
23.4008	832	1	0.021	6.05	6.66				
23.4990	562	1	0.014	6.38	6.64				
23.4990	832	1	0.021	6.05	6.66				
13448-2530	HD 119623	67071	21.1589	562	1	0.014	4.95	6.61	
			21.1589	832	1	0.021	4.41	6.61	
			22.2047	562	1	0.014	7.47	6.35	
			22.2047	832	1	0.021	6.40	6.27	
13575-2301	HD 121699	68177	21.1591	562	1	0.014	4.31	6.55	
			21.1591	832	1	0.021	4.50	6.61	
			22.2047	562	1	0.014	4.38	6.05	
			22.2047	832	1	0.021	3.90	5.93	
13585-2458	HD 121847	68269	19.3872	562	1	0.014	7.04	7.31	
			19.3872	832	1	0.021	8.41	7.78	
			20.1926	562	2	0.014	3.65	5.89	
			20.1926	832	2	0.021	2.31	5.60	
13587+1439	HD 121908	68279	21.1592	562	1	0.014	0.00	5.36	
			21.1592	832	1	0.021	5.73	6.31	
14142+1805	TOK 723	69549	21.1591	562	3	0.014	0.00	5.15	
			21.1591	832	3	0.021	6.06	5.97	
14479-1250	HD 130325	72373	23.1714	562	1	0.014	7.64	5.85	
			23.1714	832	1	0.021	5.98	5.90	
14501+0050	HD 136799	72561	19.3868	562	11	0.014	0.00	3.40	
			19.3868	832	11	0.021	7.80	5.36	
14509-1603	DSG 17Aa,Ab	72622	20.1927	562	5	0.014	0.00	4.65	Resolved on 832, same epoch.
			23.1714	562	4	0.014	7.14	6.12	Resolved on 562 and 832 on 19.3872.
			23.1714	832	4	0.021	6.02	5.84	
14576-0010	HD 132132	73193	19.3872	562	1	0.014	0.00	6.76	
			19.3872	832	1	0.021	9.68	7.35	
15066-1615	HD 133774	73945	19.3872	562	4	0.014	9.65	7.36	
			19.3872	832	4	0.021	9.21	7.74	
			20.1927	562	2	0.014	0.00	4.94	
			20.1927	832	2	0.021	0.63	5.00	
15092+1431	HIP 74165	74165	23.2644	562	2	0.014	0.00	4.08	Resolved on 562 and 832 on 21.1592.
			23.2644	832	2	0.021	5.82	5.63	
15224+1234	HD 136831	75230	21.1592	562	1	0.014	0.00	5.21	
			21.1592	832	1	0.021	4.10	5.93	
			23.2644	562	1	0.014	0.00	3.51	
			23.2644	832	1	0.021	0.00	4.56	
15258+1526	HD 137471	75530	19.3872	562	3	0.014	0.00	5.35	
			19.3872	832	3	0.021	8.33	6.91	
			20.1953	562	2	0.014	0.00	4.98	

Table 4 continued on next page

Table 4 (continued)

WDS	DD	HIP	Epoch	Filt	Ncub	MinSep	Det@0.15	Det@1.00	Comments
			+2000.0 yr			"	mag	mag	
			20.1953	832	2	0.021	7.04	5.73	
15317+0053	TOK 48	76031	23.1688	562	2	0.014	0.00	5.18	Resolved on 832, same epoch.
15343-0542	HD 138763	76233	21.1592	562	1	0.014	0.00	5.93	
			21.1592	832	1	0.021	4.57	6.32	
			22.1995	562	1	0.014	0.00	5.42	
			22.1995	832	1	0.021	4.48	6.09	
			23.1688	562	2	0.014	0.00	5.45	
			23.1688	832	2	0.021	6.28	6.07	
15344-0911	HD 138764	76243	19.3816	562	5	0.014	8.30	6.82	
			19.3816	832	5	0.021	7.81	7.24	
15351+0140	HD 138936	76291	23.1688	562	1	0.014	0.00	5.36	
			23.1688	832	1	0.021	6.58	6.29	
15365+1607	DSG 18Aa,Ab	76424	19.3873	562	3	0.014	0.00	6.17	Resolved on 832, same epoch.
			20.1956	562	5	0.014	0.00	4.84	Resolved on 832, same epoch.
16142-5047	TOK 409	79576	19.3817	562	6	0.014	6.40	5.22	
			19.3817	832	2	0.021	8.07	6.65	Resolved on 832, same epoch.
			20.1927	562	5	0.014	0.00	5.78	Resolved on 832, same epoch.
16153-4722	HD 145842	79653	19.3817	562	4	0.014	7.91	6.94	
			19.3817	832	4	0.021	7.83	7.15	
			20.1927	562	5	0.014	6.01	5.87	
			20.1927	832	5	0.021	4.62	5.94	
16308-6138	HD 148291	80874	19.3817	562	3	0.014	5.03	5.00	
			19.3817	832	3	0.021	8.28	7.23	
16314-2632	HD 148760	80910	20.1954	562	2	0.014	4.27	5.63	
			20.1954	832	2	0.021	3.26	5.42	
16315-3901	HDS 2335Aa,Ab	80925	19.3816	562	5	0.014	8.48	6.70	
			19.3816	832	5	0.021	8.74	7.27	
16329+0315	DSG 7Aab,c	81023	19.4640	562	4	0.014	0.00	5.68	Resolved on 832, same epoch.
			23.1688	562	2	0.014	0.00	4.94	Resolved on 832, same epoch.
16348-0412	DSG 20Aa,Ab	81170	19.3818	562	3	0.014	2.94	5.16	
			19.3818	832	3	0.021	7.68	6.82	
			19.3846	562	7	0.014	2.94	5.16	
			19.3846	832	7	0.021	7.68	6.82	
			19.7045	562	5	0.014	0.00	4.42	
			19.7045	832	5	0.021	0.00	5.83	
16364-0220	HD 149661	81300	19.3846	562	1	0.014	0.00	6.21	
			19.3846	832	1	0.021	8.38	7.22	
16391-2759	HD 149960	81521	21.5471	832	2	0.021	6.61	5.99	Resolved on 562 and 832 on.
			22.1995	562	5	0.014	0.00	4.49	20.1956 and 23.2617.
			22.1995	832	5	0.021	1.88	5.31	
16416-2749	HD 150367	81731	21.5471	832	1	0.021	5.57	6.04	
			22.1995	562	1	0.014	0.00	5.23	
			22.1995	832	1	0.021	1.70	5.95	
			23.2617	562	1	0.014	5.73	6.38	
			23.2617	832	1	0.021	5.95	6.13	
16468-3923	HD 151078	82135	19.3817	562	3	0.014	7.61	6.99	
			19.3817	832	3	0.021	8.47	7.37	
16478+0515	HD 151525	82216	19.4640	562	1	0.014	0.00	6.67	Resolved on 832, same epoch.
			19.5376	562	3	0.014	0.00	6.67	Resolved on 832, same epoch.
16510-3645	HD 151770	82447	19.3817	562	6	0.014	8.79	6.30	
			19.3817	832	6	0.021	8.79	7.09	
16516-4114	HD 151804	82493	19.3817	562	2	0.014	8.61	6.92	
			19.3817	832	2	0.021	8.05	7.18	
16600-2506	HD 153336	83176	19.3817	562	3	0.014	9.80	7.12	
			19.3817	832	3	0.021	7.81	7.14	
			20.1956	562	2	0.014	4.62	5.90	
			20.1956	832	2	0.021	3.79	5.70	
17062-2134	HD 154418	83684	23.4010	562	1	0.014	5.69	6.41	
			23.4010	832	1	0.021	4.21	6.28	
17082-1737	HD 154779	83854	19.6989	562	2	0.014	0.00	6.03	
			19.6989	832	2	0.021	7.15	6.73	
17098-1031	TOK 414	83962	19.3846	562	1	0.014	6.21	6.59	
			19.3846	832	1	0.021	8.49	7.32	
			19.6989	562	2	0.014	0.00	6.05	
			19.6989	832	2	0.021	6.15	6.92	

Table 4 continued on next page

Table 4 (continued)

WDS	DD	HIP	Epoch	Filt	Ncub	MinSep	Det@0.15	Det@1.00	Comments
			+2000.0 yr			"	mag	mag	
17127-2136	OCC 1096	84198	22.1996	562	3	0.014	0.00	4.45	Resolved on 832, same epoch.
17206-1920	OCC 529Aa,Ab	84856	19.6989	562	5	0.014	6.48	6.12	
			19.6989	832	5	0.021	8.79	6.86	
17280-0813	HD 158170	85474	22.2050	562	1	0.014	0.00	5.26	
			22.2050	832	1	0.021	4.06	6.01	
			23.5020	562	1	0.014	0.00	5.84	
			23.5020	832	1	0.021	5.83	6.66	
17547+2016	HIP 87693	87693	23.2620	562	2	0.014	0.00	4.60	
			23.2620	832	2	0.021	0.00	5.66	
18005+1930	HD 164447	88172	23.2620	562	1	0.014	0.00	5.02	
			23.2620	832	1	0.021	0.00	5.80	
18029-2417	HIP 88380	88380	19.3820	562	1	0.014	9.28	6.95	
			19.3820	832	1	0.021	8.18	7.16	
18100-3243	HD 165978	89010	21.7139	562	1	0.014	6.85	6.67	
			21.7139	832	1	0.021	5.16	6.77	
			22.2024	562	1	0.014	0.00	5.11	
			22.2024	832	1	0.021	1.35	5.53	
			22.3719	562	1	0.014	0.00	4.96	
			22.3719	832	1	0.021	3.06	5.48	
			23.2645	562	1	0.014	7.43	6.43	
			23.2645	832	1	0.021	7.52	6.59	
			23.4011	562	1	0.014	7.43	6.43	
			23.4011	832	1	0.021	7.52	6.59	
18111-2546	HD 166295	89097	21.5500	832	1	0.021	3.90	5.23	
			22.2024	562	1	0.014	0.00	4.99	
			22.2024	832	1	0.021	0.81	5.29	
			22.2024	562	1	0.014	0.00	3.68	
			22.2024	832	1	0.021	0.00	4.83	
18127+0249	HD 166917	89242	22.2024	562	1	0.014	0.00	3.68	
			22.2024	832	1	0.021	0.00	4.83	
			19.3765	562	1	0.014	0.00	6.38	
			19.3765	832	1	0.021	8.21	7.69	
18192+0716	HD 168387	89772	19.3820	562	3	0.014	0.00	6.38	
			19.3820	832	3	0.021	8.21	7.69	
			19.3820	562	1	0.014	8.26	6.89	
18229-3640	HD 168733	90074	19.3820	562	1	0.014	8.26	6.89	
			19.3820	832	1	0.021	8.06	7.05	
18267-3024	TOK 421	90397	19.3821	562	5	0.014	9.63	6.66	
			19.3821	832	5	0.021	8.53	7.10	
18354-3253	HD 171296	91137	21.7140	562	1	0.014	5.85	6.65	
			21.7140	832	1	0.021	5.45	6.66	
			22.3721	562	1	0.014	0.00	5.17	
			22.3721	832	1	0.021	3.43	5.52	
19182-3823	LWR 16AC	94863	19.3848	562	5	0.014	8.50	6.19	
			19.3848	832	5	0.021	8.86	6.97	
19185+0025	HD 180973	94883	21.7194	562	1	0.014	0.00	5.72	
			21.7194	832	1	0.021	4.38	6.45	
			22.3721	562	1	0.014	0.00	4.82	
			22.3721	832	1	0.021	4.10	5.83	
19197-3525	HD 180885	94986	19.3848	562	3	0.014	9.43	7.28	
			19.3848	832	3	0.021	8.92	7.55	
20339+1004	HD 195922	101473	21.7141	562	1	0.014	0.00	4.72	
			21.7141	832	1	0.021	0.00	5.62	
			22.3748	562	1	0.014	0.00	5.50	
			22.3748	832	1	0.021	6.98	6.43	
			22.7682	562	1	0.014	0.00	5.53	
			22.7682	832	1	0.021	6.79	6.28	
			23.4995	562	1	0.014	0.00	5.18	
20339-2710	HD 195719	101472	22.7627	562	2	0.014	0.00	5.02	Resolved on 832 in 21.5476.
			22.7627	832	2	0.021	4.67	5.72	Resolved on 562 and 832 on 21.7141 and 22.3721.
			23.4995	562	2	0.016	3.53	3.08	:
			23.4995	832	2	0.026	4.89	4.63	:
			23.4995	562	1	0.014	0.00	5.39	:
20359-2646	HD 196081	101629	21.5476	832	1	0.021	2.84	5.39	
20399+1115	CVN 17Aa,Ab	101966	22.7682	562	2	0.014	0.00	5.62	Resolved on 832, same epoch.
			23.4995	562	1	0.014	0.00	5.03	Resolved on 832, same epoch.

Table 4 continued on next page

Table 4 (continued)

WDS	DD	HIP	Epoch	Filt	Ncub	MinSep	Det@0.15	Det@1.00	Comments
			+2000.0 yr			"	mag	mag	
20414-2560	HD 196947	102094	22.7627	562	1	0.014	6.35	6.11	
			21.7141	562	1	0.014	6.52	6.32	
			21.7141	832	1	0.021	6.81	6.09	
			22.3721	562	1	0.014	3.83	5.74	
			22.3721	832	1	0.021	3.29	5.51	
			23.4995	562	1	0.014	0.00	6.15	
			23.4995	832	1	0.021	6.04	6.90	
21041+0300	DSG 6Aa,Ab	103987	19.4642	832	1	0.021	5.05	7.12	Triple on HIP 103987, unresolved with Zorro.
21047+0257	HD 200661	104041	21.7142	562	1	0.014	0.00	5.64	
			21.7142	832	1	0.021	5.83	6.22	
			22.3722	562	1	0.014	0.00	4.87	
			22.3722	832	1	0.021	5.99	6.05	
			22.7682	562	1	0.014	0.00	5.69	
			22.7682	832	1	0.021	6.32	6.38	
21150-2047	HD 202206	104903	21.7140	562	2	0.014	7.36	6.09	
			21.7140	832	2	0.021	5.78	6.21	
			22.3722	562	2	0.014	5.05	6.09	
			22.3722	832	2	0.021	5.96	6.04	
			22.7627	562	2	0.014	7.54	6.16	
			22.7627	832	2	0.021	6.90	6.54	
21229+0649	HD 203562	105570	19.4642	562	1	0.014	0.00	6.08	
			19.4642	832	1	0.021	7.62	6.63	
			19.7401	562	2	0.014	0.00	4.23	
			19.7401	832	2	0.021	4.72	5.43	
21241-2245	HD 203639	105662	21.7140	562	1	0.014	6.87	6.10	
			21.7140	832	1	0.021	5.12	6.13	
			22.3722	562	1	0.014	4.55	5.98	
			22.3722	832	1	0.021	5.33	5.80	
			22.7627	562	1	0.014	6.98	6.34	
			22.7627	832	1	0.021	5.66	6.49	
22033-2954	HD 209335	108871	22.7628	562	1	0.014	4.93	5.81	
			22.7628	832	1	0.021	3.67	5.84	
22069-2937	LSC 101	109172	19.6937	562	5	0.014	6.89	6.28	
			19.6937	832	5	0.021	6.47	6.33	
			22.7628	562	2	0.014	5.38	6.18	
			22.7628	832	2	0.021	5.16	6.18	
22110-2114	HD 210464	109509	22.7628	562	1	0.014	0.00	5.11	
			22.7628	832	1	0.021	2.26	5.34	
22128-2053	HD 210737	109652	19.6937	562	5	0.014	6.57	6.16	
			19.6937	832	5	0.021	5.53	6.36	
			22.7628	562	2	0.014	0.00	5.98	
			22.7628	832	2	0.021	5.66	6.18	
22143-2746	HD 210934	109789	19.6938	562	2	0.014	6.93	6.57	
			19.6938	832	2	0.021	7.40	6.68	
22171-0523	HD 211434	110023	19.6940	562	2	0.014	0.00	5.60	
			19.6940	832	2	0.021	6.56	6.46	
			19.7401	562	2	0.014	0.00	5.60	
			19.7401	832	2	0.021	6.56	6.46	
			19.7703	562	2	0.014	0.00	5.60	
			19.7703	832	2	0.021	6.56	6.46	
22216-2136	HD 212010	110391	19.6940	562	2	0.014	0.00	6.38	
			19.6940	832	2	0.021	6.71	6.55	
22584-0125	HD 217131	113433	19.6940	562	2	0.014	0.00	5.74	
			19.6940	832	2	0.021	6.90	6.75	
			23.5028	562	1	0.014	0.00	5.80	
			23.5028	832	1	0.021	6.53	6.83	
23098-1431	HD 218639	114371	19.7703	562	2	0.014	3.86	5.43	
			19.7703	832	2	0.021	2.93	5.70	
23179-1348	HD 219702	115038	20.9010	562	2	0.014	0.00	4.65	
			20.9010	832	2	0.021	0.00	5.64	
			20.9064	562	2	0.014	0.00	4.65	
			20.9064	832	1	0.021	0.00	5.64	
			21.5507	832	1	0.021	4.86	4.50	
			21.7144	562	2	0.014	6.40	6.06	
			21.7144	832	2	0.021	5.78	6.16	

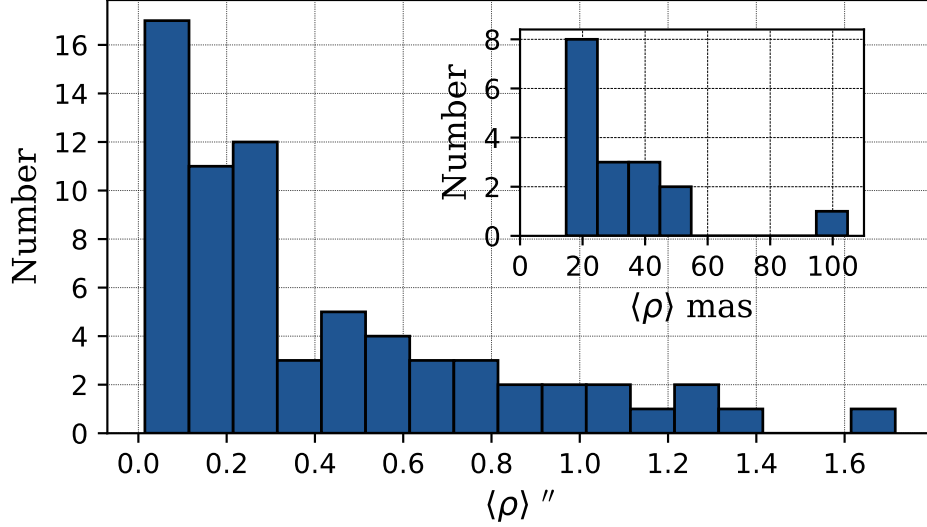


Figure 11. Histogram of mean ρ in bins of $0''.1$, computed over all epochs and all filters, for all the resolutions presented in Table 2. The inlet shows the histogram for objects with ρ smaller than 100 mas in bins of 10 mas.

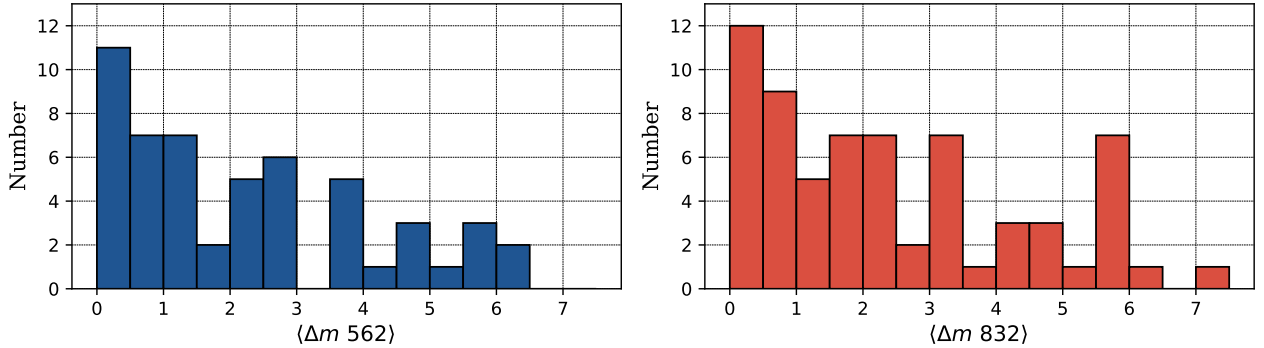


Figure 12. Histogram of mean Δm in bins of 0.5 mag, computed over all epochs for the blue filter (left) and the red filter (right), for all the resolutions presented in Table 2.

In Table 4 we present the list of unresolved targets. Here we also include PSF objects that were assumed to be single-stars, so it is no surprise that most of them are included in this table¹². The meaning of the first six columns in this table is the same as that of Table 2. The seventh column gives the angular resolution in arcsec, while the eighth and ninth columns give the 5σ magnitude difference -the detection limits of possible companions- at 0.15 and $1.00''$ respectively. Four PSF stars were serendipitously found to be new binaries, so they were moved to Table 2.

4.1. Preliminary orbits

With the available Zorro measurements, it was possible to calculate tentative orbits for some targets. However, we must emphasize that in most cases a follow-up will be required to complete the orbital coverage. Orbits derived from the present data should be considered preliminary; they are presented here only with the purpose of evaluating Zorro's

¹² because they are not listed in the WDS, they do not have a DD name, instead we adopt the HD or HIP number for them.

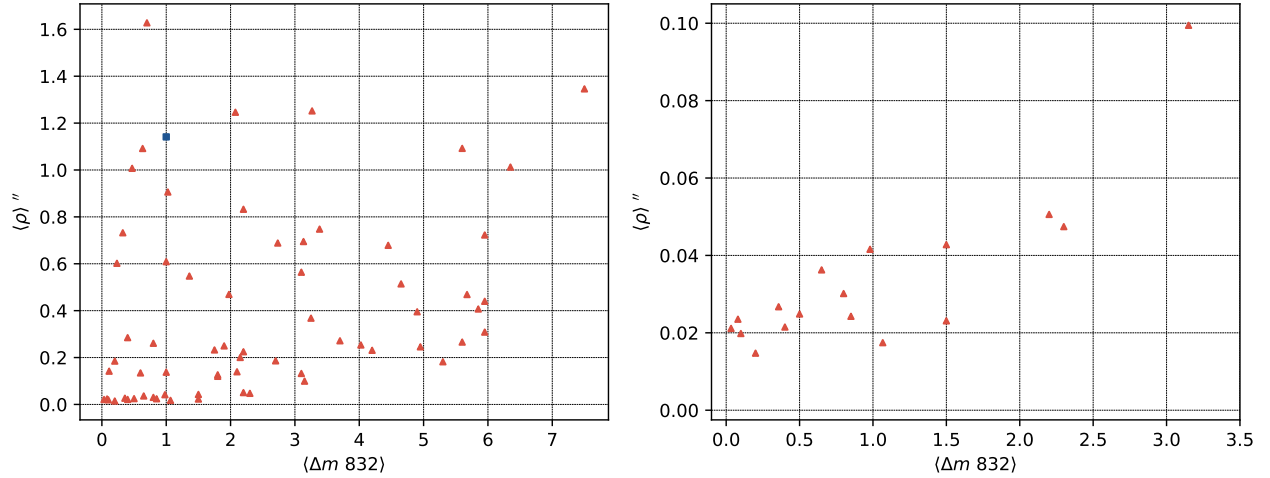


Figure 13. Average ρ of the components (over all epochs) as a function of the mean Δm in the red filter for all the resolutions presented in Table 2. The left panel is for the whole sample, while the right panel is for objects with ρ less than 100 mas. In the left panel, the blue square indicates the only object with no detection in the red filter (STF 1998AB), for this we plot the blue filter contrast instead.

capabilities. As a strategy, all pairs that could possibly be observed and followed up with smaller facilities have been moved to SOAR, while all very tight and/or faint companions will be continued to observe with Zorro@GS.

We note that, in Table 2, most objects with large ρ (larger than about $0''.4$) are calibration binaries, while tighter systems are our program targets. All objects in this table with the comment "Was PSF star" means they are newly confirmed binaries (four objects in total) with red companions of various ρ and a relatively large Δm . The most extreme case is HIP 82216, with a companion having $\Delta m \sim 6.0$ in the 832 filter and undetected in the 562 filter. There are also seven other new binaries which are either very tight (e.g., HIP 74165 and HIP 101472) or have large Δm (e.g. HIP 5146 and HIP 19120); mostly detected in the red channel only.

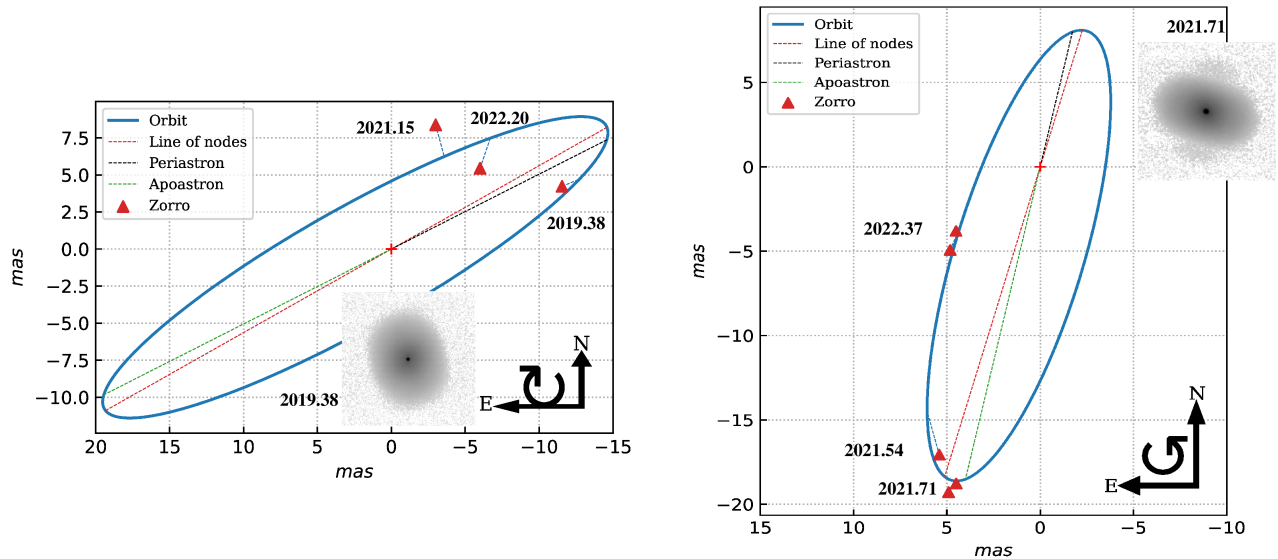


Figure 14. Preliminary visual orbits for HIP 76400 Aa1,Aa2 (left, $P=368.6$ days, $a=19.5$ mas) and HIP 101472 Aa,Ab (right, $P=354.9$ days, $a=13.9$ mas) derived by joint fitting of Zorro positions and available RVs. The inserts show the Speckle power spectra recorded near maximum ρ at 832 nm, with the same orientation.

Of particular interest are, of course, objects resolved for the first time. Figure 14 illustrates tentative combined spectro-interferometric orbits based on our Zorro data. Their visual orbital elements are listed in Table 5.

HIP 76400 (HD 139059, WDS 15362–0623, primary G6V) is a quadruple system composed of an internal double-line spectroscopic binary Aa1,Aa2 unresolved until now, with a companion Ab at $0.3''$ (Tok 301Aa,Ab), and another distant companion, B, at $80''$ (TOK 301AB). In our solution for Aa1,Aa2, the outer 70-yr orbit of Aa,Ab was fitted as well (it causes a substantial trend in the systemic velocities). For comparison, we also give the orbital parameters derived from the SB9 spectroscopic orbit of HIP 76400Aa1,Aa2.

HIP 101472 (HD 195719, WDS 20339–2710, primary G8V) is a triple system (possibly belonging to the Thick-Disk, Tokovinin (2019)) composed of an internal double-line spectroscopic binary Aa,Ab not resolved until now, with a faint companion B at $53''$ (CBL 178) that exhibits very small motion, and has no published orbit (period estimated at 200 kyr). In Table 5 we also show the (purely) astrometric orbit Aa,Ab from the non-single catalog produced by Gaia DR3 (Gaia Collaboration 2022)¹³.

Table 5. Tentative orbital elements for HIP 76400 Aa1,Aa2 and HIP 101472 from a joint astrometric/spectroscopic solution.

Pair	P days	T yr	e	a mas	Ω °	ω °	i °
Hip 76400 Aa1,Aa2	368.6	2018.3	0.143	19.5	119.4	192.3	102.0
SB9	368.51	2018.32	0.1370	—	—	192.0	—
Hip 101472	354.9	2016.4	0.397	13.9	344.4	12.2	74.1
Gaia DR3	353.98	—	0.410	—	356.9	33.3	91.2

Both systems have periods close to one yr, which makes it difficult to adequately sample the orbits, due to the yearly visibility cycles, fixed telescope schedules, and the need to observe as close to the meridian as possible.

These two cases are a good example of the limitations of the Zorro@GS setup. Their semi-major axes (~ 19 mas and ~ 15 mas) are below the diffraction limit of Gemini at 832 nm, so our tentative resolutions do not yield accurate measurements of the positions. Even if more data are accumulated, the prospect of measuring masses with sufficient (a few percent) accuracy for targets like these is unlikely. To constrain the inclination of these edge-on orbits, the pairs must be resolved at ρ substantially less than the maximum, below the diffraction limit. A long-baseline interferometer like VLTI is needed in these cases.

In a forthcoming paper, we will publish orbits for other targets in our sample, combining them with new RV measurements acquired by our team with the FEROS Echelle spectrograph at the MPG 2.2 m telescope at ESO/La Silla.

4.2. Comments on individual objects

In this section, comments regarding multiplicity are mostly based on Tokovinin’s Multiple Star Catalogue (MSC¹⁴, Tokovinin (1997, 2018b)).

HIP 7869 = 01412–6741 = HD 10607 is a nearby quadruple system of 2+2 architecture. The outer $33''$ common proper-motion pair (CPM hereafter) A,B is known as LDS 56; its estimated period is 76 kyr. The 12.4 mag secondary star B was resolved at SOAR as a $0''.49$ pair; it also has double transits in Gaia, indicating a double source. The 8.32 mag G0V primary star A has double lines (Nordström et al. 2004). It has been resolved by Zorro twice, but only in the red channel; in 2019.54 and 2020.90, at ρ of 25.6 and 34.7 mas respectively, with a moderate $\Delta m \approx 0.8$ mag (Figure 15); the pair was unresolved on two subsequent visits in 2021.72 and 2022.76 (see Table 2). The estimated period of Aa,Ab is 3 yr. Both A and B are independently detected as astrometric binaries by Gaia DR3 (RUWE 8.5 and 5.2), so their parallaxes (12.67 and 13.04 mas) are unreliable. The masses range from 0.4 to 1.1 M_{\odot} . As we collect

¹³ The values for Ω and ω have been corrected for their 180 deg ambiguity in Gaia DR3, to match our joint RV/ astrometric solution

¹⁴ Updated version available at <http://www.ctio.noirlab.edu/~atokovin/stars/>

more epochs, a good prospect exists for a combined inner orbit.

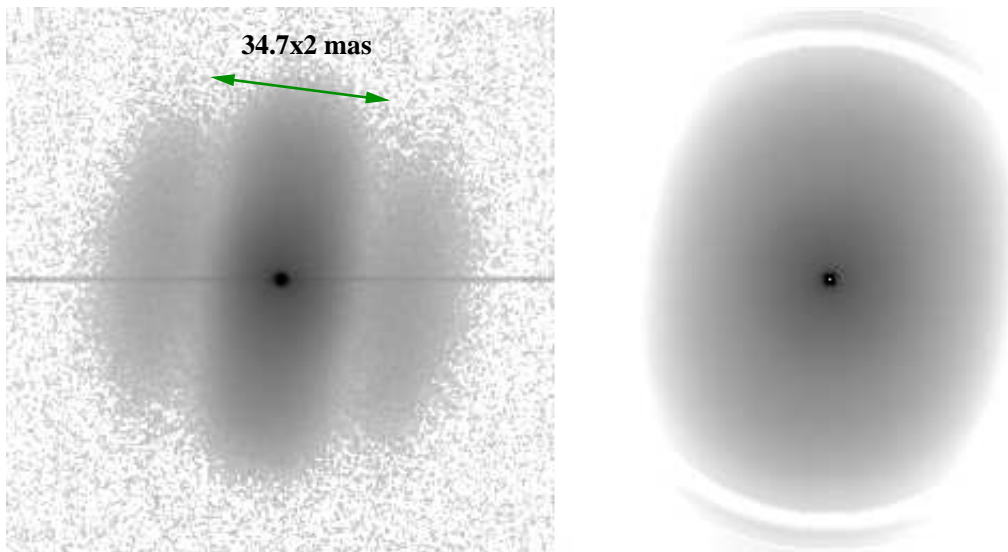


Figure 15. The power spectrum of HIP 7869 (component A) recorded on 2020.90 at 832 nm (left), and its model accounting for the AD (right).

HIP 30953 = 06298–5014 = HD 46273. This is a 2+2 quadruple system with an outer ρ of $12''.2$ (DUN 30). Both pairs A,B, and C,D have known visual orbits with periods of 53 and 99 yr, respectively. The pair A,B (R 65) has been observed with Zorro eight times, covering the periastron of its eccentric ($e = 0.97$) orbit in 2021.39. Double lines were expected near the periastron, but unfortunately no RVs were secured at this epoch. The residuals to the latest orbit¹⁵ (see also Table 2) indicates that it should be updated. Interestingly, pairs A,B and C,D move in opposite directions (inclinations 33 and 157°), excluding their coplanarity. The mass ratios in both pairs are close to one, but the component’s masses are different; 1.5 and $0.8 M_\odot$. The dynamical parallaxes deduced from the estimated masses and orbits are 20.1 and 21.5 mas and agree with the Hipparcos parallax of 19.4 mas. Gaia gives no parallaxes for these pairs. Interestingly, Trilling et al. (2007) found a 16 AU debris disk around A.

HIP 38625 = 07546–0125 = HD 64606, KOV is a triple system at 20 pc from the Sun (GJ 292.2). WDS lists two pairs, HDS1125AB at $4''.9$ and YSC 198Aa,Ab at $0''.5$ with similar magnitude differences of 4 mag. However, the $4''.9$ pair is spurious; it is not confirmed by Gaia and most likely results from the wrong interpretation of the double-star signal in the Hipparcos data reduction (a similar case was recently documented at SOAR). Star A is also a spectroscopic binary with $P = 450$ days (Latham et al. 2002). Its estimated semimajor axis is 66 mas, but the RV amplitude implies a minimum mass ratio of 0.25 , making it a poor candidate for speckle resolution. Nevertheless, the star was visited by Zorro five times, with ρ decreasing from $0''.79$ in 2020 to $0''.74$ in 2022 and little change in θ (direct motion). So, this pair has opened up from $0''.52$ in 2010, when it was resolved by Horch et al. (2017), and now is closing again. Its estimated period is 30 yr, and a preliminary orbit can be fitted to the data (albeit on a very short arc). The estimated amplitude of the wobble caused by the subsystem is 13 mas, so the speckle data should be fitted by two Keplerian orbits to determine the inclination of the subsystem Aa,Ab. The object has fast PM, large RV (102.2 km s^{-1}), and is located slightly below the standard main sequence (metal-poor).

¹⁵ In Circular 207, available at <https://www.usc.gal/astro/circularing.html>.

HIP 55505 = 11221–2447 = HD 98800, K4V according to SIMBAD, the primary is a T Tauri star TWA 4 in a quadruple system consisting of close spectroscopic pairs Aa,Ab and Ba,Bb on a 205 yr orbit around each other. We have not resolved the inner pairs and measured the outer pair I 507AB which is closing down, approaching periastron.

HIP 57421 = 11464–2758 = HD 102301, G0V is a strange triple system with comparable ρ between components (trapezium type). The inner $0''.2$ pair A,B (LSC 49) was discovered by Horch et al. (2017) in 2012. A fainter star C at $0''.5$ from A (DSG 13) was first measured in 2016 (Horch et al. 2019). The object has been visited four times with Zorro, and C was confirmed at 832 nm (but never detected in the blue filter) with a magnitude difference of 5.6 mag (Figure 16). The mean magnitude difference between A and B is 2.98 and 2.70 mag at 562 and 823 nm, respectively. Observations of this system at SOAR resolved only the pair A,B because component C was below the detection limit. Zorro measured A,C with an angle 180° from that of Horch et al. (2017). The position of A,C is stable over time, confirming that this system is bound. The projected ρ imply periods of 50 and 150 yr for A,B and AB,C, respectively. The pair A,B has turned from 98° in 2012 to 40° in 2023 with little change in ρ , suggesting a quasi-circular face-on orbit with a period of ~ 70 yr. The angle of A,C has changed only by $-3^\circ.5$ in 6 yr, a speed that corresponds to a 600 yr circular orbit. A plausible dynamically stable configuration would be a wide orbit of C around AB, where C is seen at close ρ owing to projection. In such case its slow motion is natural.

HIP 59426 = 12114–1647 = HD 105913 has been known as a triple with an outer $4''.7$ pair S 634 (ADS 8444) and an inner spectroscopic subsystem Aa,Ab with a period of 211 days (Tokovinin 2019). This triple has been resolved at SOAR and its combined inner orbit was published. Gaia DR3 independently determined an astrometric and SB1 orbit of Aa,Ab, although its amplitude is severely reduced by blending (the mass ratio is 0.87). The purpose of Zorro observations has been to measure the inner subsystem more accurately for mass estimation. Unexpectedly, another faint star Ac has been detected in 2020.04 at 832 nm at $0''.33$ with $\Delta I = 5.9$ mag. The detection is secure in each of the five data cubes. So, Zorro observations reveal this system as a new 3+1 quadruple.

The ρ of Aab,Ac implies a period of 25 yr. Motion in this orbit should leave a signature in the astrometry and RVs. Indeed, a PM anomaly of 6 mas yr^{-1} has been detected by Brandt (Brandt 2018, 2019), and the PMs of A and B are substantially different. The 211 day subsystem cannot produce such a large effect, so astrometry indirectly confirms the existence of Ac. No obvious trend is found in the RVs of the spectroscopic pair measured in 2017–2019. The latest spectrum taken in 2023 also matches the orbit. However, the very first observation in 2008 does differ from the orbit by 3 km s^{-1} . The Aab,Ac pair can be presently near elongation, corresponding to a slow RV variation. The RV amplitude can be reduced by the face-on orbit orientation.

HIP 58669 = 12018–3439 = HD 104471 is a classical solar-type triple system composed of three similar stars. The outer pair I 215 has a combined visual-spectroscopic orbit with $P = 156$ yr, and its main component is a double-lined spectroscopic binary with a period of 148 days (Tokovinin et al. 2015). The semimajor axis of Aa,Ab is 13 mas, and it has been resolved in 2017.43 at similar ρ (Horch et al. 2019). We visited this object four times between 2019 and 2022. So far, it has been processed as a binary, but the inner pair is marginally resolved (Figure 17). As we accumulate more epochs, and the data are reprocessed as triple, the measurements of Aa,Ab will allow a determination of its combined orbit, which will define its relative orientation with respect to A,B. The prospect of accurate mass measurement is however uncertain, considering only marginal resolutions.

RST 2802 = 12314–5659 = HD 108938. This is a triple-lined system of three similar G8V stars. The outer pair RST 2802 is separated at $1''.2$ and has an estimated period of 1.4 kyr. The inner SB2 subsystem Aa,Ab has a period of 343 days, implying a semimajor axis of 8.4 mas (the parallax of star B is 6.35 mas, Tokovinin (2022)). This system has been observed with Zorro four times in hope of resolving the inner pair. The power spectrum might be slightly elongated, but this resolution is uncertain and we fitted only the binary-star model, measuring the outer $1''.25$ pair. Our calibration is not accurate enough for detecting astrometric wobble caused by the subsystem with an estimated amplitude of 2 mas.

HIP 63162 = 12565–2635 = HD 112375 is a visual triple with ρ of $13''.8$ and $0''.15$; the inner pair YSC 216 Aa,Ab has been measured here three times. It has turned by 63° since its discovery in 2011 by Horch et al. (2017). The motion matches the estimated period of 60 yr, but the orbit is not yet sufficiently constrained to be of any use.

HIP 63377 = 12592–6256 = HD 112636 was noted as double-lined by Nordström et al. (2004), and has an astrometric signature (RUWE 10.0 in DR3). The outer $0''.45$ pair TOK 722 with substantial contrast ($\Delta I = 2.5$ mag) has been resolved at SOAR in 2016. The inner pair Aa,Ab has been securely resolved by Zorro in 2019, 2021, and 2023 (see Figure 18) and marginally resolved in 2022.37. The estimated period of Aa,Ab is 3 yr. A spectrum taken with

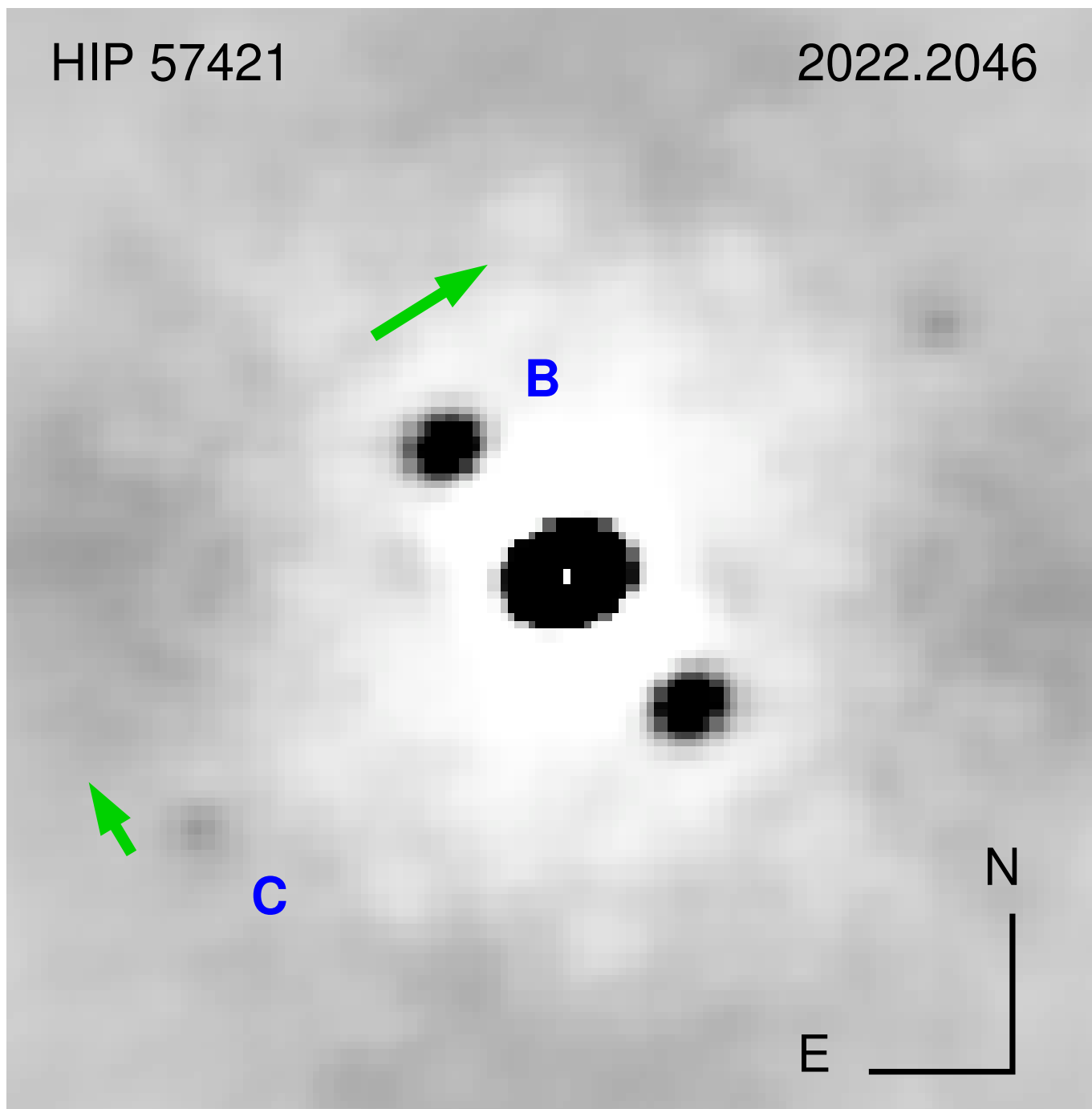


Figure 16. Speckle ACF of the triple system HIP 57421 recorded on 2022.20 at 823 nm (in negative rendering). The inner $0.18''$ pair is A,B, and the faint tertiary C is seen at nearly orthogonal angle at $0''.46$. Green arrows show the direction of motion.

CHIRON in 2023 January clearly shows double lines. This is a good candidate for continued speckle and spectroscopic monitoring for a determination of the inner orbit and masses.

HIP 68587 = 14025–2440 = HD 122445, G3V is a triple system where the $0''.5$ visual pair B 263 (period 161 yr) contains a single-lined spectroscopic subsystem with a period of 2.738 yr according to Griffin, who also noted a trend in its center of mass velocity. The corresponding semimajor axis is 31 mas. However, the full spectroscopic elements remain unpublished, and Roger Griffin passed away. The subsystem Aa,Ab has been tentatively resolved in

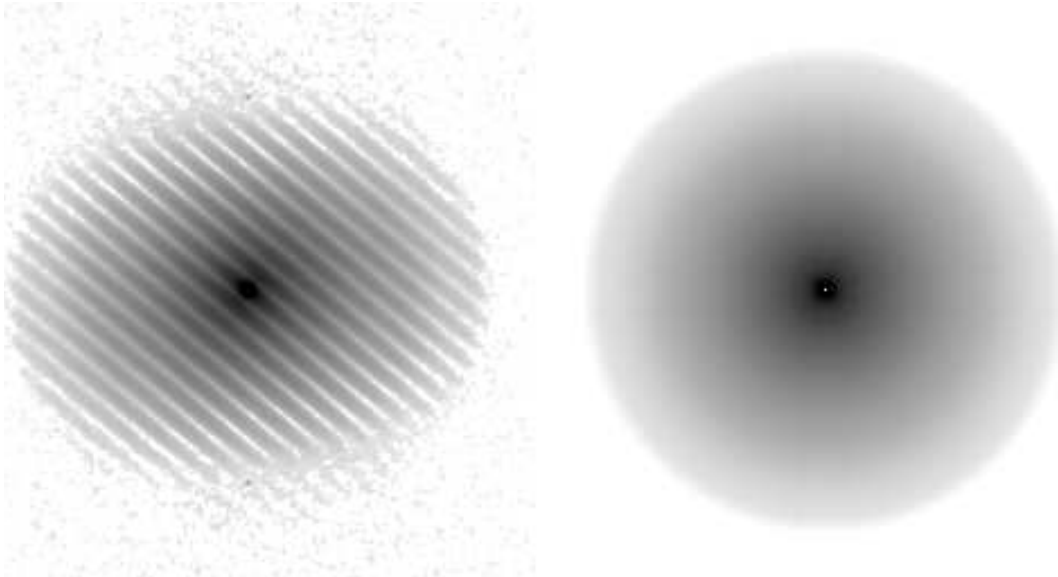


Figure 17. Power spectrum of HIP 58669 (left) and its model (right) taken on 2021.0359 at 832 nm. The fringes correspond to the A,B pair at a ρ of $0''.27$. Note the loss of contrast and the inversion of fringe phase in the upper and lower areas, indicating the resolution of Aa,Ab.

2017.42 by Horch et al. (2019) at 10 mas ρ with a small magnitude difference. The object has been visited by Zorro three times and only the A,B binary was measured. Although the existence of Aa,Ab leaves no doubt, its published resolution remains unconfirmed.

HIP 72622 = 14509–1603 = HD 130841, A3IV, $\alpha 2$ Lib is a naked-eye quadruple system of 2+2 hierarchy located at 23 pc. The outer CPM pair has a ρ of $231''$ and an estimated period of 170 kyr. Its secondary component B (HIP 72603, HD 130819) is a single-lined spectroscopic binary with a period of 14.3 yr (Duquennoy & Mayor 1991) resolved as BEU 19. The primary star A is also a single-lined SB1 with $P = 70.3$ days (Fuhrmann et al. 2014) resolved as DSG 17 in 2017 by Horch et al. (2019). It has been resolved in 2019 and 2020 by Zorro at 27 and 18 mas, respectively, and unresolved in 2023. Using these observations and the published RVs, a visual-spectroscopic orbit of Aa,Ab can be computed. It is unlikely that the orbits of Aa,Ab and Ba,Bb are aligned, given the large outer ρ .

HIP 76400 = 15362–0623 = HD 139059 is a 3+1 quadruple system. The outer $80''$ pair A,B and the intermediate $0''.4$ pair Aa,Ab are both designated as TOK 301 in the WDS. Furthermore, star A is a triple-lined spectroscopic system with an inner period of 368.5 days (Tokovinin 2022). Its estimated axis of 20 mas prompted Zorro observations aimed to resolve Aa1,Aa2. In three visits, we securely measured the pair Aa,Ab and noted a slight elongation of the power spectrum due to partially resolved Aa1,Aa2 (Figure 19). Instead of fitting a triple-star model, we estimated the positions of Aa1,Aa2 by fitting a close binary with a $\Delta m = 0$ constraint to the red channel only. These positions roughly agree with the spectroscopic elements (see Table 5).

HIP 76424 = 15365+1607 = HD 139225 is a bright but uninteresting triple with outer ρ of $35''.5$ (UC 3033) and inner ρ of $1''$ (DSG 18 Aa,Ab). The long estimated periods of 50 kyr and 250 yr do not favor orbit determination in this century. We measured the inner pair in 2019 and 2020 only in the red channel. Its position has not changed since its discovery in 2014 by Horch et al. (2019). The measured Δm at 823 nm is large (6.4 mag)

HIP 81023 = 16329+0315 = HD 149162 belongs to a late-type quintuple system. The outermost CPM pair A,BC (LEP 79) has a ρ of $252''$ and an estimated period of 770 kyr, while the period of the $6''.3$ pair B,C (DAM 649) is 7 kyr. Stars A, B, and C have similar PMs and parallaxes in Gaia DR3. Component A itself hosts three stars: the inner spectroscopic pair Aa,Ab with a period of 226 days (Latham et al. 2002) and a low-mass star Ac at $0''.3$. Both

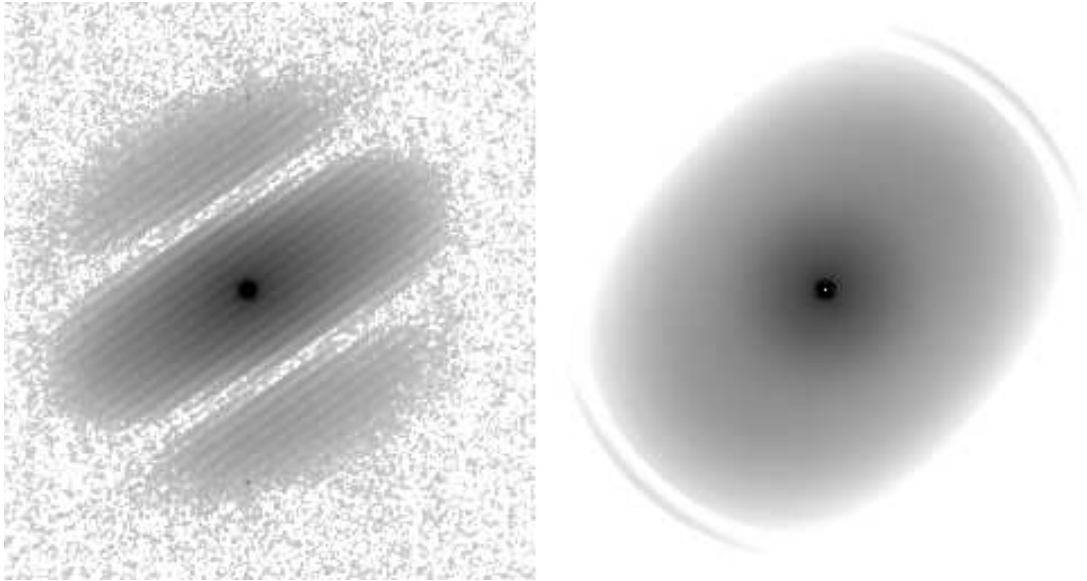


Figure 18. Power spectrum of HIP 63377 taken in 2019.531 at 832 nm and showing resolution of the inner subsystem.

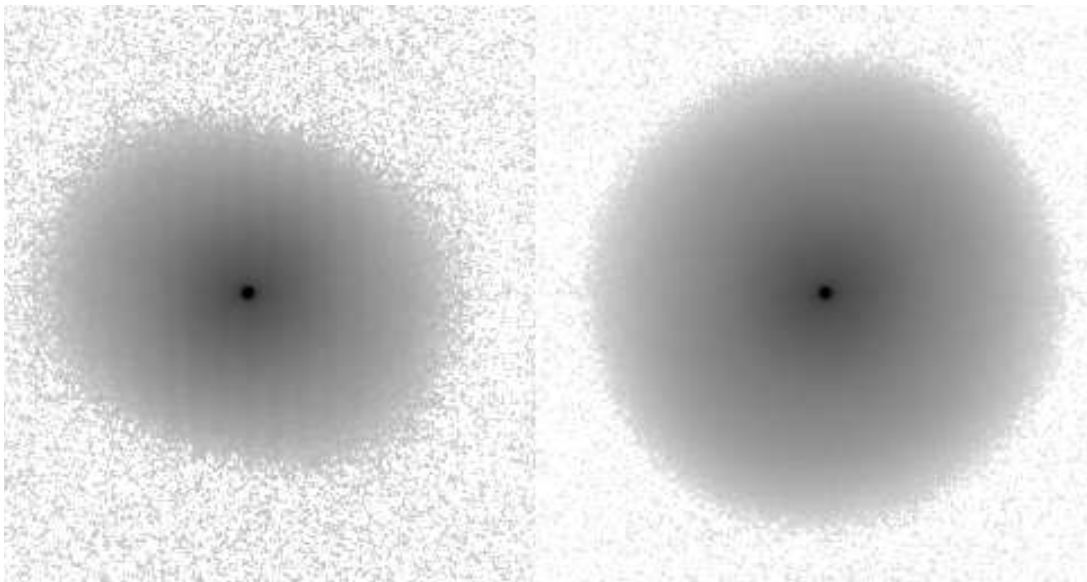


Figure 19. Power spectrum of HIP 76400 taken on 2019.38 at 832 nm. The fine low-contrast fringes are produced by the companion Ab at $0''.21$, and the elongation indicates partial resolution of Aa1,Aa2 at 25 mas.

pairs were resolved by Horch in 2013 and bear the name DSG 7 in the WDS. Videla et al. (2022) have done a joint spectroscopic (SB1) and astrometric solution, obtaining a semimajor axis of 22 mas. We observed this target with Zorro in 2019.46, 2019.54, and 2023.17 at zenith distances of 35–39° and fitted a binary-star model that corresponds to the intermediate Aab,Ac pair. The power spectrum is slightly elongated, suggesting partial resolution of Aa,Ab, but uncorrected AD prevents reliable estimation of its parameters; data in the blue channel are hopelessly distorted by AD. Given these discouraging results, the object will not be observed regularly in the future. The estimated period of Aab,Ac is 30 yr, and our measures of this pair will be useful in a future orbit calculation.

HIP 82730 = 16546–0609 is listed in the WDS as a triple system with two companions B and C at ρ of 0''.35 and 0''.66, respectively, discovered by Horch et al. (2012) in 2012.57. However, further measurements between 2015 through 2017 by Horch et al. (2020) feature only the A,B pair. This object was observed by Zorro in 2019 twice, and we also do not confirm the existence of additional component C. This system is therefore a simple binary.

HIP 84430 = 17157–0949 = HD 156034 is a resolved triple system where the visual orbits of A,B and Ba,Bb (A 2592 and TOK 53) with periods of 137 and 5.26 yr, respectively, are well constrained (Tokovinin 2021). Our measurement of this triple in 2022.21 and 2023.50 agrees with both orbits.

HIP 88937 = 18093–2607 = HD 165896 is a triple system consisting of the 1''.3 visual pair Aa,Ab and a double-lined spectroscopic subsystem Aa1, Aa2 with a period of 38 days according to its unpublished orbit listed in the MSC. The corresponding semimajor axis of 6 mas does not favor resolution with Zorro and, indeed, we measured only Aa,Ab in three visits. The estimated period of this pair is 260 yr, and the observed motion is slow. WDS lists another two faint companions B and C which are unrelated, as evidenced by the fast relative motion. The sky in this region is very crowded.

HIP 101472 = 20339–2710 = HD 195719 is a triple system composed of the 52 CPM pair A,B (CBL 178) and the double-lined binary Aa,Ab with a period of 355 days and a mass ratio of 0.92 (Tokovinin 2019). Gaia DR3 provided an astrometric orbit of this pair with an inclination of 91° (edge-on). The semimajor axis of 14 mas prompted Zorro observations aimed to resolve this pair. Observations in 2021.55, 2021.71, and 2022.37 measured ρ of 18, 19, and 15 mas, respectively; the last measurement below the diffraction limit is tentative. An orbit fitted to these data is presented in Figure 14.

5. CONCLUSIONS

In this paper we report on the astrometric characterization of the Zorro speckle camera mounted on the 8.1 m GS telescope, based on measurements of binary systems obtained in the context of our survey of southern hemisphere low-metallicity binary and multiple stellar systems. We show that Zorro@GS is a powerful facility for the study of tight visual binary systems and systems with faint secondary components (or the combination of both).

Zorro@GS allows to resolve binary systems even slightly below its natural diffraction limit of 20 mas, which proved to be critical for the discovery of tight multiple systems among our targets and for the study of the orbital architecture of known compact hierarchical systems we included in our program.

We show that, with proper calibration, astrometric data (ρ , θ and Δm) of excellent quality can be obtained. For targets with ρ smaller than 0''.4, an overall precision of 1 mas in the radial and tangential directions is achieved, while the uncertainty in θ is 0''.2. A repeatability study in relative photometry indicates a precision of about 0.1 mag both in the blue and red filters.

Simultaneous blue (562 nm) and red (832 nm) images can be acquired, but the orientation and scale of the two cameras differ, and this has to be considered for high-precision relative astrometry. We compare the ρ and θ of well-measured binaries with ρ between 50 mas and 1''.2 (typically around 10 such pairs per observing run), which allows us to put them on a common system with an uncertainty smaller than 0.6%. In this way the blue and red measurements become commensurable, and can be considered equivalent, but independent, in the subsequent orbital analysis. We perform this relative calibration in every observing run, because the instrument sometimes has to be removed from the telescope. In each observing run we also observed at least two astrometric calibration binaries, which allow us to estimate a fractional correction to the absolute plate scale and orientation in the sky. These are long-period (slow motion) bright binaries with ρ between 0''.5 and 1''.2, that have plenty of modern interferometric measurements, typically from our SOAR program (albeit not necessarily good orbits).

Given certain orbital architectures, however, the limitations of the Zorro@GS setup become evident when the semimajor axis is below the natural diffraction limit of Gemini at 832 nm, in which case the resolutions do not yield accurate measurements of the positions. Even if more data is secured, the prospect of measuring masses with sufficient (a few

percent) accuracy for targets like these is unlikely. We report on two examples of this kind: HIP 76400 (semimajor axis of 19.5 mas) and HIP 101472 (semimajor axis of 13.9 mas).

We have also found that, due to the lack of an atmospheric dispersion corrector at Gemini, the blue images are systematically worse than those in the red channel, despite its smaller formal diffraction limit. This means that no detection might be possible in the blue filter if the dispersion happens to be along the θ of the companion, despite being above the diffraction limit. This is a severe limitation of the instrument in its present form.

Here we present relative astrometry and contrast brightness in both Zorro filters for 70 pairs in 64 distinct systems (six are hierarchical triples). Eleven new binaries have been found (among these, four PSF stars that were considered to be bona-fide single stars until now), most of them with small ρ (down to 15 mas) and large Δm (up to $\Delta m = 6$ in the red channel).

We plan to continue observing the most interesting targets with Zorro, as well as adding new promising objects, with the medium-term goal of extending the sample to the low-metallicity regime (currently our lowest metallicity object has $[\text{Fe}/\text{H}] = -1.72$). In the longer term, we hope that our observations could contribute to the advance of our knowledge of stellar masses for a wide range of metallicities.

RAM, EC and MD acknowledge support from FONDECYT/ANID grant # 124 0049. RAM also acknowledges support from ANID, Fondo GEMINI, Astrónomo de Soporte GEMINI-ANID grant # 3223 AS0002. We acknowledge many discussions with Dr. Elliot Horch, who provided inspiration, expert guidance, and interesting targets for GS prior to publication, especially in the early stages of this work. Finally we thank an anonymous referee, his/her suggestions and comments were of great help to improve the readability of our paper.

Facilities: NOIRLab:Gemini 8.1 m-South+ZORRO, ESO: La Silla, MPG2.2m+FEROS

Software: IDL

REFERENCES

- Anguita-Aguero, J., Mendez, R. A., Clavería, R. M., & Costa, E. 2022, *AJ*, 163, 118, doi: [10.3847/1538-3881/ac478c](https://doi.org/10.3847/1538-3881/ac478c)
- Anguita-Aguero, J., Mendez, R. A., Videla, M., et al. 2023, *AJ*, 166, 172, doi: [10.3847/1538-3881/acf297](https://doi.org/10.3847/1538-3881/acf297)
- Benedict, G. F., Henry, T. J., Franz, O. G., et al. 2016, *AJ*, 152, 141, doi: [10.3847/0004-6256/152/5/141](https://doi.org/10.3847/0004-6256/152/5/141)
- Boyajian, T. S., McAlister, H. A., van Belle, G., et al. 2012a, *ApJ*, 746, 101, doi: [10.1088/0004-637X/746/1/101](https://doi.org/10.1088/0004-637X/746/1/101)
- Boyajian, T. S., von Braun, K., van Belle, G., et al. 2012b, *ApJ*, 757, 112, doi: [10.1088/0004-637X/757/2/112](https://doi.org/10.1088/0004-637X/757/2/112)
- Brandt, T. D. 2018, *ApJS*, 239, 31, doi: [10.3847/1538-4365/aaec06](https://doi.org/10.3847/1538-4365/aaec06)
- . 2019, *ApJS*, 241, 39, doi: [10.3847/1538-4365/ab13b2](https://doi.org/10.3847/1538-4365/ab13b2)
- Davidson, James W., J., Baptista, B. J., Horch, E. P., Franz, O., & van Altena, W. F. 2009, *AJ*, 138, 1354, doi: [10.1088/0004-6256/138/5/1354](https://doi.org/10.1088/0004-6256/138/5/1354)
- Duquenois, A., & Mayor, M. 1991, *A&A*, 248, 485
- Eddington, A. S. 1924, *MNRAS*, 84, 308, doi: [10.1093/mnras/84.5.308](https://doi.org/10.1093/mnras/84.5.308)
- Feiden, G. A., & Chaboyer, B. 2012, *ApJ*, 757, 42, doi: [10.1088/0004-637X/757/1/42](https://doi.org/10.1088/0004-637X/757/1/42)
- Fuhrmann, K., Chini, R., Barr, A., et al. 2014, *MNRAS*, 437, 2303, doi: [10.1093/mnras/stt2046](https://doi.org/10.1093/mnras/stt2046)
- Gafeira, R., Patacas, C., & Fernandes, J. 2012, *Ap&SS*, 341, 405, doi: [10.1007/s10509-012-1125-3](https://doi.org/10.1007/s10509-012-1125-3)
- Gaia Collaboration. 2022, VizieR Online Data Catalog: Gaia DR3 Part 3. Non-single stars (Gaia Collaboration, 2022), VizieR On-line Data Catalog: I/357. Originally published in: *Astron. Astrophys.*, in prep. (2022)
- Gratton, R. G., Fusi Pecci, F., Carretta, E., et al. 1997, *ApJ*, 491, 749, doi: [10.1086/304987](https://doi.org/10.1086/304987)
- Horch, E. P., Howell, S. B., Everett, M. E., & Ciardi, D. R. 2012, *AJ*, 144, 165, doi: [10.1088/0004-6256/144/6/165](https://doi.org/10.1088/0004-6256/144/6/165)
- Horch, E. P., Veillette, D. R., Baena Gallé, R., et al. 2009, *AJ*, 137, 5057, doi: [10.1088/0004-6256/137/6/5057](https://doi.org/10.1088/0004-6256/137/6/5057)
- Horch, E. P., van Altena, W. F., Demarque, P., et al. 2015, *AJ*, 149, 151, doi: [10.1088/0004-6256/149/5/151](https://doi.org/10.1088/0004-6256/149/5/151)
- Horch, E. P., Casetti-Dinescu, D. I., Camarata, M. A., et al. 2017, *AJ*, 153, 212, doi: [10.3847/1538-3881/aa6749](https://doi.org/10.3847/1538-3881/aa6749)
- Horch, E. P., Tokovinin, A., Weiss, S. A., et al. 2019, *AJ*, 157, 56, doi: [10.3847/1538-3881/aaf87e](https://doi.org/10.3847/1538-3881/aaf87e)
- Horch, E. P., van Belle, G. T., Davidson, James W., J., et al. 2020, *AJ*, 159, 233, doi: [10.3847/1538-3881/ab87a6](https://doi.org/10.3847/1538-3881/ab87a6)

- Iben, Jr., I. 2013, *Stellar Evolution Physics, Volume 1: Physical Processes in Stellar Interiors*
- Kahler, H. 1972, *A&A*, 20, 105
- Latham, D. W., Stefanik, R. P., Torres, G., et al. 2002, *AJ*, 124, 1144, doi: [10.1086/341384](https://doi.org/10.1086/341384)
- Mann, A. W., Dupuy, T., Kraus, A. L., et al. 2019, *ApJ*, 871, 63, doi: [10.3847/1538-4357/aaf3bc](https://doi.org/10.3847/1538-4357/aaf3bc)
- Massey, P., & Meyer, M. 2001, in *Encyclopedia of Astronomy and Astrophysics*, ed. P. Murdin, 1882, doi: [10.1888/0333750888/1882](https://doi.org/10.1888/0333750888/1882)
- Mendez, R. A., Claveria, R. M., Orchard, M. E., & Silva, J. F. 2017, *AJ*, 154, 187, doi: [10.3847/1538-3881/aa8d6f](https://doi.org/10.3847/1538-3881/aa8d6f)
- Moe, M., & Di Stefano, R. 2017, *ApJS*, 230, 15, doi: [10.3847/1538-4365/aa6fb6](https://doi.org/10.3847/1538-4365/aa6fb6)
- Moe, M., & Kratter, K. M. 2018, *ApJ*, 854, 44, doi: [10.3847/1538-4357/aaa6d2](https://doi.org/10.3847/1538-4357/aaa6d2)
- Nordström, B., Mayor, M., Andersen, J., et al. 2004, *A&A*, 418, 989, doi: [10.1051/0004-6361:20035959](https://doi.org/10.1051/0004-6361:20035959)
- Reid, I. N. 1997, *AJ*, 114, 161, doi: [10.1086/118462](https://doi.org/10.1086/118462)
- Spada, F., Demarque, P., Kim, Y. C., & Sills, A. 2013, *ApJ*, 776, 87, doi: [10.1088/0004-637X/776/2/87](https://doi.org/10.1088/0004-637X/776/2/87)
- Tighe, R., Tokovinin, A., Schurter, P., Martínez, M., & Cantarutti, R. 2016, in *Society of Photo-Optical Instrumentation Engineers (SPIE) Conference Series*, Vol. 9908, *Ground-based and Airborne Instrumentation for Astronomy VI*, ed. C. J. Evans, L. Simard, & H. Takami, 99083B, doi: [10.1117/12.2233681](https://doi.org/10.1117/12.2233681)
- Tokovinin, A. 2018a, *PASP*, 130, 035002, doi: [10.1088/1538-3873/aaa7d9](https://doi.org/10.1088/1538-3873/aaa7d9)
- . 2018b, *Astrophysical Journal, Supplement*, 235, 6, doi: [10.3847/1538-4365/aaa1a5](https://doi.org/10.3847/1538-4365/aaa1a5)
- . 2019, *AJ*, 158, 222, doi: [10.3847/1538-3881/ab4c94](https://doi.org/10.3847/1538-3881/ab4c94)
- . 2021, *AJ*, 161, 144, doi: [10.3847/1538-3881/abda42](https://doi.org/10.3847/1538-3881/abda42)
- . 2022, *AJ*, 163, 161, doi: [10.3847/1538-3881/ac5330](https://doi.org/10.3847/1538-3881/ac5330)
- . 2023, *AJ*, 165, 220, doi: [10.3847/1538-3881/acca19](https://doi.org/10.3847/1538-3881/acca19)
- Tokovinin, A., Everett, M. E., Horch, E. P., Torres, G., & Latham, D. W. 2019, *AJ*, 158, 167, doi: [10.3847/1538-3881/ab4137](https://doi.org/10.3847/1538-3881/ab4137)
- Tokovinin, A., & Latham, D. W. 2020, *AJ*, 160, 251, doi: [10.3847/1538-3881/abbad4](https://doi.org/10.3847/1538-3881/abbad4)
- Tokovinin, A., Mason, B. D., & Hartkopf, W. I. 2010, *AJ*, 139, 743, doi: [10.1088/0004-6256/139/2/743](https://doi.org/10.1088/0004-6256/139/2/743)
- Tokovinin, A., Mason, B. D., Mendez, R. A., & Costa, E. 2022, *AJ*, 164, 58, doi: [10.3847/1538-3881/ac78e7](https://doi.org/10.3847/1538-3881/ac78e7)
- Tokovinin, A., Pribulla, T., & Fischer, D. 2015, *AJ*, 149, 8, doi: [10.1088/0004-6256/149/1/8](https://doi.org/10.1088/0004-6256/149/1/8)
- Tokovinin, A. A. 1997, *Astronomy and Astrophysics, Supplement*, 124, 75, doi: [10.1051/aas:1997181](https://doi.org/10.1051/aas:1997181)
- Torres, G., Andersen, J., & Giménez, A. 2010, *A&A Rv*, 18, 67, doi: [10.1007/s00159-009-0025-1](https://doi.org/10.1007/s00159-009-0025-1)
- Trilling, D. E., Stansberry, J. A., Stapelfeldt, K. R., et al. 2007, *ApJ*, 658, 1289, doi: [10.1086/511668](https://doi.org/10.1086/511668)
- Videla, M., Mendez, R. A., Clavería, R. M., Silva, J. F., & Orchard, M. E. 2022, *AJ*, 163, 220, doi: [10.3847/1538-3881/ac5ab4](https://doi.org/10.3847/1538-3881/ac5ab4)